

**AN EMPIRICAL CORRELATION FOR WATER FLOODING
PERFORMANCE IN A LAYERED RESERVOIR**

BY

SHAMS KALAM

A Thesis Presented to the
DEANSHIP OF GRADUATE STUDIES

KING FAHD UNIVERSITY OF PETROLEUM & MINERALS

DHAHRAN, SAUDI ARABIA

1963 ١٣٨٣

In Partial Fulfillment of the
Requirements for the Degree of

MASTER OF SCIENCE

In

Petroleum Engineering

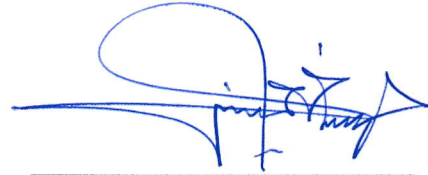
March 2016

KING FAHD UNIVERSITY OF PETROLEUM & MINERALS

DHAHRAN- 31261, SAUDI ARABIA

DEANSHIP OF GRADUATE STUDIES

This thesis, written by **SHAMS KALAM** under the direction of his thesis advisor and approved by his thesis committee, has been presented and accepted by the Dean of Graduate Studies, in partial fulfillment of the requirements for the degree of **MASTER OF SCIENCE IN PETROLEUM ENGINEERING**.



Dr. Sidqi A. Abu-Khamsin
(Advisor)



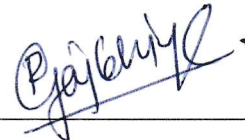
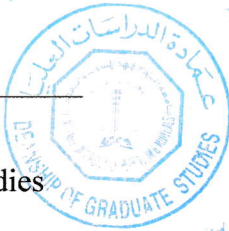
Dr. Abdullah S. Sultan
Department Chairman



Dr. Hasan Y. Al-Yousef
(Member)



Dr. Salam A. Zummo
Dean of Graduate Studies



Dr. Rahul N. Gajbhiye
(Member)

6/10/16

Date

© Shams Kalam

2016

Dedication

I dedicate my work to my parents, sisters and family who have been supporting and encouraging me in all my endeavors.

ACKNOWLEDGEMENTS

First of all I would like to thank Almighty Allah for His countless blessings to complete my research at KFUPM. I am also thankful to KFUPM for providing me scholarship and ground to gain knowledge and enhance my technical and soft skills. After that I would like to express my honest appreciation and sincere gratitude to my thesis advisor Dr. Sidqi Abu-Khamsin and my thesis committee members Dr. Hasan Al-Yousef and Dr. Rahul Gajbhiye for their continuous support throughout my research period. I especially acknowledge the constant support of Dr. Sidqi Abu-Khamsin and I am highly grateful to him for his precious time and commitment. His precious guidance and encouragement helped me grow confidence both academically and personally. I am also highly thankful to Dr. Hasan Al-Yousef. My research goals couldn't be achieved without his advices and guidance.

I would like to thank my parents, sisters and family for their strong support and encouragement throughout my stay at KFUPM.

Special thanks are due to the Department of Petroleum Engineering at King Fahd University of Petroleum & Minerals, including Faculty, Staff and Fellow Graduate Students who contributed directly or indirectly to the accomplishments of this work.

I am also thankful to Rizwan Ahmed Khan, Muzammil Hussain Rammay and M. Sarim Jamal for spending time with me on discussing and resolving issues related to my thesis work. At the end, I am so grateful to all my friends at KFUPM especially Usama Yousuf, Ahmed Mehboob, Mirza Talha Baig, Muzammil Shakeel, Abdul Qadeer, Waqas Ahmed

Khan, Zeeshan Tariq, Mohammad Danish Hashmat, M. Mansoor Alam, Arbab Latif, Ali
Khalid and Zaid Zaffar.

TABLE OF CONTENTS

ACKNOWLEDGEMENTS	iv
LIST OF TABLES	ix
LIST OF FIGURES	x
LIST OF ABBREVIATIONS	xxi
THESIS ABSTRACT (ENGLISH)	xxiii
THESIS ABSTRACT (ARABIC).....	xxv
CHAPTER 1 INTRODUCTION.....	1
1.1 Factors Affecting Flood Performance.....	2
1.1.1 Mobility Ratio.....	2
1.1.2 Reservoir Heterogeneity	5
1.2 Modeling Flood Performance	7
1.2.1 Areal Sweep Efficiency	7
1.2.2 Vertical Sweep Efficiency	7
1.2.3 Displacement Efficiency.....	8
CHAPTER 2 LITERATURE REVIEW.....	10
CHAPTER 3 PROBLEM STATEMENT.....	16
3.1 Knowledge Gap	16
3.2 Objectives	17
3.3 Research Methodology	17
CHAPTER 4 DEVELOPMENT OF THE SIMULATION MODEL AND THE INPUT DATA.....	19

4.1 Development of Simulation Model.....	19
4.1.1 Input Data Calculations.....	22
4.1.2 Simulation Model Description.....	30
4.2 Extraction of Simulated Data.....	39
4.2.1 Simulation Model Sensitivity Analysis	41
CHAPTER 5 SIMULATION RESULTS.....	49
5.1 Effect of Mobility Ratio.....	49
5.2 Effect of Reservoir Heterogeneity	51
5.3 Effect of Permeability Anisotropy Ratio	52
5.4 Effect of Wettability	55
CHAPTER 6 DEVELOPMENT AND TESTING OF THE MATHEMATICAL CORRELATION	61
6.1 Artificial Neural Networks	61
6.2 Correlation Development.....	64
6.2.1 Input Normalization.....	67
6.2.2 Output De-Normalization	68
6.3 Correlation Testing	72
6.3.1 Case 1: Wettability Indicator=0.8.....	73
6.3.2 Case 2: Wettability Indicator=1.51	75
6.3.3 Wettability Indicator Testing.....	77
6.4 Comparison with Field Data	79
6.4.1 Case 1: Field A.....	79
6.4.2 Case 2: Field B.....	82

6.5 Comparison with Craig-Geffen-Morse Method.....	85
CHAPTER 7	88
7.1 Conclusions.....	88
7.2 Recommendations for Future Work.....	89
REFERENCES.....	90
APPENDIX.....	92
VITAE.....	131

LIST OF TABLES

Table 4.1: Reservoir permeability data.....	23
Table 4.2: Cumulative frequency distribution table	23
Table 4.3: $k_{84.1}$ values.....	25
Table 4.4: Layered permeability values for each V	26
Table 4.5: Relative permeability curves construction.....	27
Table 4.6: Oil viscosities for different mobility ratios.....	29
Table 4.7: Simulation Model Characteristics.....	32
Table 4.8: Values of input variables	33
Table 4.9: Properties of randomly sorted simulation models	46
Table 6.1: Dependent and independent variables for the new correlation.....	63
Table 6.2: Statistical Description of the Input and Output Data Used for Training ...	68
Table 6.3: Weights and Bias Values for RF _M Artificial Neural Network Model	69
Table 6.4: Accuracy measurement of training and testing data.....	71
Table 6.5: Correlation testing parameters.....	72
Table 6.6: Correlation testing parameters (with several values of WI)	77
Table 6.7: Data for Field A	80
Table 6.8: Data for Field B	83

LIST OF FIGURES

Figure 1.1: Characterization of reservoir heterogeneity by permeability variation.....	6
Figure 3.1: Work flow for this study	18
Figure 4.1: Single five spot pattern unit.....	21
Figure 4.2: Quadrant of a five-spot pattern unit (shaded).....	21
Figure 4.3: Dykstra-Parsons coefficient of permeability variation plot	24
Figure 4.4: Dykstra-Parsons permeability variation plot at $V=0.1$ to 0.9	25
Figure 4.5: Relative permeability curves for all systems.....	27
Figure 4.6: Fractional flow curve for system 2 at mobility ratios 0.1 to 4	30
Figure 4.7: Top view, water front before breakthrough, system 2, $M=0.1$, $V=0.5$, $k_z/k_x=0.1$	34
Figure 4.8: Top view, water front before breakthrough, system 2, $M=2$, $V=0.5$, $k_z/k_x=0.1$	35
Figure 4.9: Top view, at breakthrough, system 2, $V=0.5$, $M=1$, $k_z/k_x=0.1$	36
Figure 4.10: Side view, at breakthrough, system 2, $V=0.5$, $M=1$, $k_z/k_x=0.1$	36
Figure 4.11: 3D view, at breakthrough, system 2, $V=0.5$, $M=1$, $k_z/k_x=0.1$	37
Figure 4.12: Top view, system 2, $V=0.5$, $M=1$, $k_z/k_x=0.1$, $f_w=70\%$	38
Figure 4.13: Side view, system 2, $V=0.5$, $M=1$, $k_z/k_x=0.1$, $f_w=70\%$	38
Figure 4.14: 3D view, system 2, $V=0.5$, $M=1$, $k_z/k_x=0.1$, $f_w=70\%$	39
Figure 4.15: Grid size optimization, system2, $M=1$, $V=0.7$, $f_w=95\%$, $k_z/k_x=0.1$	40
Figure 4.16: Time optimization, system2, $M=1$, $V=0.7$, $f_w=95\%$, $k_z/k_x=0.1$	41

Figure 4.17: Area sensitivity for system 2 with $V=0.5$, $M=0.5$, $k_z/k_x=0.1$	42
Figure 4.18: Area sensitivity for system 2 with $V=0.5$, $M=1$, $k_z/k_x=0.1$	43
Figure 4.19: Area sensitivity for system 2 with $V=0.5$, $M=4$, $k_z/k_x=0.1$	43
Figure 4.20: Thickness sensitivity for system 2 with $V=0.5$, $M=0.5$, $k_z/k_x=0.1$	44
Figure 4.21: Thickness sensitivity for system 2 with $V=0.5$, $M=1$, $k_z/k_x=0.1$	45
Figure 4.22: Thickness sensitivity for system 2 with $V=0.5$, $M=4$, $k_z/k_x=0.1$	45
Figure 4.23: Side View of simulation model with random sorting 01.....	46
Figure 4.24: Side View of simulation model with random sorting 02.....	47
Figure 4.25: Side View of simulation model with random sorting 03.....	47
Figure 4.26: Sensitivity of oil recovery to the layer permeability sorting for system=2, $V=0.6$, $M=1.5$, $k_z/k_x=0.15$, $f_w=0$ to 95%	48
Figure 5.1: Effect of mobility ratio on oil recovery factor at water breakthrough	50
Figure 5.2: Effect of mobility ratio on oil recovery factor beyond water breakthrough at $f_w=0.7$	50
Figure 5.3: Effect of permeability variation on oil recovery factor at water breakthrough	51
Figure 5.4: Effect of permeability variation on oil recovery factor beyond water breakthrough at $f_w=0.7$	52
Figure 5.5: Effect of crossflow on oil recovery at water breakthrough for $M=0.1$	53
Figure 5.6: Effect of crossflow on oil recovery at water breakthrough for $M=4$	54
Figure 5.7: Effect of crossflow on oil recovery beyond water breakthrough for $M=0.1$	54

Figure 5.8: Effect of crossflow on oil recovery beyond water breakthrough for M=4.....	55
Figure 5.9: Effect of wettability on oil recovery at water breakthrough with M=0.1, $k_z/k_x=0$	56
Figure 5.10: Effect of wettability on oil recovery efficiency at water breakthrough with M=4, $k_z/k_x=0.2$	57
Figure 5.11: Effect of wettability on movable oil recovery efficiency at water breakthrough with M=0.1, $k_z/k_x =0$	57
Figure 5.12: Effect of wettability indicator on movable oil recovery efficiency at water breakthrough with M=4, $k_z/k_x =0.2$	58
Figure 5.13: Effect of wettability indicator on oil recovery efficiency beyond water breakthrough at M=0.1, $k_z/k_x=0$	58
Figure 5.14: Effect of wettability indicator on oil recovery efficiency beyond water breakthrough at M=4, $k_z/k_x=0$	59
Figure 5.15: Effect of wettability indicator on movable oil recovery efficiency beyond water breakthrough at M=0.1, $k_z/k_x=0$	59
Figure 5.16: Effect of wettability indicator on movable oil recovery efficiency beyond water breakthrough at M=4, $k_z/k_x=0$	60
Figure 6.1: Topology of a Basic ANN network.....	63
Figure 6.2: Topology of RF _M prediction FFNN-based model	65
Figure 6.3: Scatter plot for training data.....	71
Figure 6.4: Scatter plot for testing data.....	72

Figure 6.5: Relative permeability curves for case 1	73
Figure 6.6: Fractional flow curve for case 1	74
Figure 6.7: Comparison between simulator and new correlation at several M	74
Figure 6.8: Relative permeability curves for case 2	75
Figure 6.9: Fractional flow curves for several M	76
Figure 6.10: Comparison between simulator and new correlation at several M	76
Figure 6.11: Relative permeability curves for 5 other systems	78
Figure 6.12: Fractional flow curves for 5 new systems	78
Figure 6.13: Scatter plot for WI testing between simulator vs. new correlation	79
Figure 6.14: Relative permeability curves for field A	81
Figure 6.15: Fractional flow curve for field A	81
Figure 6.16: Comparison of water flood performance of two different wells from Field A with the new correlation	82
Figure 6.17: Relative permeability curves for field B	84
Figure 6.18: Fractional flow curve for field B	84
Figure 6.19: Comparison of water flood performance of two different wells from Field B with the new correlation.....	85
Figure 6.20 Fractional flow curve for System 2 at M=1.062	86
Figure 6.21: Comparison of new correlation with the CGM Method.....	87
Figure A.1: Recovery factors at breakthrough without crossflow ($\alpha=0$) for system 1	92

Figure A.2: Recovery factors at breakthrough with crossflow ($\alpha=0.05$) for system 1	92
Figure A.3: Recovery factors at breakthrough with crossflow ($\alpha=0.1$) for system 1 ..	93
Figure A.4: Recovery factors at breakthrough with crossflow ($\alpha=0.2$) for system 1 ..	93
Figure A.5: Recovery factors at breakthrough with crossflow ($\alpha=0.3$) for system 1 ..	94
Figure A.6: Recovery factors after breakthrough ($f_w=0.3$) without crossflow ($\alpha=0$) for system 1	94
Figure A.7: Recovery factors after breakthrough ($f_w=0.3$) with crossflow ($\alpha=0.05$) for system 1	95
Figure A.8: Recovery factors after breakthrough ($f_w=0.3$) with crossflow ($\alpha=0.1$) for system 1	95
Figure A.9: Recovery factors after breakthrough ($f_w=0.3$) with crossflow ($\alpha=0.2$) for system 1	96
Figure A.10: Recovery factors after breakthrough ($f_w=0.3$) with crossflow ($\alpha=0.3$) for system 1	96
Figure A.11: Recovery factors after breakthrough ($f_w=0.5$) without crossflow ($\alpha=0$) for system 1	97
Figure A.12: Recovery factors after breakthrough ($f_w=0.5$) with crossflow ($\alpha=0.05$) for system 1	97
Figure A.13: Recovery factors after breakthrough ($f_w=0.5$) with crossflow ($\alpha=0.1$) for system 1	98

Figure A.14: Recovery factors after breakthrough ($f_w=0.5$) with crossflow ($\alpha=0.2$) for system 1	98
Figure A.15: Recovery factors after breakthrough ($f_w=0.5$) with crossflow ($\alpha=0.3$) for system 1	99
Figure A.16: Recovery factors after breakthrough ($f_w=0.7$) without crossflow ($\alpha=0$) for system 1	99
Figure A.17: Recovery factors after breakthrough ($f_w=0.7$) with crossflow ($\alpha=0.05$) for system 1	100
Figure A.18: Recovery factors after breakthrough ($f_w=0.7$) with crossflow ($\alpha=0.1$) for system 1	100
Figure A. 19: Recovery factors after breakthrough ($f_w=0.7$) with crossflow ($\alpha=0.2$) for system 1	101
Figure A.20: Recovery factors after breakthrough ($f_w=0.7$) with crossflow ($\alpha=0.3$) for system 1	101
Figure A.21: Recovery factors after breakthrough ($f_w =0.95$) without crossflow ($\alpha=0$) for system 1	102
Figure A.22: Recovery factors after breakthrough ($f_w=0.95$) with crossflow ($\alpha=0.05$) for system 1	102
Figure A.23: Recovery factors after breakthrough ($f_w=0.95$) with crossflow ($\alpha=0.1$) for system 1	103
Figure A.24: Recovery factors after breakthrough ($f_w=0.95$) with crossflow ($\alpha=0.2$) for system 1	103

Figure A.25: Recovery factors after breakthrough ($f_w=0.95$) with crossflow ($\alpha=0.3$) for system 1	104
Figure A.26: Recovery factors at breakthrough without crossflow ($\alpha=0$) for system 2	105
Figure A.27: Recovery factors at breakthrough with crossflow ($\alpha=0.05$) for system 2	105
Figure A.28: Recovery factors at breakthrough with crossflow ($\alpha=0.1$) for system 2	106
Figure A.29: Recovery factors at breakthrough with crossflow ($\alpha=0.2$) for system 2	106
Figure A.30: Recovery factors at breakthrough with crossflow ($\alpha=0.3$) for system 2	107
Figure A.31: Recovery factors after breakthrough ($f_w=0.3$) without crossflow ($\alpha=0$) for system 2.....	107
Figure A.32: Recovery factors after breakthrough ($f_w=0.3$) with crossflow ($\alpha=0.05$) for system 2.....	108
Figure A.33: Recovery factors after breakthrough ($f_w=0.3$) with crossflow ($\alpha=0.1$) for system 2.....	108
Figure A.34: Recovery factors after breakthrough ($f_w=0.3$) with crossflow ($\alpha=0.2$) for system 2.....	109
Figure A.35: Recovery factors after breakthrough ($f_w=0.3$) with crossflow ($\alpha=0.3$) for system 2.....	109

Figure A.36: Recovery factors after breakthrough ($f_w=0.5$) without crossflow ($\alpha=0$) for system 2.....	110
Figure A.37: Recovery factors after breakthrough ($f_w=0.5$) with crossflow ($\alpha=0.05$) for system 2.....	110
Figure A.38: Recovery factors after breakthrough ($f_w =0.5$) with crossflow ($\alpha=0.1$) for system 2.....	111
Figure A.39: Recovery factors after breakthrough ($f_w=0.5$) with crossflow ($\alpha=0.2$) for system 2.....	111
Figure A.40: Recovery factors after breakthrough ($f_w=0.5$) with crossflow ($\alpha=0.3$) for system 2.....	112
Figure A.41: Recovery factors after breakthrough ($f_w=0.7$) without crossflow ($\alpha=0$) for system 2.....	112
Figure A.42: Recovery factors after breakthrough ($f_w=0.7$) with crossflow ($\alpha=0.05$) for system 2.....	113
Figure A.43: Recovery factors after breakthrough ($f_w=0.7$) with crossflow ($\alpha=0.1$) for system 2.....	113
Figure A.44: Recovery factors after breakthrough ($f_w=0.7$) with crossflow ($\alpha=0.2$) for system 2.....	114
Figure A.45: Recovery factors after breakthrough ($f_w=0.7$) with crossflow ($\alpha=0.3$) for system 2.....	114
Figure A.46: Recovery factors after breakthrough ($f_w=0.95$) without crossflow ($\alpha=0$) for system 2.....	115

Figure A.47: Recovery factors after breakthrough ($f_w=0.95$) with crossflow ($\alpha=0.05$) for system 2.....	115
Figure A.48: Recovery factors after breakthrough ($f_w=0.95$) with crossflow ($\alpha=0.1$) for system 2.....	116
Figure A.49: Recovery factors after breakthrough ($f_w=0.95$) with crossflow ($\alpha=0.2$) for system 2.....	116
Figure A.50: Recovery factors after breakthrough ($f_w=0.95$) with crossflow ($\alpha=0.3$) for system 2.....	117
Figure A.51: Recovery factors at breakthrough without crossflow ($\alpha=0$) for system 3	118
Figure A.52 Recovery factors at breakthrough with crossflow ($\alpha=0.05$) for system 3	118
Figure A.53: Recovery factors at breakthrough with crossflow ($\alpha=0.1$) for system 3	119
Figure A.54: Recovery factors at breakthrough with crossflow ($\alpha=0.2$) for system 3	119
Figure A.55: Recovery factors at breakthrough with crossflow ($\alpha=0.3$) for system 3	120
Figure A.56: Recovery factors after breakthrough ($f_w=0.3$) without crossflow ($\alpha=0$) for system 3.....	120
Figure A.57: Recovery factors after breakthrough ($f_w=0.3$) with crossflow ($\alpha=0.05$) for system 3.....	121

Figure A.58: Recovery factors after breakthrough ($f_w=0.3$) with crossflow ($\alpha=0.1$) for system 3.....	121
Figure A.59: Recovery factors after breakthrough ($f_w=0.3$) with crossflow ($\alpha=0.2$) for system 3.....	122
Figure A.60: Recovery factors after breakthrough ($f_w=0.3$) with crossflow ($\alpha=0.3$) for system 3.....	122
Figure A.61: Recovery factors after breakthrough ($f_w=0.5$) without crossflow ($\alpha=0$) for system 3.....	123
Figure A.62: Recovery factors after breakthrough ($f_w=0.5$) with crossflow ($\alpha=0.05$) for system 3.....	123
Figure A.63: Recovery factors after breakthrough ($f_w=0.5$) with crossflow ($\alpha=0.1$) for system 3.....	124
Figure A.64: Recovery factors after breakthrough ($f_w=0.5$) with crossflow ($\alpha=0.2$) for system 3.....	124
Figure A.65: Recovery factors after breakthrough ($f_w=0.5$) with crossflow ($\alpha=0.3$) for system 3.....	125
Figure A.66: Recovery factors after breakthrough ($f_w=0.7$) without crossflow ($\alpha=0$) for system 3.....	125
Figure A.67: Recovery factors after breakthrough ($f_w=0.7$) with crossflow ($\alpha=0.05$) for system 3.....	126
Figure A.68: Recovery factors after breakthrough ($f_w=0.7$) with crossflow ($\alpha=0.1$) for system 3.....	126

Figure A.69: Recovery factors after breakthrough ($f_w=0.7$) with crossflow ($\alpha=0.2$) for system 3.....	127
Figure A.70: Recovery factors after breakthrough ($f_w=0.7$) with crossflow ($\alpha=0.3$) for system 3.....	127
Figure A.71: Recovery factors after breakthrough ($f_w=0.95$) without crossflow ($\alpha=0$) for system 3.....	128
Figure A.72: Recovery factors after breakthrough ($f_w=0.95$) with crossflow ($\alpha=0.05$) for system 3.....	128
Figure A.73: Recovery factors after breakthrough ($f_w=0.95$) with crossflow ($\alpha=0.1$) for system 3.....	129
Figure A.74: Recovery factors after breakthrough ($f_w=0.95$) with crossflow ($\alpha=0.2$) for system 3.....	129
Figure A.75: Recovery factors after breakthrough ($f_w=0.95$) with crossflow ($\alpha=0.3$) for system 3.....	130

LIST OF ABBREVIATIONS

List of Abbreviations are as follows

ANN	:	Artificial Neural Networks
α	:	Permeability Anisotropy Ratio
B_o	:	Oil formation volume factor, RB/STB
B_w	:	Water formation volume factor, RB/STB
E_R	:	Recovery efficiency
E_A	:	Areal sweep efficiency
E_v	:	Vertical sweep efficiency
E_D	:	Displacement efficiency
E_{VOL}	:	Volumetric Sweep Efficiency
FFNN	:	Feedforward Neural Network
f_w	:	Production Water Cut
k_z/k_x	:	Permeability Anisotropy Ratio
k_{50}	:	Mean permeability, mD
$k_{84.1}$:	Permeability at one standard deviation above mean value, mD
$(k_{rw})_{S_{or}}$:	Water relative permeability endpoint
$(k_{ro})_{S_{wi}}$:	Oil relative permeability endpoint

M	:	Mobility Ratio
M_{CGM}	:	CGM's Mobility Ratio
NMR	:	Nuclear Magnetic Resonance
N_F	:	Number of flooded cells
N_T	:	Total number of cells
n_w	:	Corey's oil exponents
n_o	:	Corey's water exponents
S_{wi}	:	Initial water saturation
$\overline{S_w}$:	Average water saturation
S_g	:	Gas saturation
$\overline{S_{wf}}$:	Average water saturation behind the flood front
S_{or}	:	Residual oil saturation
μ_o	:	Oil Viscosity. cP
μ_w	:	Water Viscosity. cP
V	:	Dykstra-Parsons Permeability Variation Coefficient
V_p	:	Pore volume of reservoir, cu-ft
WI	:	Wettability Indicator
WOR	:	Water Oil Ratio

ABSTRACT

Full Name : Shams Kalam

Thesis Title : An Empirical Correlation for Water Flooding Performance in a Layered Reservoir

Major Field : Petroleum Engineering

Date of Degree : March 2016

Water flooding is an oil recovery technique usually employed after the primary depletion phase of an oil reservoir's development. Several methods exist to predict the performance of a water flood but each is based on one or more simplifying assumptions. For heterogeneous reservoirs, commercial simulators can predict water-flooding performance fairly accurately but they are expensive and time consuming. Therefore, a need exists for a ready-to-use correlation that can produce a good and quick estimate.

In this study, a general empirical correlation is presented to estimate the movable oil recovery in both communicating and non-communicating stratified oil reservoirs undergoing five-spot water-flooding at and beyond water breakthrough. The new correlation was developed by the artificial neural networks technique utilizing thousands of data points from simulation runs covering a wide range of variables. The new correlation's input variables are the flood mobility ratio (M), the reservoir's Dykstra-Parsons coefficient of permeability variation (V) and permeability anisotropy ratio (k_z/k_x),

the producing water cut (f_w) and the wettability indicator (WI). WI is a new parameter introduced in this study as a simple measure of wettability and is based only on features of the relative permeability curves.

The new correlation matches all simulator results with high accuracy. It also matches the results of simulation runs that were not utilized in developing the new correlation. Furthermore, the new correlation predicts the performance of two different field projects with good accuracy.

ملخص الرسالة

الاسم الكامل : شمس كلام

عنوان الرسالة : علاقة تجريبية لأداء الغمر المائي في المكامن الطبقيّة

التخصص : هندسة النفط

تاريخ الدرجة العلمية : مارس 2016

الغمر المائي هو أحد تقنيات استخلاص الزيت وتستخدم عادة بعد مرحلة النضوب الأولي لتطوير المكمن النفطي. توجد عدة طرق للتنبؤ بأداء الغمر المائي، وتعتمد كل طريقة على افتراض تبسيطي أو أكثر. ويمكن التنبؤ بأداء الغمر المائي للمكامن غير المتجانسة عن طريق برامج المحاكاة التجارية بدقة جيدة لكنها تستهلك الكثير من الوقت وتكلفة مادية مرتفعة. نتيجة لذلك، هنالك حاجة لعلاقة رياضية تستطيع توفير تقدير جيد وسريع.

في هذه الدراسة، تم تقديم علاقة تجريبية عامة لتقدير كمية الزيت القابل للتحرك المستخلص من المكامن الزيتية ذات الطبقات المتصلة وغير المتصلة والتي تخضع للغمر المائي خماسي النقاط عند الإختراق المائي وما بعده. وتم انشاء العلاقة باستخدام تقنية الشبكات العصبية الصناعية بالاستفادة من آلاف النتائج من عمليات المحاكاة التي تغطي مدى واسع من المتغيرات. والمتغيرات التي تتطلبها العلاقة هي نسبة حركية الغمر، معامل دايكستر-بارسنز لتفاوت النفاذية ونسبة تباين النفاذية (النفاذية في الاتجاه الرأسي / النفاذية في الاتجاه الأفقي) للمكمن، نسبة الماء المنتج، ومؤشر التبلل. ومؤشر التبلل متغير جديد قدم في هذه الدراسة ويسئل من سمات لمنحنيات النفاذية النسبية.

تتطابق العلاقة مع نتائج المحاكاة بدقة عالية. كما تتطابق أيضا مع نتائج حالات المحاكاة التي لم تستخدم في انشاء العلاقة. بالإضافة إلى ذلك، فإن العلاقة الجديدة تتبأت بأداء مشروعين حقلين مختلفين بدقة جيدة.

CHAPTER 1

INTRODUCTION

Water flooding is an oil recovery technique usually employed after the primary depletion phase of an oil reservoir's development. In 1865, the very first water flood occurred in the Pithole City area of Pennsylvania, USA, as a result of an accidental water injection (API, Dallas, Tex., 1961). Now, it has become a standard practice since the middle of the 20th century, and it usually provides an additional 10 to 20 percent of oil recovery from the reservoir. Water was injected only in a single well to improve the oil recovery in the earliest routine of water flooding. In 1924, the first five-spot pattern flood was applied in the southern part of the Bradford field in Pennsylvania, USA (Fettke, C.R, 1938).

Water flooding involves injection of water in a well or pattern of wells to displace oil towards a producer. When the flood front's leading edge arrives at the producing well, water breakthrough takes place. After breakthrough, both oil and water are produced and the water cut increases continuously. A precise evaluation of the water flood performance plays an important role for better reservoir management, accurate decision making and the overall project economics.

1.1 Factors Affecting Flood Performance

1.1.1 Mobility Ratio

A key factor in the performance of a water flood is the flood's mobility ratio (M). It is a function of viscosity and fluid relative permeabilities, which depend on water saturation. The mobility ratio will be explained in detail later in this subsection.

The relative permeability to a fluid is the ratio of its effective permeability to some reference permeability, which is usually the effective permeability to oil at the irreducible water saturation $(k_{ro})_{S_{wi}}$. This makes the relative permeability to oil at S_{wi} always equal to 1.0. Corey's relative permeability functions (Molina, 1980) can be used to construct the relative permeability curves for given oil and water exponents known as Corey's exponents. Corey's exponent is approximately equal to 4.0 for the wetting phase and 2.0 for the non-wetting phase. Corey's type functions for relative permeability curves are of the form:

$$k_{rw} = (k_{rw})_{S_{or}} \left[\frac{S_w - S_{wi}}{1 - S_{wi} - S_{or}} \right]^{n_w} \quad 1.1a$$

$$k_{ro} = (k_{ro})_{S_{wi}} \left[\frac{1 - S_w - S_{or}}{1 - S_{wi} - S_{or}} \right]^{n_o} \quad 1.1b$$

Where $(k_{rw})_{S_{or}}$ and $(k_{ro})_{S_{wi}}$ are the water and oil relative permeability endpoints, respectively, and n_w and n_o are the water and oil Corey exponents, respectively. These correlations were used in this research work to generate relative permeability curves.

Among other things, the shape and magnitude of the relative permeability curves are influenced by the wettability of the reservoir rock, which can be assessed or quantified by a number of techniques such as the Contact Angle, Amott, NMR (Nuclear Magnetic Resonance) etc. Wettability of a reservoir strongly affects oil recovery efficiency in water-flooding projects. In a preferentially water-wet system, the oil recovery at breakthrough is high, while water breakthrough occurs earlier in preferentially oil-wet system. Water flooding is less efficient in oil-wet systems than water wet ones, since a large amount of water is required to recover more oil.

In this study, a new parameter - termed the wettability indicator (WI) - is introduced as a crude measure of wettability. WI is based only on features of the relative permeability curves, which are the crossover water saturation and relative permeability to water at residual oil saturation, as expressed in equation 1.1c.

$$WI = \frac{\text{Crossover Water Saturation } (S_{co})}{\text{Relative Permeability to Water at Residual Oil Saturation } (k_{rwe})} \quad 1.1c$$

The crossover water saturation is the water saturation at which the relative permeability curves of oil and water intersect each other. WI is less than 1 for oil-wet systems and greater than 1 for water-wet systems.

A flood mobility ratio is the mobility of the displacing phase to the mobility of the displaced phase. It can be estimated using water relative permeability evaluated at the maximum possible water saturation and the oil relative permeability measured at the initial water saturation.

$$M = \frac{\lambda_{\text{Displacing}}}{\lambda_{\text{Displaced}}} \quad 1.2a$$

$$M = \frac{(k_{rw})_{S_{or}} \mu_o}{(k_{ro})_{S_{wi}} \mu_w} \quad 1.2b$$

Where,

$\lambda_{\text{Displacing}}$ = mobility of the water (displacing phase)

$\lambda_{\text{Displaced}}$ = mobility of the oil (displaced phase)

$(k_{rw})_{S_{or}}$ = relative permeability to water at residual saturation of oil, fraction

$(k_{ro})_{S_{wi}}$ = relative permeability to oil at the initial saturation of water, fraction

μ_w = viscosity of water, cP

μ_o = viscosity of oil, cP

The above definition of mobility ratio is called endpoint mobility ratio. Another definition for M (Eq. 1.2c) considers k_{rw} and k_{ro} both at the average water saturation behind the front ($\overline{S_{wf}}$) instead of $(k_{rw})_{S_{or}}$. Namely, the mobility of the displacing phase incorporates the mobilities of both water and oil evaluated at $\overline{S_{wf}}$, while the displaced phase is oil at initial conditions. This definition better represents frontal displacement in the porous media and was employed in this study. CGM method defines the mobility ratio (M_{CGM}) in a similar way except that oil mobility is not considered in the displacing phase as shown in Equation 1.2d.

$$M = \frac{\left(\frac{k_{rw}}{\mu_w} + \frac{k_{ro}}{\mu_o} \right)_{S_{wf}}}{\left(\frac{k_{ro}}{\mu_o} \right)_{S_{wi}}} \quad 1.2c$$

$$M_{CGM} = \frac{\left(\frac{k_{rw}}{\mu_w} \right)_{S_{wf}}}{\left(\frac{k_{ro}}{\mu_o} \right)_{S_{wi}}} \quad 1.2d$$

1.1.2 Reservoir Heterogeneity

Reservoirs exist with various degrees of heterogeneity that stem from the reservoir's geological history. As a measure of reservoir heterogeneity, Dykstra and Parsons introduced the coefficient of permeability variation (V) (Dykstra and Parsons, 1950). Since permeability is created in the reservoir rock during the geological process, which is a natural process, it can be assumed that the rock permeability is log-normally distributed.

The coefficient V could be determined by the following procedure:

1. Order the permeability of the layers in decreasing values.
2. Determine for each value the percent of values with greater permeability and express each number as cumulative percentage, or "percent greater than".
3. Plot the data on log-probability scale, with permeability in the log scale and percent in the probability scale.
4. Draw the best fit line on this graph.

5. Find the mean value of permeability (k_{50}) and the value at one standard deviation above mean value ($k_{84.1}$).

6. Compute the Dykstra-Parsons coefficient V using the expression:

$$V = \frac{k_{50} - k_{84.1}}{k_{50}} \quad 1.3$$

Figure 1.1 shows a typical reservoir heterogeneity graph for several values of Dykstra-Parsons coefficients V . The larger the value of V the greater the degree of heterogeneity of the reservoir. For V equals to 0, the reservoir is considered to be completely homogenous and for V equals to 1.0, the reservoir is considered to be completely heterogeneous. Most reservoirs have Dykstra-Parsons coefficients between 0.5 and 0.9.

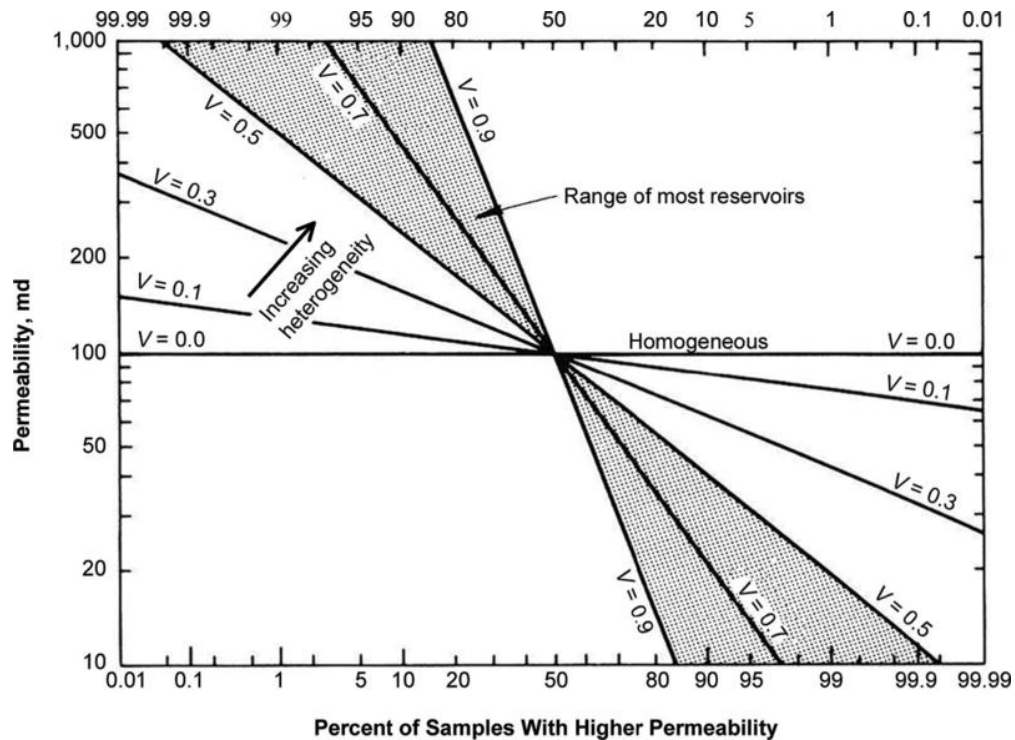


Figure 1.1: Characterization of reservoir heterogeneity by permeability variation

(from Waterflooding by G. Paul Willhite, SPE textbook series, v3, 1986)

The vertical to horizontal permeability ratio (k_z/k_x or α) is often used to quantify permeability anisotropy, which accounts for the amount of communication between the layers of a reservoir. α is an important influencing parameter of heterogeneous reservoirs in water flooding projects.

1.2 Modeling Flood Performance

The recovery factor (RF) is one of the key parameters that determines the economic feasibility of a water-flood project. RF is the ratio of the amount of oil produced by the project to the initial oil in place before water flooding. It can be estimated by the product of the areal, vertical and displacement sweep efficiencies, which are defined below.

1.2.1 Areal Sweep Efficiency

The areal sweep efficiency (E_A) is defined as the fractional reservoir area contacted by water. E_A depends on the injection pattern, total volume of injected fluid, mobility ratio (M), and areal heterogeneity (including directional and permeability fractures). Published correlations to estimate areal sweep efficiency are available at several mobility ratios (CGM, 1955).

1.2.2 Vertical Sweep Efficiency

Vertical sweep efficiency (E_v) is the fraction of the vertical section of the reservoir contacted by water. It is strongly influenced by the reservoir's vertical heterogeneity, total

volume of injected fluid, fluid mobilities and gravity segregation. Experimental correlations are available to evaluate E_v for different mobility ratio values (Dykstra and Parsons, 1950). The product of areal and vertical sweep efficiencies is known as volumetric sweep efficiency or conformance.

1.2.3 Displacement Efficiency

The displacement efficiency (E_D) is the fraction of oil that has been displaced out of the flooded zone by the flood water. It depends mainly on the rock's relative permeability characteristics and on the fluid viscosities. It can be estimated by:

$$E_D = \frac{\overline{S_w} - S_{wi} - S_g}{1 - S_{wi} - S_g} \quad 1.4$$

Where,

S_{wi} = initial water saturation in the flooded volume of the reservoir, fraction

$\overline{S_w}$ = average water saturation in the flooded volume of the reservoir, fraction

S_g = gas saturation in the flooded volume of the reservoir, fraction

Therefore, the recovery factor (RF) is estimated by Eq. 1.5a:

$$RF = E_A \cdot E_V \cdot E_D \quad 1.5a$$

Since a fraction of the oil cannot be recovered by ordinary means, the movable oil recovery efficiency (RF_M) is more pertinent in water-flood recovery performance than RF and, under ideal conditions, RF_M can approach 100%. It is defined mathematically as:

$$RF_M = \frac{N_P}{V_P(1 - S_{wi} - S_{or}) / B_o} \quad 1.5b$$

Where,

N_P = Cumulative oil produced, STB

V_P = Reservoir pore volume, RB

B_o = Oil formation volume factor, RB/STB

S_{wi} = Initial water saturation, dimensionless

S_{or} = Residual oil saturation, dimensionless

RF_M = Movable recovery factor, dimensionless

With the inception of water flooding a plethora of research studies have come to the limelight. Each focusing on the phenomena of oil displacement by water in a porous medium and factors influencing its sweep efficiencies. The past few decades are a testament to the efforts of modeling and forecasting this phenomena. A number of different models and correlations were brought forward by different researchers. Some dealt with the estimation of volumetric sweep efficiency while others focused on areal and vertical sweep efficiency prediction. All these efficiencies are important input parameters in determining recovery efficiency.

For this study an extensive literature review was conducted to study the methods developed to estimate various efficiencies used to predict water flood performance. A review of previous research works carried out on the subject is presented and discussed briefly in the following chapter.

CHAPTER 2

LITERATURE REVIEW

An extensive literature review of past research works on water flooding performance prediction is presented briefly in the following paragraphs.

Dykstra and Parsons developed an empirical correlation for a non-communicating stratified reservoir (Dykstra and Parsons, 1950). The results of the series of water flooding tests in the laboratory were correlated which shows that the oil recovery is a function of mobility ratio, permeability variation and water oil ratio. The assumptions of Dykstra-Parsons method include: immiscible displacement, linear flow, piston-like displacement, no cross-flow between layers, negligible gravity effects and horizontal layers.

The Craig-Geffen-Morse prediction method (CGM) was introduced to estimate water-flood performance (Craig et al., 1955). It is based on the Buckley-Leverett theory that is concerned with displacement mechanisms and considers oil displacement by water in either a linear or a radial system. The method estimates oil recovery with the required volume of water injected for that recovery in a water flooding system as a function of time. The method was based on experimental work in which X-ray shadowgraphs permitted observation of the gross fluid movement within the models.

In the paper by Johnson (Johnson, 1956), the correlation between V , mobility ratio, initial water saturation and fractional oil recovery corresponding to a given producing water-oil

ratio were shown on a single graph. This was done by plotting V with mobility ratio to illustrate lines of constant $R(1 - S_w.WOR^{-0.2})$.

A method was developed by Martin et al. (Martin et al., 1960) that allows the evaluation of water-flood oil recovery from depleted stratified reservoirs. The new method is especially useful for evaluating the optimum formation pressure at which to start a flood in order to produce the greatest total yield of primary and secondary oil. This method modified the Dykstra-Parsons equation to allow for liquid resaturation of the free gas space in each individual layer. Other modifications allow for layer-to-layer variations of porosity and initial and final saturations, but the effects of these latter modifications are not believed to be large enough to justify their use in water-flood prediction.

The objective of the study by Guerrero et al. (Guerrero et al., 1961) was to analyze and compare different methods used to estimate water-flood reserves and performance. All assumptions involved in each method are presented and discussed in the paper. Reserves and performance predictions by each method on two water floods are shown and compared with actual histories. The results show that none of the methods gave completely satisfactory performance predictions for both floods.

In 1966 a numerical study (Craig et al., 1966) for water-flood performance in a stratified system with crossflow was carried out. In this study, the performance of water flooding a water-wet layered system with crossflow was calculated using finite difference method. The effects of different parameters on the oil displacement efficiency, water saturation and crossflow rates were estimated without gravitational affect. Also, it was found that Crossflow because of viscous and capillary forces have major effect on oil recovery.

A mathematical model was developed by McGuire (McGuire, 1968) in which the original assumptions of Dykstra and Parsons were made with two exceptions. First, the difference in the two fluids was one of the viscosities only i.e. there were no relative permeability effects. Second, crossflow between strata was allowed. The mathematical model developed here is capable of predicting breakthrough efficiency in a stratified system with a degree of accuracy comparable with laboratory investigations. Also, it was concluded that Crossflow promotes dissipation of the front.

The research work by Warner (Warner, 1968) focused on a layered Burbank sand water-flooding project in Osage County, Oklahoma, USA. Stiles and Dykstra-Parsons methods were compared with the predicted real performance. The performance of this project showed that when reservoir or economic conditions prevent the use of mechanical and chemical means of mobility control, the highly stratified reservoirs can be successfully and economically water-flooded.

A paper by Craig (Craig, 1970) describes the reservoir description effect on water flooding performance forecast. It was found that in the 5-spot water-flooding pattern, the effect of mobility ratio on breakthrough volumetric sweep efficiency is higher in the range of 0.1 to 10. It is also noted that at any range of permeability variation and mobility ratio, volumetric sweep efficiency at breakthrough reduces with a larger number of layers.

Predicted WOR-recovery performance using the standard Dykstra-Parsons method, the modified Dykstra-Parsons and the numerical model for different layered systems were studied by Mobarak and Salem (Mobarak and Salem, 1975). Results showed good agreement between the performance predicted by the modified Dykstra-Parsons method

and the numerical model. Over a wide range of WOR, the difference between recovered oil as a fraction of oil in place does not exceed 5 percent. On the other hand, the standard Dykstra-Parsons method shows low oil recoveries over the whole range of WOR.

The work of Osman (Osman, 1981) presented a study of fluid flow in heterogeneous porous media. The major part related to a modification to the Dykstra-Parsons method to predict water-flooding performance of multi-layered composite reservoirs. The alteration considers the change in reservoir properties and dimensions both vertically and horizontally. Both Constant Injection Rate (CIR) and Constant Injection Pressure drop (CIP) were noticed. It was concluded that water-flooding performance in stratified composite linear reservoirs is controlled by the mobility ratio.

A Study of Dykstra-Parsons curves was carried out in 1981 (deSouza and Brigham, 1981). This work carries Dykstra-Parsons study further, which involves the coverage calculation for different permeability variations. Mobility ratio and WOR are considered as fixed parameters in this research. The notion was to combine the curves found in their research into a single curve so that wide range of parameters can be considered, which are useful in reservoir displacements. Vertical sweep efficiency curves were successfully grouped into a single curve.

The log-normal permeability distribution has often been used to describe the permeability distribution of stratified, heterogeneous reservoirs. With this distribution, an expression can be derived for fraction of flow capacity versus fraction of thickness, pseudo-relative permeability. Another expression relates vertical sweep efficiency versus water oil ratio,

sweep efficiency of a finite surfactant slug with adsorption, and layer permeabilities in a layered reservoir model (Hirasaki, 1984).

In the paper by El-Khatib (El-Khatib, 1985), a mathematical correlation was developed for water flooding performance in linear stratified systems with and without crossflows. The model forecasts the fractional oil recovery, water cut, total volume injected, and change in injection rate at the water breakthrough in the successive layers. It was found that crossflow between layers improves the oil recovery for systems with mobility ratios less than 1 and retards oil recovery for systems with mobility ratios greater than 1.

Fassihi (Fassihi, 1986) introduced two new statistical correlations for vertical sweep efficiency (E_v) and areal sweep efficiency (E_A), which were obtained by applying non-linear regression technique on a data set given by Dyes, Caudle and Erickson. Use of these correlations can help the water-flood performance estimations for mobility ratios from 0 to 10.

Tiab (Tiab, 1986) introduced a modification to the Dykstra-Parsons method for layered composite reservoirs. In this correlation, the layers were assumed to consist of numerous blocks with several different transmissibility (kh/μ) and storage ($\phi C_t h$). It was concluded that water-flooding performance in layered-composite reservoirs is basically controlled by mobility ratio.

Pande et al. (Pande et al., 1987) studied the inclusion of frontal advance theory in water flooding process. Outcomes show that this theory can be applied to flow in heterogeneous systems for processes that show linear behavior. In such a case, a particular saturation moves at a constant velocity through the porous medium. Performance of displacement for

2-D, Dykstra-Parsons model is correctly replicated using 1-D, frontal advance theory for displacements having unit mobility ratio.

El-Khatib (El-Khatib, 1999) published an analytical model for water flooding performance of stratified reservoirs with crossflow. The water flooding performance is shown in terms of vertical coverage as a function of the producing water-oil ratio. Expressions were also derived for pseudorelative permeability functions, dimensionless time and fractional flow curves. A procedure and empirical correlations were developed to estimate oil recovery factor at several water oil ratios.

In 2009, Espinel et al. (Espinel et al., 2009) studied straight-line zone of the semi-log plot between water-oil ratio and recovery factor. Results were correlated in terms of the Dykstra-Parsons coefficient and mobility ratio. They used end point mobility ratio concept which considers relative permeability to water at the maximum water saturation resulting in optimistic results.

In 2012, El-Khatib (El-Khatib, 2012) also developed a correlation for the prediction of water-flooding performance in layered, inclined reservoirs. The gravitational effect is shown in the fractional flow formula by a dimensionless gravity number. This gravity number incorporates the dip angle from the horizontal and the difference in densities of oil and water. Dimensionless time, fractional oil recovery, injectivity ratio and water cut at times of water breakthrough can be estimated by this model in the successive layers. The outcomes were compared with the performance of reservoirs having dip with crossflow. For favorable and unit mobility ratios, the effect of crossflow between layers was found to advance fractional oil recovery and vice versa.

CHAPTER 3

PROBLEM STATEMENT

3.1 Knowledge Gap

During the last 65 years, several attempts have been made to forecast water-flood performance and ultimate oil recovery by modeling the sweeping process of water displacing oil through the porous medium. Water flood performance is mostly affected by reservoir heterogeneity and permeability anisotropy ratio, rock wettability and the flood mobility ratio. Those methods are either analytical or empirical, and are based upon several assumptions that many times are either ignored or violated.

Numerical simulation is one of the most powerful tools used in the oil and gas industry for guiding reservoir management decisions. Reservoir simulators allow engineers to forecast and visualize reservoir performance efficiently. But simulation is a costly and time consuming process. Empirical correlations are useful in providing quick answers with reasonable accuracy and, in some instances, are as accurate as reservoir simulation.

For heterogeneous reservoirs, the Dykstra-Parsons correlation and all its subsequent modifications and expansions does not consider pattern flooding and assumes piston like displacement with no cross-flow between the layers. Therefore, there is a need to develop a correlation to predict oil recovery in pattern water flooding projects in communicating and non-communicating stratified reservoirs for a wide range of rock wettability.

3.2 Objectives

The objective of this study was to develop a correlation to predict the movable oil recovery for a 5-spot pattern flood that captures the effect of the following parameters/scenarios:

- Reservoir heterogeneity
- A wide range of mobility ratio
- With and without crossflow between layers of a reservoir
- Rock wettability
- At and beyond water breakthrough

The new correlation allows the estimation of recoverable oil for any possible combination of mobility ratio (M), permeability variation (V), permeability anisotropy ratio (k_z/k_x), rock wettability and water cut (f_w).

3.3 RESEARCH METHODOLOGY

To develop the new empirical correlation, water-flood performance was obtained by numerical simulation employing ECLIPSE commercial simulator. The simulated results were then processed by the artificial neural networks technique.

The ranges of the parameters varied in the simulation runs were:

- mobility ratio (M): 0.1 - 4
- permeability variation (V): 0.1 – 0.9
- Vertical-horizontal permeability ratio (k_z/k_x): 0 – 0.3

- Wettability Indicator (WI): 0.5 - 3
- Producing water cut (f_w): 0 to 95%

The mobility ratio was varied by changing the oil viscosity while the wettability indicator was varied by changing the shape of the relative permeability curves.

The roadmap of this study is summarized in the following flowchart:

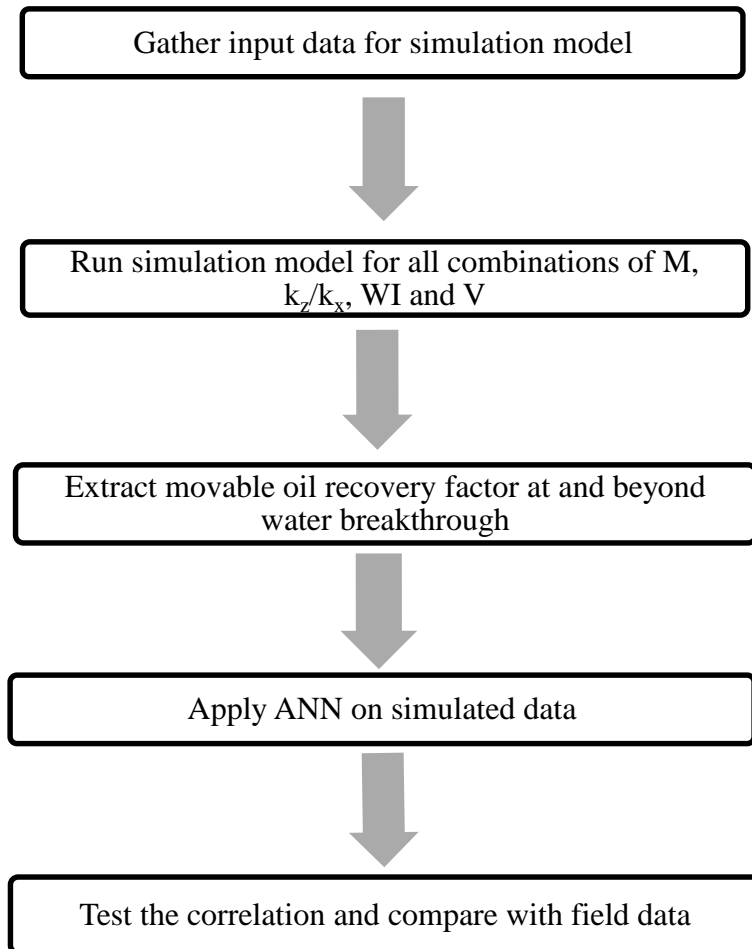


Figure 3.1: Work flow for this study

CHAPTER 4

DEVELOPMENT OF THE SIMULATION MODEL AND THE INPUT DATA

In order to make the proposed correlation, a simulation model was prepared to generate the recovery data. This chapter details all the work conducted to develop the simulation model. Extraction of the recovery data is presented later.

4.1 Development of Simulation Model

ECLIPSE 100 simulator was used to build the simulation model. ECLIPSE 100 is a 3D, multi-phase, fully-implicit, black oil simulator used for general purposes. It can simulate 1, 2 or 3 phase systems with variety of grid geometry.

The ECLIPSE 100 input data file consists of eight main sections (five compulsory and three optional). These are described briefly below:

RUNSPEC: General model characteristics (Title, model dimensions, phases, etc.)

GRID: Grid geometry and basic rock properties (Cell size, reservoir depth, porosity, absolute permeability of each layer etc.

EDIT: Modification of processed GRID data (optional section)

PROPS: PVT and SCAL properties (Properties tables of reservoir rock and fluids as functions of fluid pressures, and saturations (density, compressibility, viscosity, relative permeability, etc.))

REGIONS: Subdivision of reservoir into regions for calculation of saturation properties, PVT Properties etc. (optional section)

SOLUTION: Initialization (Specification of initial conditions in reservoir by either using specified fluid contact depths or reading from a restart file)

SUMMARY: Request output like FOPT, WWCT, FOE etc. (optional section)

SCHEDULE: Specification of operations to be simulated (production and injection controls and constraints), and output reports time-steps are required. Tuning of simulation can also be specified.

The simulation case in this study was a 3D, 2-phase (oil and water), 5-spot pattern water flooding. A general five-spot pattern comprises of a production well surrounded by four injection wells. In this simulation work, a quadrant of the five spot simulation model was used to estimate the water flooding performance. It decreased the total number of cells by one-fourth, which saved significant simulation time. The schematic of a five spot unit and a quadrant of the five spot pattern flooding are shown in Figures 4.1 and 4.2 respectively.

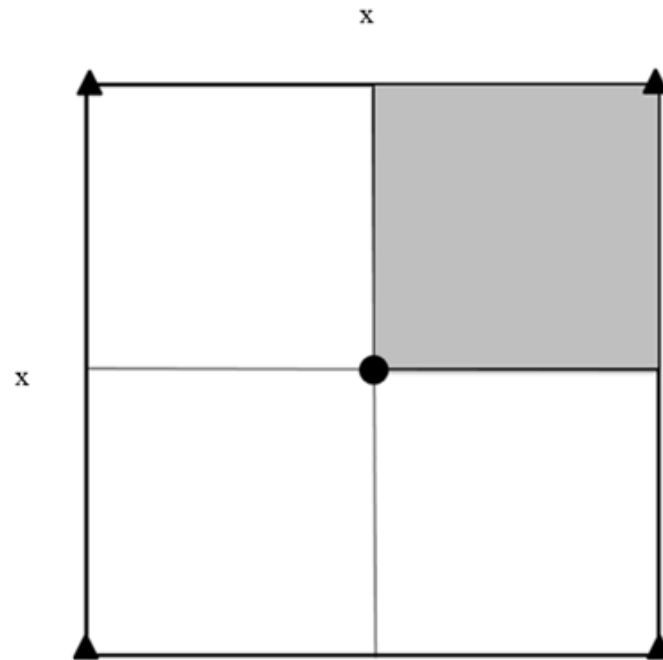


Figure 4.1: Single five spot pattern unit

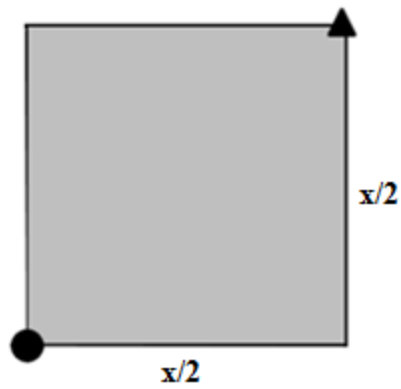


Figure 4.2: Quadrant of a five-spot pattern unit (shaded)

Assumptions and limitations of this simulation model were:

- Confined $\frac{1}{4}$ of a 5-spot pattern unit
- A heterogeneous, layered reservoir with log-normally distributed absolute permeability
- Uniform permeability in each layer

- All layers are of equal thickness
- Both crossflow and no crossflow cases were analyzed
- Relative permeabilities and fluid properties were the same for all layers
- Constant injection and production volumetric rates
- Negligible capillary pressure effects
- All layers are of equal porosity
- Liquid-filled reservoir (no initial gas saturation at all times)

4.1.1 Input Data Calculations

Gathering of input data for the simulation model required the following three main steps:

1. Reservoir heterogeneity calculation
2. Relative permeability curves construction
3. Oil viscosity calculation

4.1.1.1 Reservoir Heterogeneity Calculation

The reservoir heterogeneity was created by using Dykstra-Parsons method described in Chapter 1. Several permeability distributions, each corresponding to a selected value of the Dykstra-Parsons permeability variation coefficient (V), were used in the simulation model. To establish those permeability distributions, an arbitrary distribution is first created as shown in Table 4.1. The permeabilities are then arranged in decreasing order and the cumulative frequency distribution is calculated as shown in Table 4.2.

Table 4.1: Reservoir permeability data

Permeability, mD	Thickness, ft
2	1
40	2
45	2
120	2
80	2
145	2
110	2
74	2
48	2
5	1

Table 4.2: Cumulative frequency distribution table

Permeability (k), mD	Thickness (h), ft.	h with greater 'k'	Cumulative frequency distribution (% of h with greater k)
145	2	0	0
120	2	2	11.11
110	2	4	22.22
80	2	6	33.33
74	2	8	44.44
48	2	10	55.56
45	2	12	66.67
40	2	14	77.78
5	1	16	88.89
2	1	17	94.44
	Total = 18 ft.		

Using log-probability graph with permeability in the log scale and percent cumulative frequency in the probability scale, the best fit line was drawn to find k_{50} , which turns out to be 58 mD as illustrated in Figure 4.3. With k_{50} equals to 58 mD, $k_{84.1}$ for any value of V

was estimated with Eq. 4.1 as shown in Table 4.3. Now for each V, a graph was plotted on log-probability scale (Figure 4.4) and the permeability for each layer was calculated at the mid-point of the frequency distribution as shown in Table 4.4.

$$V = \frac{k_{50} - k_{84.1}}{k_{50}} \tag{1.3}$$

Equation 1.3 was rearranged to find $k_{84.1}$;

$$k_{84.1} = k_{50}(1 - V) \tag{4.1}$$

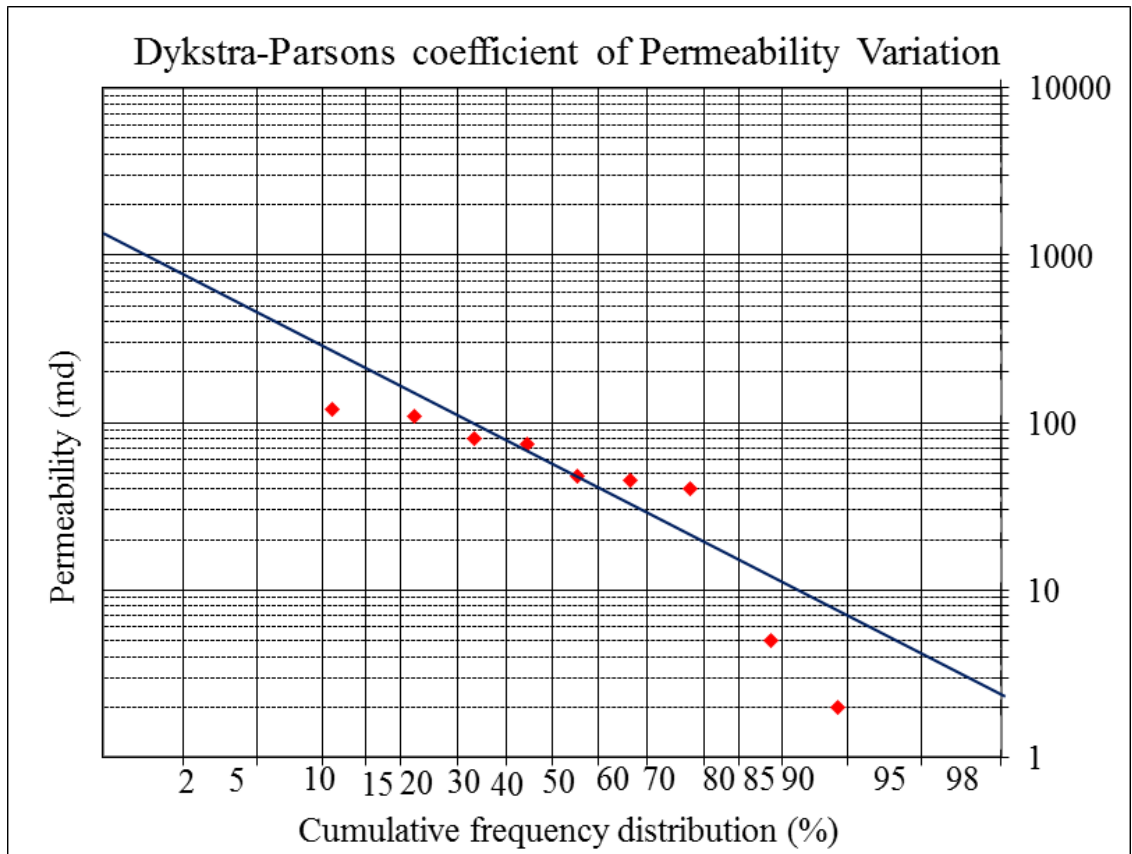


Figure 4.3: Dykstra-Parsons coefficient of permeability variation plot

Table 4.3: $k_{84.1}$ values

V	$k_{84.1}$, mD
0.1	52.2
0.3	40.6
0.5	29.0
0.7	17.4
0.9	5.8

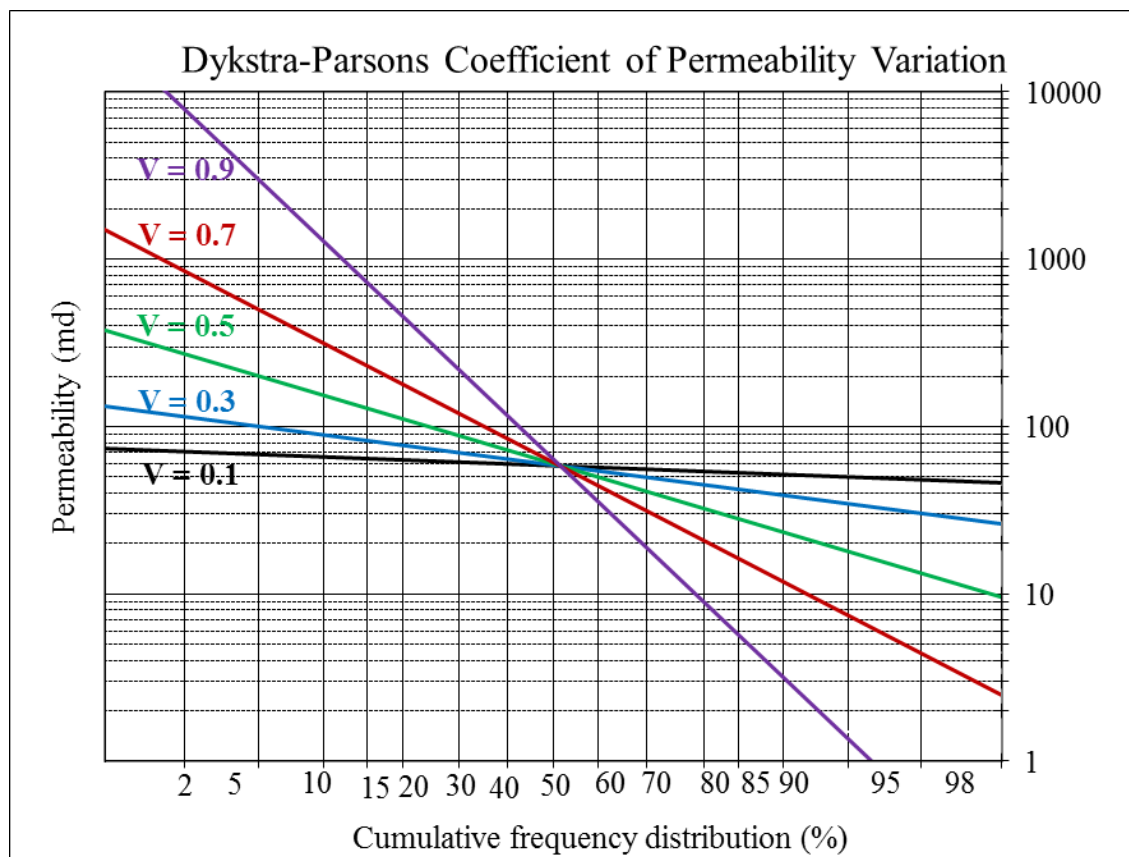


Figure 4.4: Dykstra-Parsons permeability variation plot at $V=0.1$ to 0.9

Table 4.4: Layered permeability values for each V

Layer	Mid-Point of Frequency Distribution (%)	Horizontal Permeability (mD)				
		V = 0.1	V = 0.3	V = 0.5	V = 0.7	V = 0.9
1	5	69	102	202	510	3200
2	15	65	85	140	250	750
3	25	62	72	100	160	310
4	35	61	67	80	100	170
5	45	60	61	65	75	90
6	55	60	58	57	53	50
7	65	58	52	45	38	25
8	75	58	48	36	26	14
9	85	55	43	28	16	5
10	95	51	36	18	7.5	1.5

4.1.1.2 Relative Permeability Curves Construction

Three different systems were constructed with a wide range of wettability indicator. These systems represent a strongly oil-wet reservoir, a neutral wettability reservoir and a strongly water-wet reservoir. Relative permeability curves for those systems, shown in Figure 4.5 were established using Corey's correlation described in Chapter 1. Table 4.5 lists their Corey's parameters.

Table 4.5: Relative permeability curves construction

	S_{wi}	S_{or}	k_{rwe}	k_{roe}	n_o	n_w	S_{co}	WI	Wettability
System 1	0.1	0.4	0.74	1	2	2	0.37	0.5	Oil wet
System 2	0.22	0.2	0.5	1	2	2	0.56	1.12	Neutral
System 3	0.4	0.25	0.215	1	2	2.5	0.645	3	Water wet

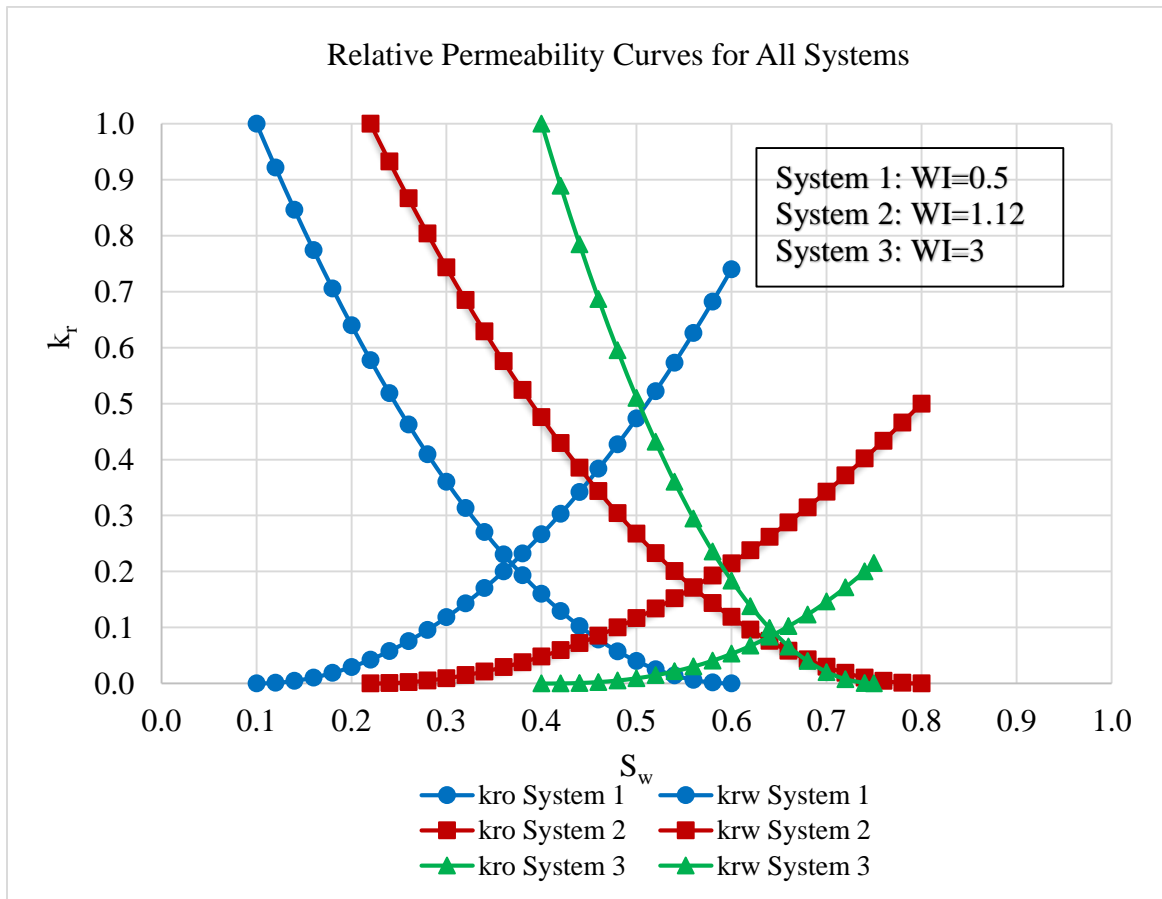


Figure 4.5: Relative permeability curves for all systems

4.1.1.3 Oil Viscosity Calculations

The mobility ratio (M) for the simulation model ranges between 0.1 and 4. Since the water viscosity was fixed at 1 cP, the oil viscosity corresponding to each mobility ratio was to be determined. However, in order to avoid convergence problems with the mobility ratio of 4 due to very high pressure levels, the water viscosity was reduced to 0.25 cP.

Since frontal displacement is assumed in the simulation model, the mobility ratio would depend on the fluid viscosities through the fractional-flow curve. Therefore, to arrive at the correct oil viscosity for a given mobility ratio, the following procedure was followed:

- 1- A value of oil viscosity was assumed.
- 2- The fractional flow curve was constructed (Eq. 4.2) using the relative permeability curves of the studied system and a water viscosity of 1 cP.

$$f_w = \frac{1}{1 + \left(\frac{k_{ro}}{k_{rw}} \right) \left(\frac{\mu_w}{\mu_o} \right)} \quad 4.2$$

- 3- The average water saturation behind the flood front ($\overline{S_{wf}}$) was found from the fractional flow curve.
- 4- Relative permeabilities to water and oil were calculated using Corey's correlations 1 and 2, respectively, at $\overline{S_{wf}}$.
- 5- Along with the assumed value of μ_o , the values of k_{ro} and k_{rw} obtained in step 4 were then plugged in Equation 1.2c to obtain the mobility ratio.

6- Steps 2 to 5 were repeated with different values of oil viscosity until the desired mobility ratio was obtained.

Using the above iterative procedure, oil viscosities corresponding to mobility ratios 0.1, 0.2, 0.5, 1, 2, and 4 for the three systems were determined as shown in Table 4.6. Figure 4.6 shows fractional flow curves for system 2 at different mobility ratios.

Table 4.6: Oil viscosities for different mobility ratios

	M	\bar{S}_w	$(k_{rw})_{\bar{S}_w}$	$(k_{ro})_{\bar{S}_w}$	μ_w , cP	μ_o , cP
System 1	0.1	0.5876	0.7037	0.0006	1	0.141
	0.2	0.5753	0.6688	0.0024	1	0.295
	0.5	0.5393	0.5712	0.0147	1	0.85
	1	0.4815	0.4308	0.0562	1	2.2
	2	0.3752	0.2242	0.2021	1	8.02
	4	0.1858	0.0218	0.6862	0.25	38
System 2	0.1	0.782	0.4694	0.001	1	0.22
	0.2	0.77	0.4496	0.0027	1	0.45
	0.5	0.73	0.3866	0.0146	1	1.25
	1	0.665	0.2943	0.0542	1	3.20
	2	0.54	0.1522	0.201	1	11.84
	4	0.782	0.4694	0.001	0.25	56.3
System 3	0.1	0.7414	0.2021	0.0006	1	0.49
	0.2	0.7331	0.19	0.0023	1	1.04
	0.5	0.7095	0.1582	0.0134	1	3.08
	1	0.6739	0.1165	0.0473	1	8.18
	2	0.6112	0.0608	0.1572	1	30.3
	4	0.5058	0.0108	0.4868	0.25	81.3

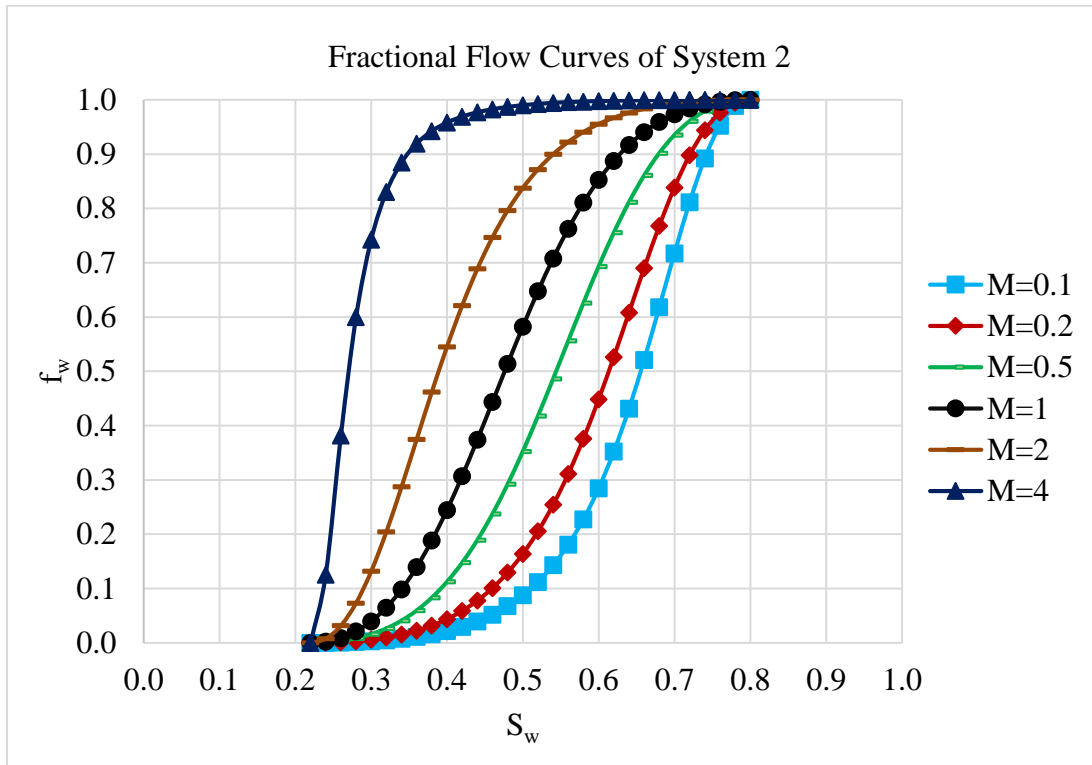


Figure 4.6: Fractional flow curve for system 2 at mobility ratios 0.1 to 4

4.1.2 Simulation Model Description

The simulation model in this study assumes a reservoir 2400 ft x 2400 ft (132.23 acres) with 250 ft total thickness. The model has grid dimensions of 80x80x10 and 64000 grid cells. The length of each cell was 30 ft in the x and y directions and 25 ft in the z direction. The reservoir was divided into 10 layers of equal thickness with different permeabilities in descending order. It was a quadrant of a 5-spot pattern water flooding model with one producer and one injector, completed in all 10 layers. Production and injection rates were kept constant. The water-flood strategy was pressure maintenance and the production

control method was reservoir voidage. The fully implicit solution method was used. Cross flow between the layers was allowed by taking non-zero anisotropy ratio, k_z/k_x . Zero anisotropy ratio signifies non-communicating layers. The description of the simulation model is summarized in Table 4.7.

Water-flood performance calculations at and after water breakthrough were computed for all possible combinations of the input variables whose values are listed in Table 4.8. The simulation model was run up to a maximum possible water cut of 95%. A total of 5000 simulated output points were obtained at different water cuts.

Table 4.7: Simulation Model Characteristics

Property/Parameter	Value/Description
Model Structure	
Flooding Pattern	5-spot
Grid dimensions, number (x,y,z)	80, 80, 10
Total number of cells	64000
Grid's size (D_x , D_y , D_z), ft	30, 30, 25
Acres, acres	132.23
Layers	10
Thickness of reservoir, ft	250
Depth, ft	8000
Water oil contact	8500
Reservoir pressure, psi	4500
Rock and Fluid Properties	
Phases	Oil and water
Water Density, lb/ft ³	63
Oil Density, lb/ft ³	63
Density ratio	1
API gravity	10
Water viscosity, μ_w , cP	0.25 and 1
Oil viscosity, μ_o , cP	Variable
Relative permeability curves	Using Corey's correlation
Medium	Variable
Porosity, fraction	0.15
Permeability variation coefficient, V	Variable

Anisotropy ratio, k_z/k_x	Variable
Simulation background	
Solution method	Fully implicit
Simulation technique	Finite difference
Operations Specification (Controls and Constraints)	
Number of producer(s)	1
Number of injector(s)	1
Production rate, stb/day	7500
Injection rate, stb/day	7500
Producer completions	80, 80, 1-10 (all layers)
Injector completions	1, 1, 1-10 (all layers)
Waterflood strategy	Pressure maintenance
Production control methods	Reservoir voidage (RESV)

Table 4.8: Values of input variables

Variable	Values
Permeability variation, V	0.1, 0.3, 0.5, 0.7, 0.9
Mobility ratio, M	0.1, 0.2, 0.5, 1, 2, 4
Anisotropy ratio, k_z/k_x	0, 0.05, 0.1, 0.2, 0.3
Wettability Indicator, WI	0.5, 1.12, 3

Examples of simulation output are shown below as follows:

- Figures 4.7 and 4.8 show water flood front before breakthrough for system 2 with two different mobility ratios.

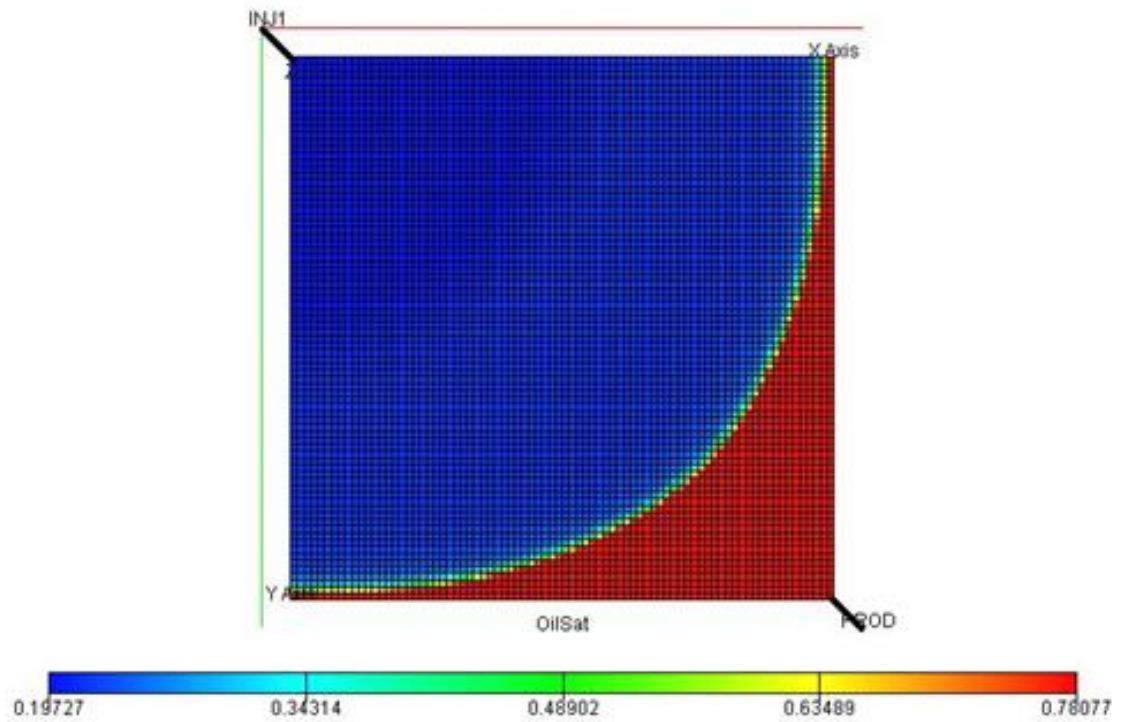


Figure 4.7: Top view, water front before breakthrough, system 2, $M=0.1$, $V=0.5$,

$$k_z/k_x=0.1$$

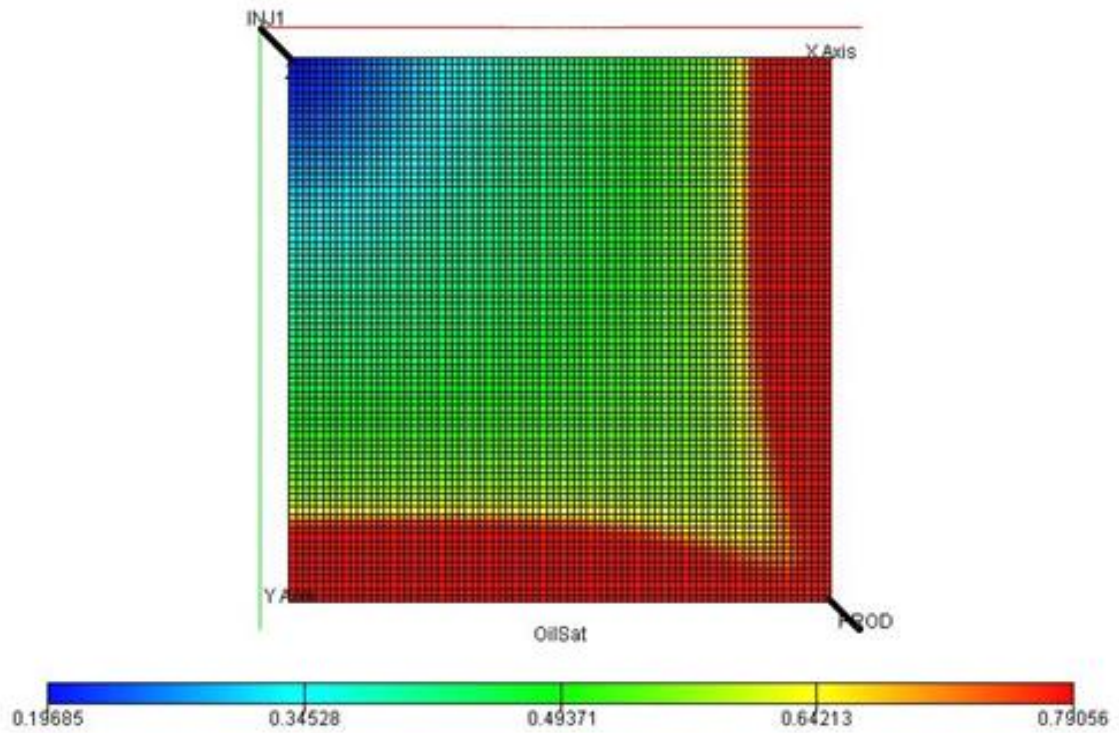


Figure 4.8: Top view, water front before breakthrough, system 2, $M=2$, $V=0.5$,
 $k_z/k_x=0.1$

- Figures 4.9, 4.10 and 4.11 show top, side and 3D view, respectively, for 'at breakthrough case' with 0.5 permeability variation coefficient, 0.1 anisotropy ratio and unit mobility ratio for system 2.

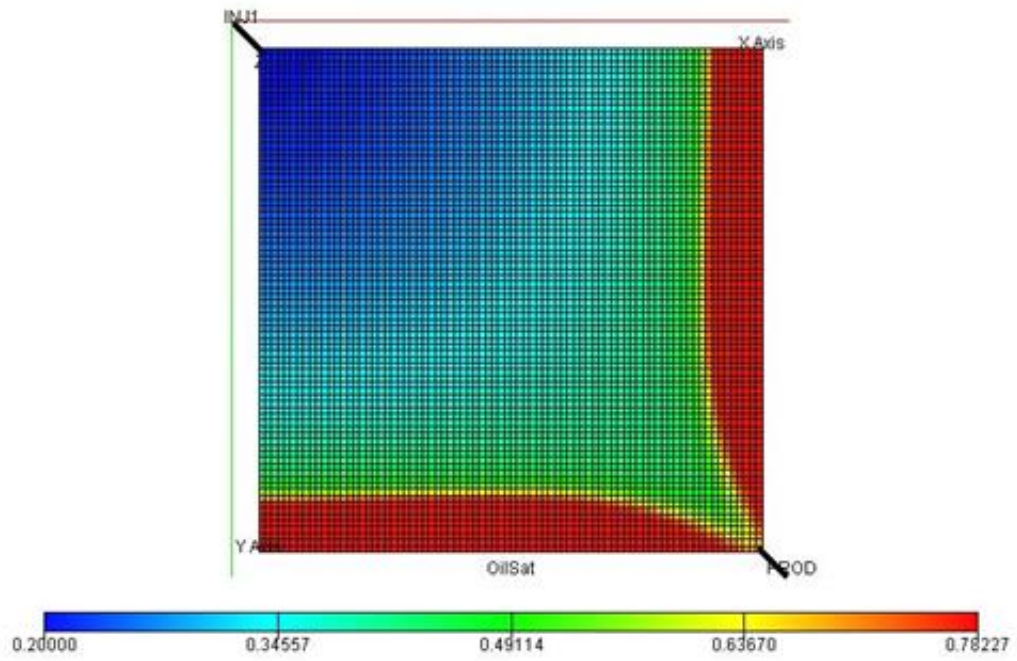


Figure 4.9: Top view, at breakthrough, system 2, $V=0.5$, $M=1$, $k_z/k_x=0.1$

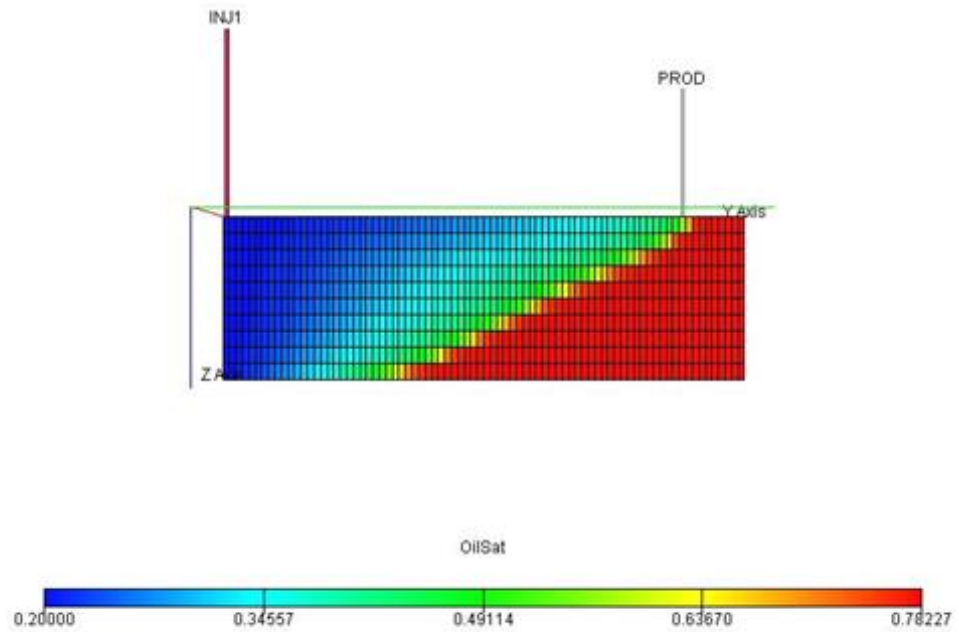


Figure 4.10: Side view, at breakthrough, system 2, $V=0.5$, $M=1$, $k_z/k_x=0.1$

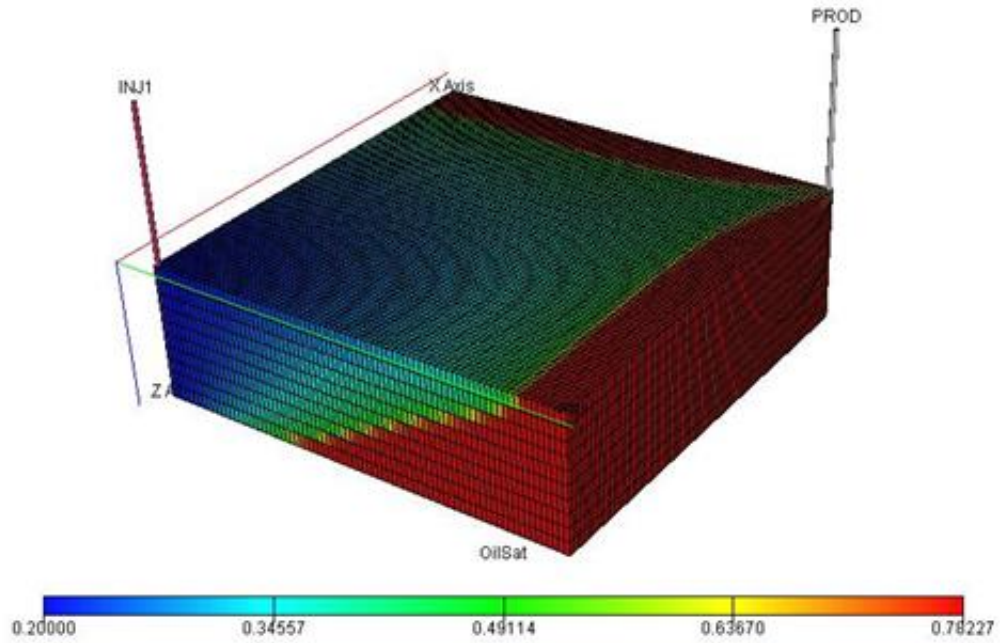


Figure 4.11: 3D view, at breakthrough, system 2, $V=0.5$, $M=1$, $k_z/k_x=0.1$

- Figures 4.12, 4.13 and 4.14 show top, side and 3D view, respectively, for 70% water cut with 0.5 permeability variation coefficient, 0.1 anisotropy ratio and unit mobility ratio for system 2.

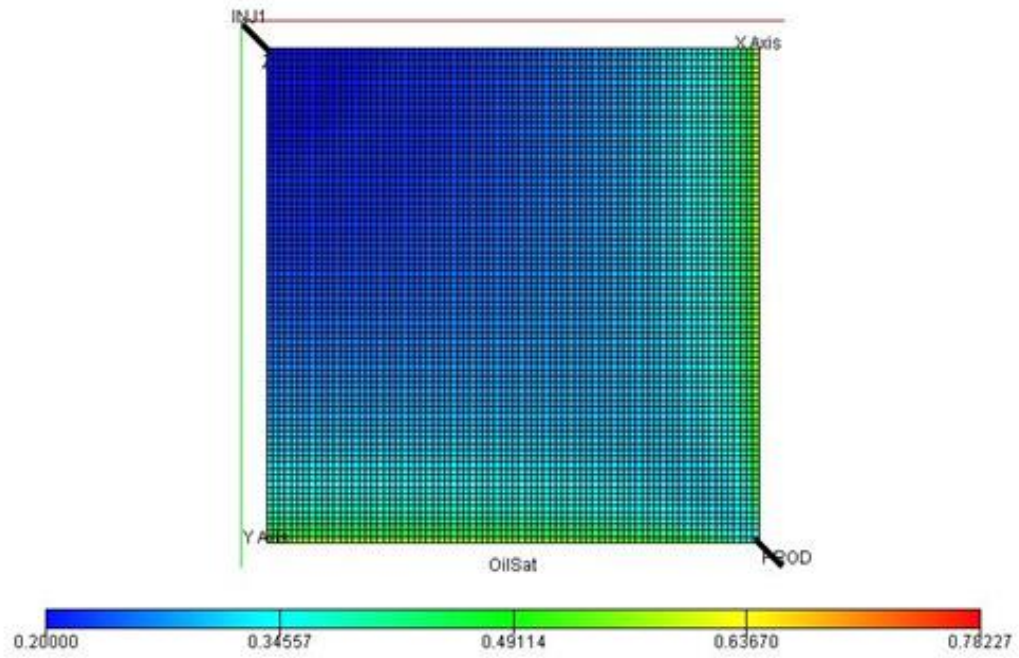


Figure 4.12: Top view, system 2, $V=0.5$, $M=1$, $k_z/k_x=0.1$, $f_w=70\%$

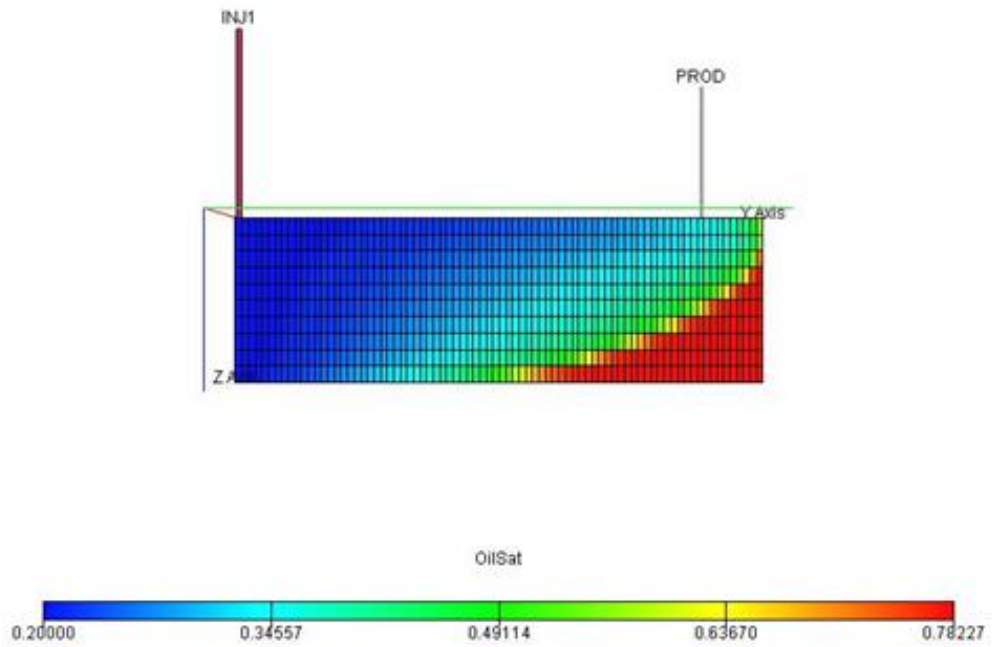


Figure 4.13: Side view, system 2, $V=0.5$, $M=1$, $k_z/k_x=0.1$, $f_w=70\%$

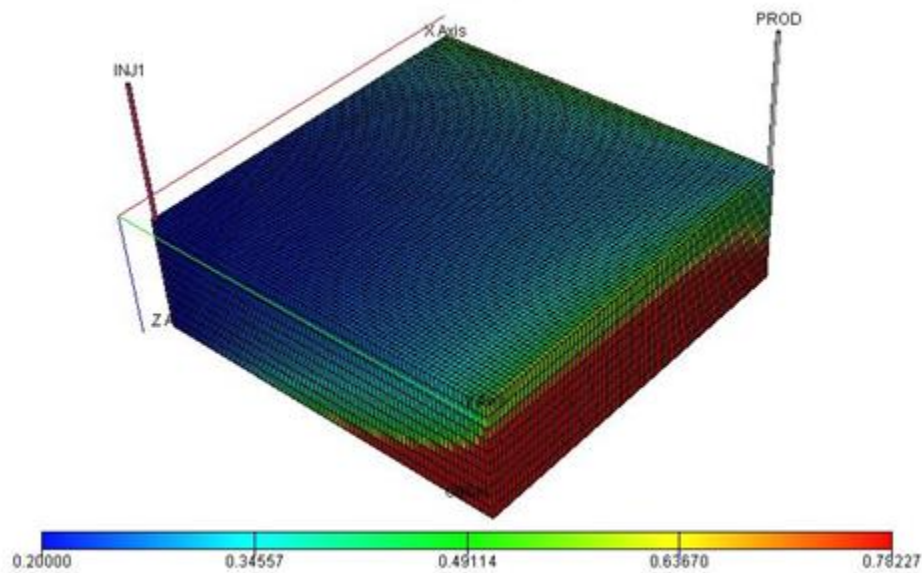


Figure 4.14: 3D view, system 2, $V=0.5$, $M=1$, $k_z/k_x=0.1$, $f_w=70\%$

4.2 Extraction of Simulated Data

The recovery factor (RF) reported by ECLIPSE is based on the initial oil in place. However, it is more relevant to consider the oil recovery that is based on the initial movable oil in place, which is the maximum volume of oil that can be produced by water flooding. Therefore, RF from the simulator was converted to RF_M by the following equation:

$$RF_M = RF \left(\frac{1 - S_{wi}}{1 - S_{wi} - S_{or}} \right) \quad 4.3$$

In order to minimize the numerical dispersion problem in the simulation model, grid size optimization was carried out by using different cell sizes resulting in 6250 to 100,000 total number of cells. The optimum grid size with respect to the output value and time was found

to be 30x30x25 in the x, y and z directions, respectively. This is demonstrated by Figures 4.15 and 4.16 for a test case with 0.7 permeability variation, 95% water cut, 0.1 anisotropy ratio, unit mobility ratio and 1.12 wettability indicator (system 2). This created a model with 64000 cells.

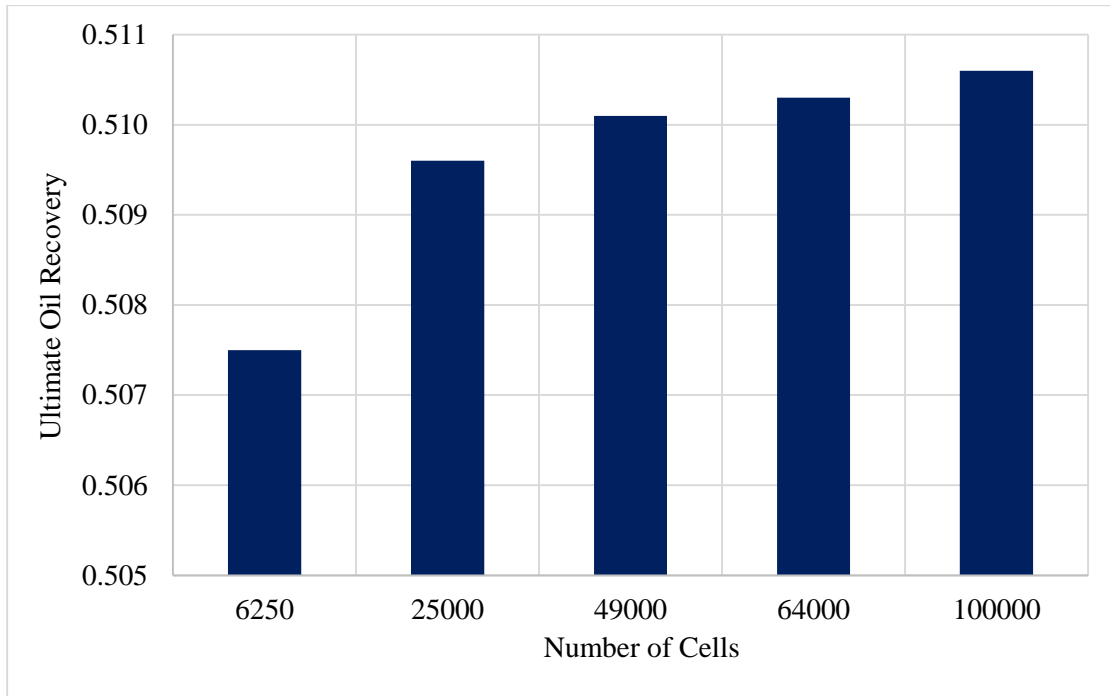


Figure 4.15: Grid size optimization, system2, $M=1$, $V=0.7$, $f_w=95\%$, $k_z/k_x=0.1$

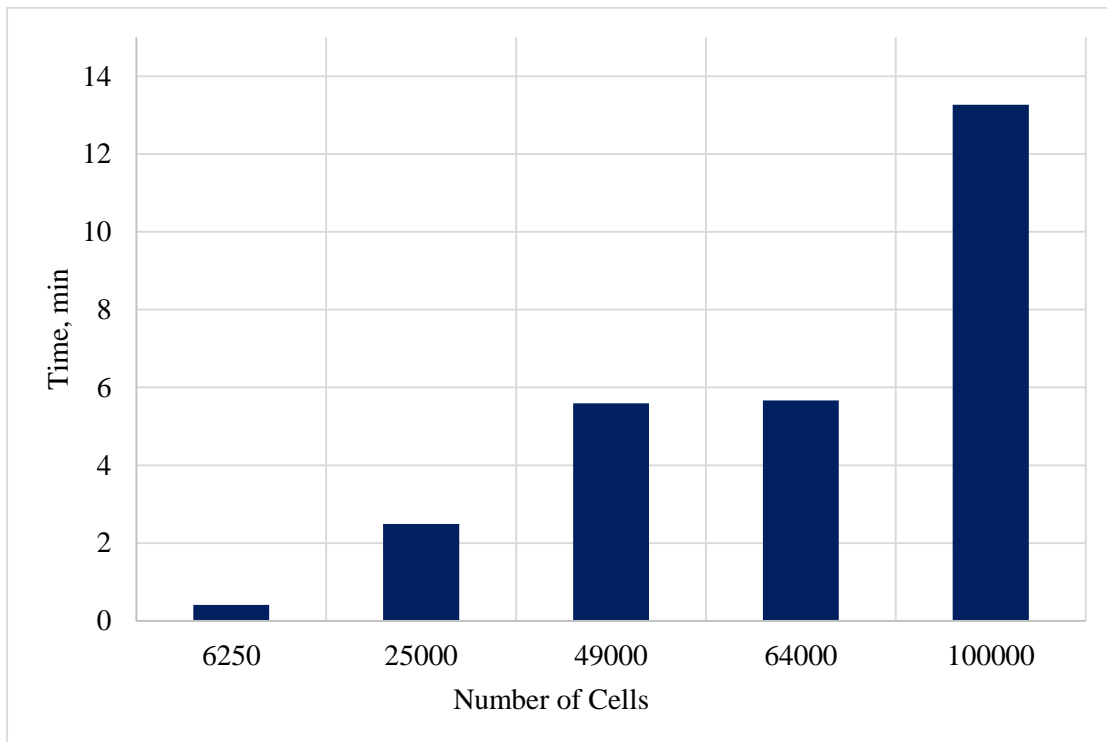


Figure 4.16: Time optimization, system2, $M=1$, $V=0.7$, $f_w=95\%$, $k_z/k_x=0.1$

4.2.1 Simulation Model Sensitivity Analysis

Sensitivity analysis was conducted to check the effect of the following parameters:

- 1- Pattern area
- 2- Reservoir thickness
- 3- Layer sorting

4.2.1.1 Pattern Area Sensitivity

Two cases were run using system 2 with different pattern areas for three mobility ratios. Figures 4.17, 4.18 and 4.19 show the area sensitivity for favorable, unit and unfavorable mobility ratios, respectively, which reveals that oil recovery does not depend on the pattern size.

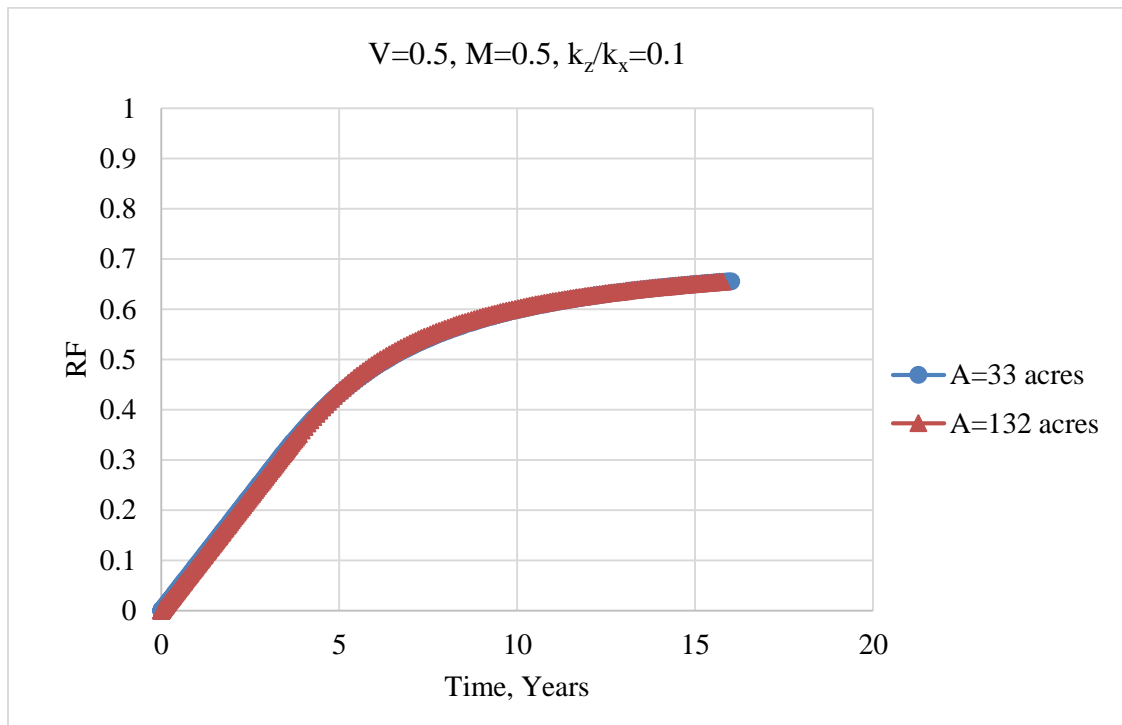


Figure 4.17: Area sensitivity for system 2 with $V=0.5$, $M=0.5$, $k_z/k_x=0.1$

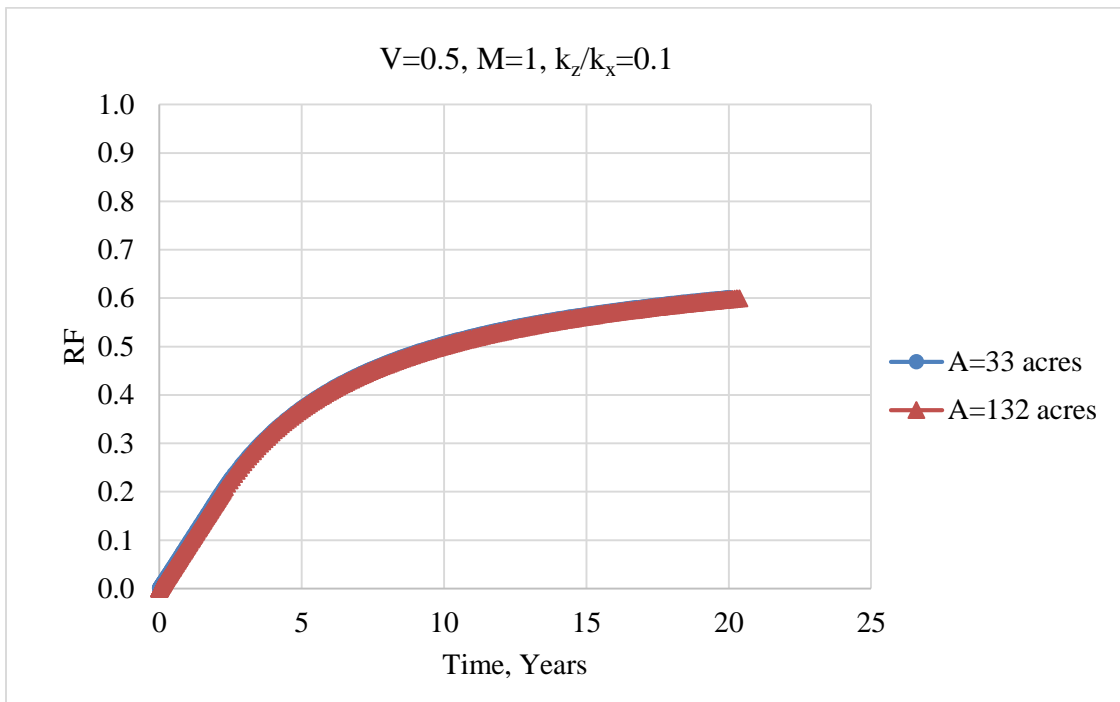


Figure 4.18: Area sensitivity for system 2 with $V=0.5, M=1, k_z/k_x=0.1$

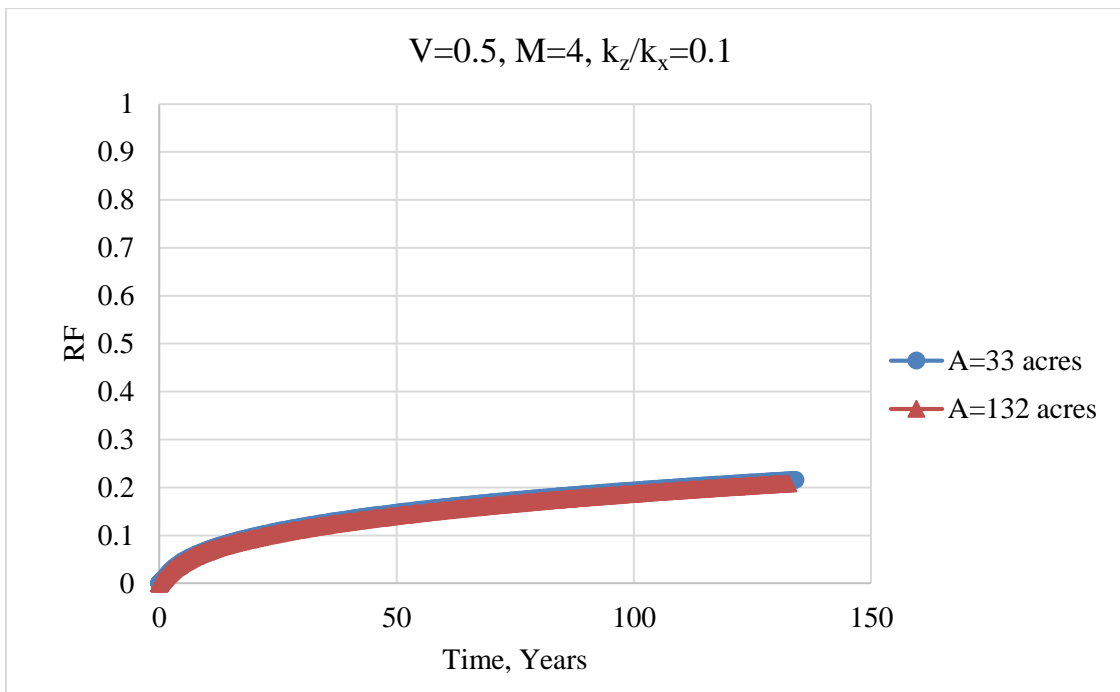


Figure 4.19: Area sensitivity for system 2 with $V=0.5, M=4, k_z/k_x=0.1$

4.2.1.2 Reservoir Thickness Sensitivity

Two cases were run using system 2 with different reservoir thicknesses for three mobility ratios. Figures 4.20, 4.21 and 4.22 show the reservoir thickness sensitivity for favorable, unit and unfavorable mobility ratios, respectively, which illustrates that oil recovery does not change with the reservoir thickness.

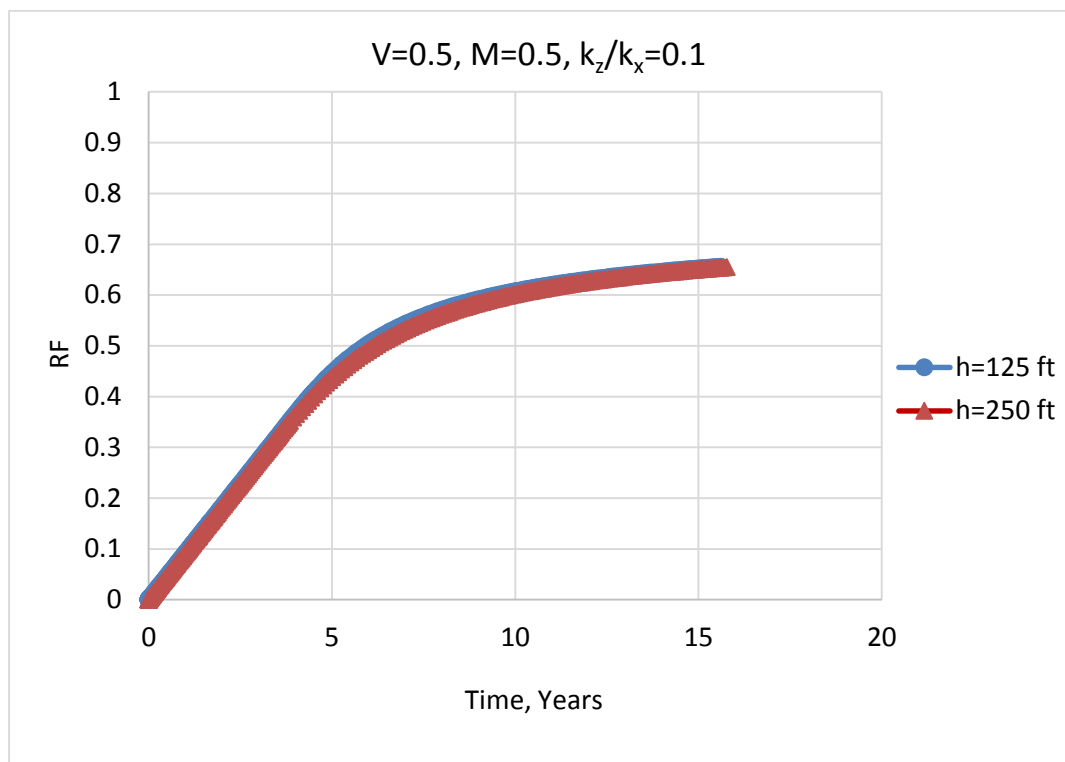


Figure 4.20: Thickness sensitivity for system 2 with $V=0.5$, $M=0.5$, $k_z/k_x=0.1$

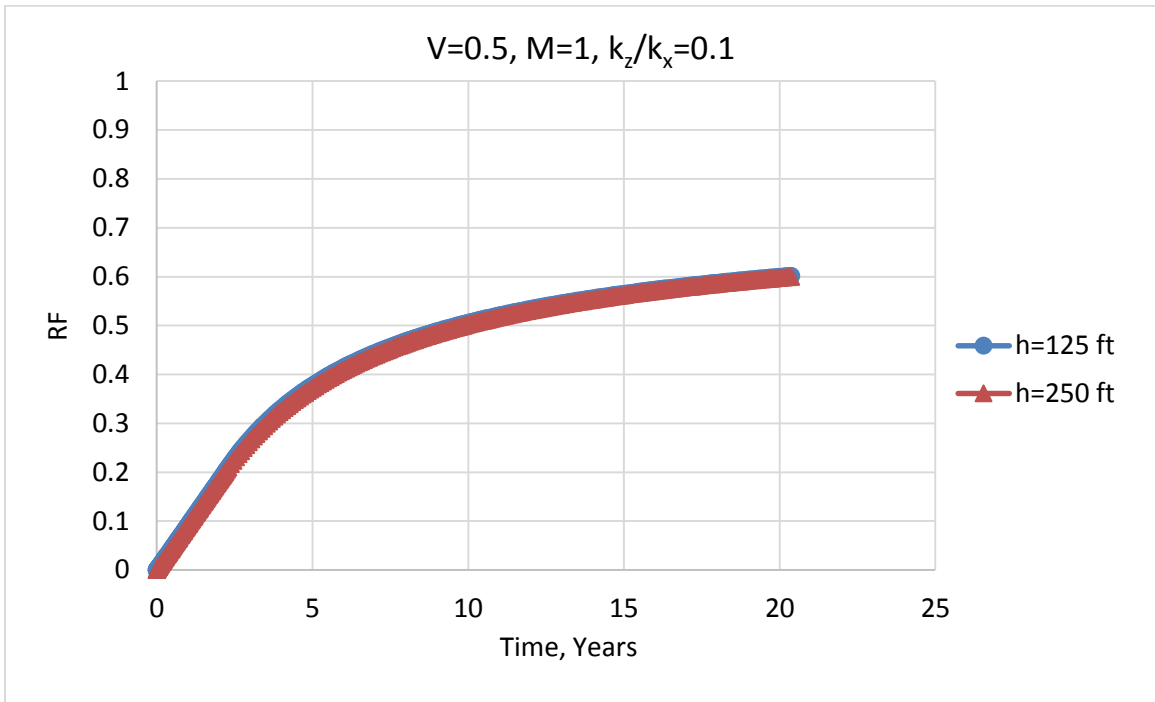


Figure 4.21: Thickness sensitivity for system 2 with $V=0.5, M=1, k_z/k_x=0.1$

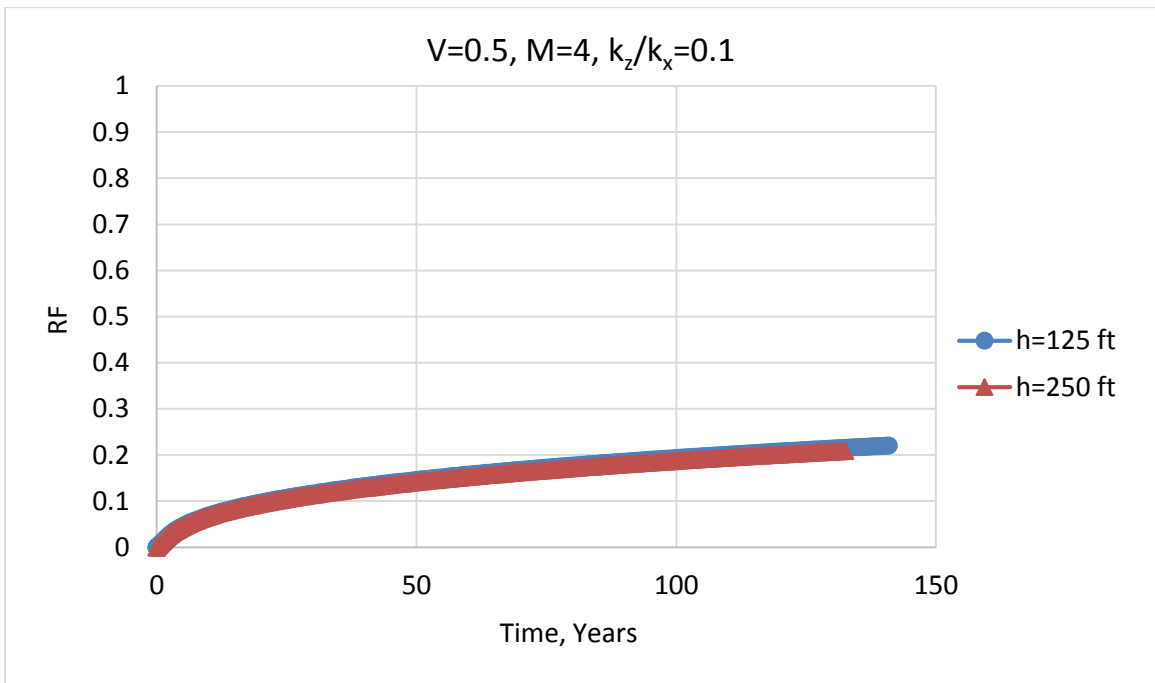


Figure 4.22: Thickness sensitivity for system 2 with $V=0.5, M=4, k_z/k_x=0.1$

4.2.1.3 Layer Sorting Sensitivity

The simulation model orders the layers with permeability in descending order. In real situations, however, the layers are randomly distributed. A reservoir with system 2 and the properties listed in Table 4.9 was arranged in three random permeability arrangements as shown in Figures 4.23, 4.24 and 4.25. Figure 4.26 shows that the oil recovery factor is insensitive to the permeability sorting at water cuts 0 to 95%.

Table 4.9: Properties of randomly sorted simulation models

Parameter	Value
Dykstra Parsons reservoir Heterogeneity Coefficient, V	0.6
Permeability anisotropy ratio, k_z/k_x	0.15
Mobility Ratio, M	1.5

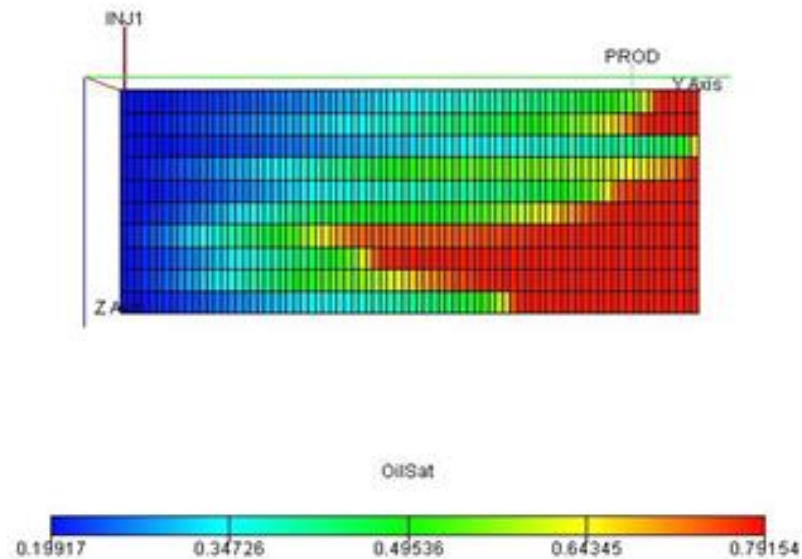


Figure 4.23: Side View of simulation model with random sorting 01

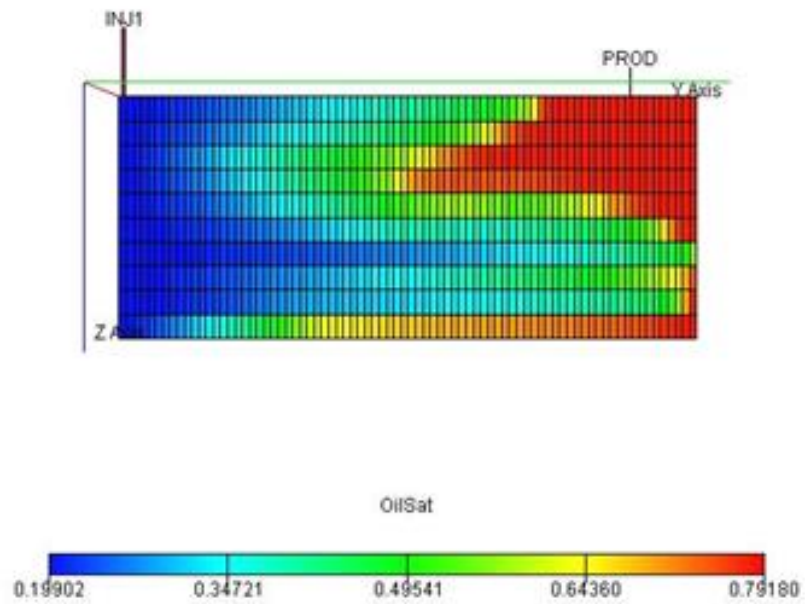


Figure 4.24: Side View of simulation model with random sorting 02

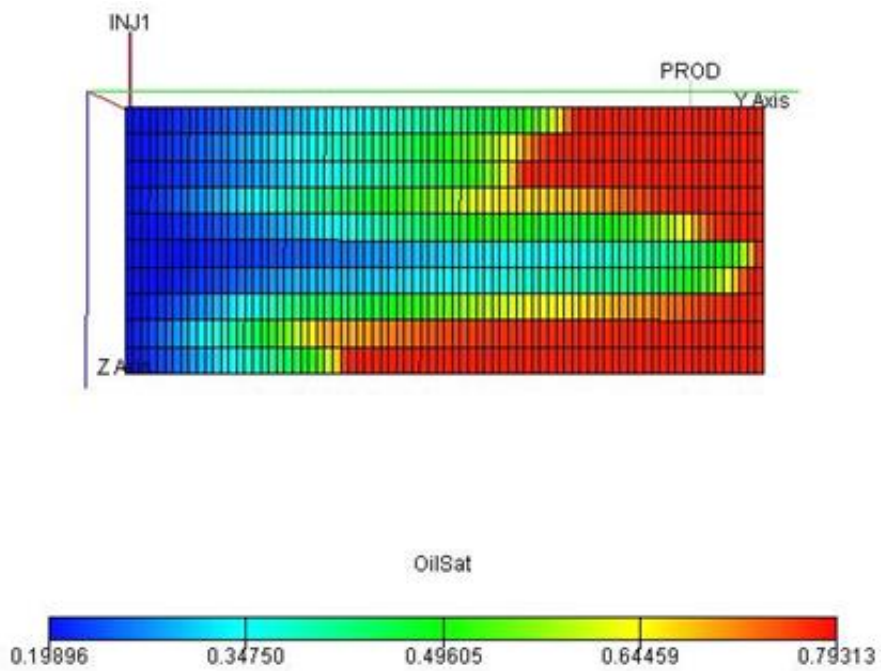


Figure 4.25: Side View of simulation model with random sorting 03

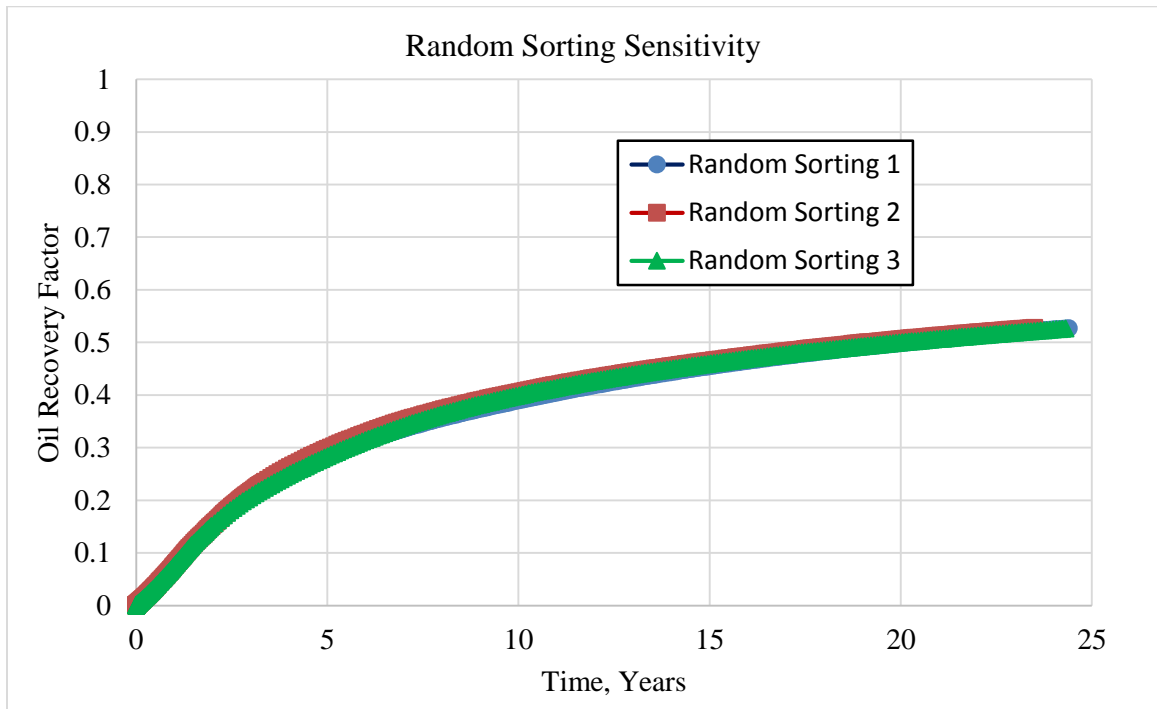


Figure 4.26: Sensitivity of oil recovery to the layer permeability sorting for system=2,
 $V=0.6$, $M=1.5$, $k_z/k_x=0.15$, $f_w=0$ to 95%

CHAPTER 5

SIMULATION RESULTS

This chapter presents and discusses the results of the simulation work. The effect of each parameter on the oil recovery will be presented in a separate section. All simulation results are presented in graphical form in the appendix.

5.1 Effect of Mobility Ratio

As explained in Chapter 1, the water-oil mobility ratio is a measure of the water injectivity of a well relative to its oil productivity. The mobility ratio has a great influence on water-flood efficiency at and beyond water breakthrough as shown in Figures 5.1 and 5.2 respectively, for system 2 with various values of V . As expected, oil reservoirs with favorable mobility ratio yield higher oil recovery (RF) as compared to unfavorable mobility ratio.

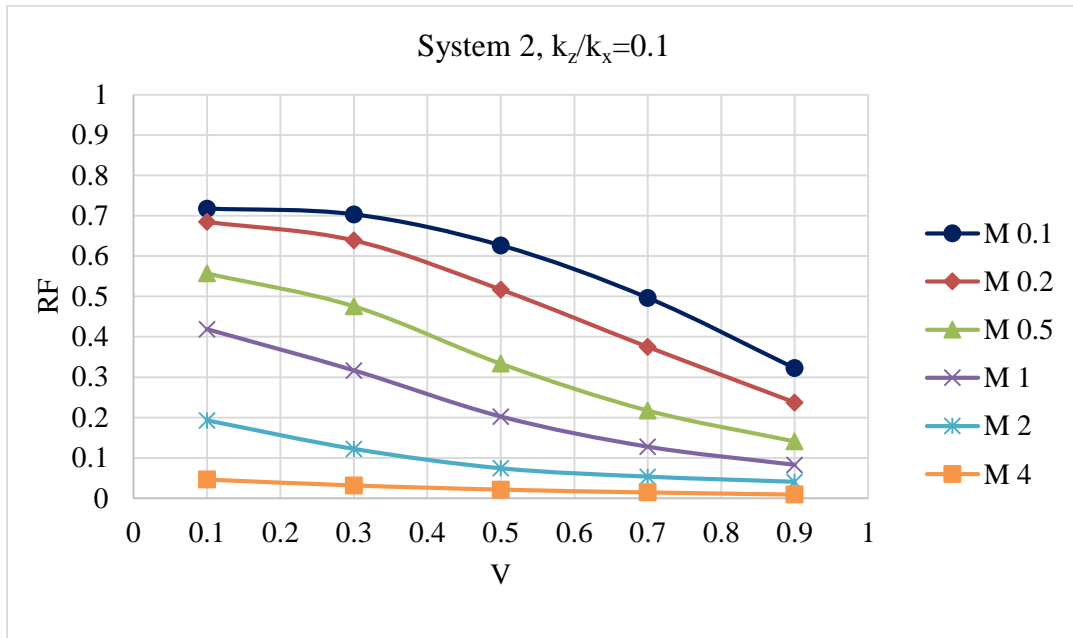


Figure 5.1: Effect of mobility ratio on oil recovery factor at water breakthrough

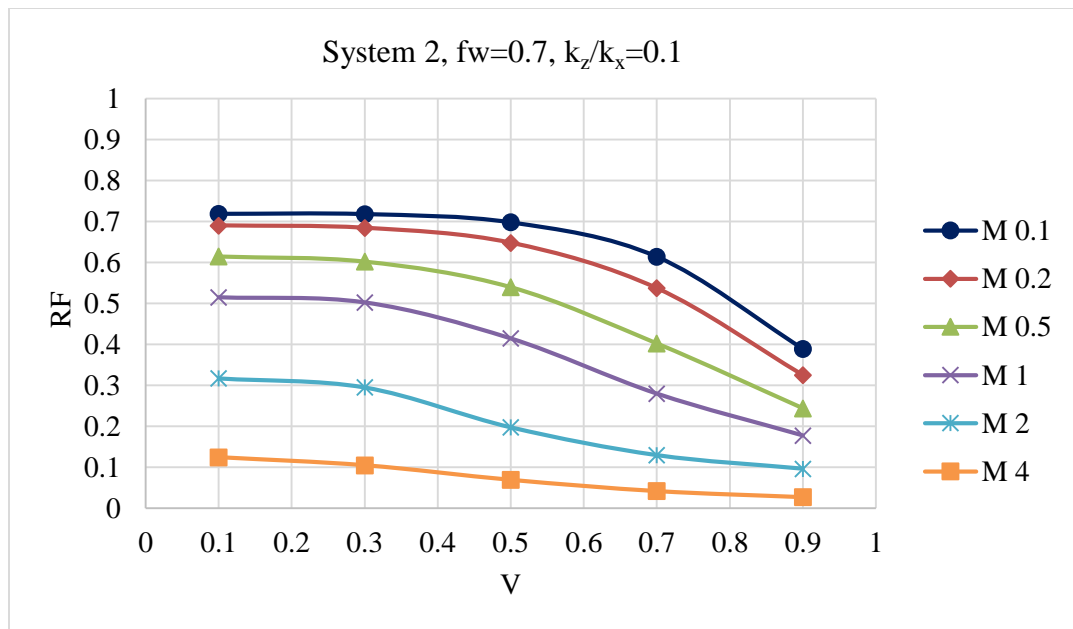


Figure 5.2: Effect of mobility ratio on oil recovery factor beyond water breakthrough at

$f_w=0.7$
50

5.2 Effect of Reservoir Heterogeneity

Oil recovery factor highly depends on the coefficient of permeability variation. Figures 5.3 and 5.4 show the effect of permeability variation on oil recovery factor at and beyond water breakthrough, respectively, for system 2 at various mobility ratios. A larger permeability variation results in poorer oil recovery.

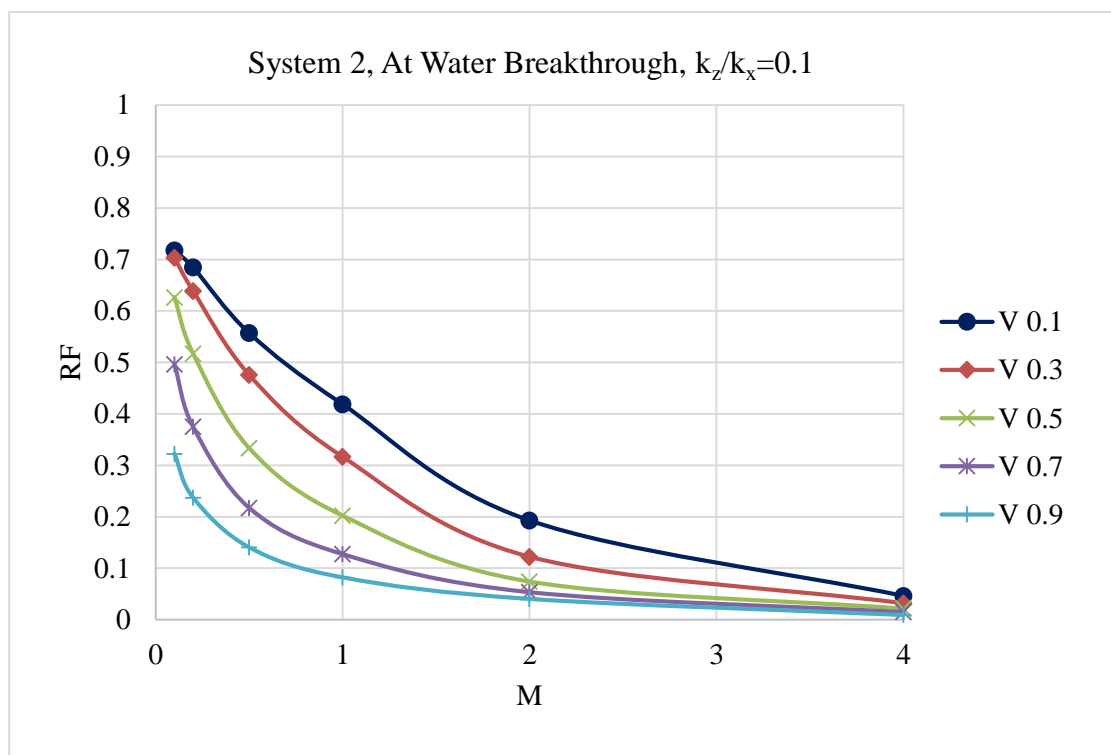


Figure 5.3: Effect of permeability variation on oil recovery factor at water breakthrough

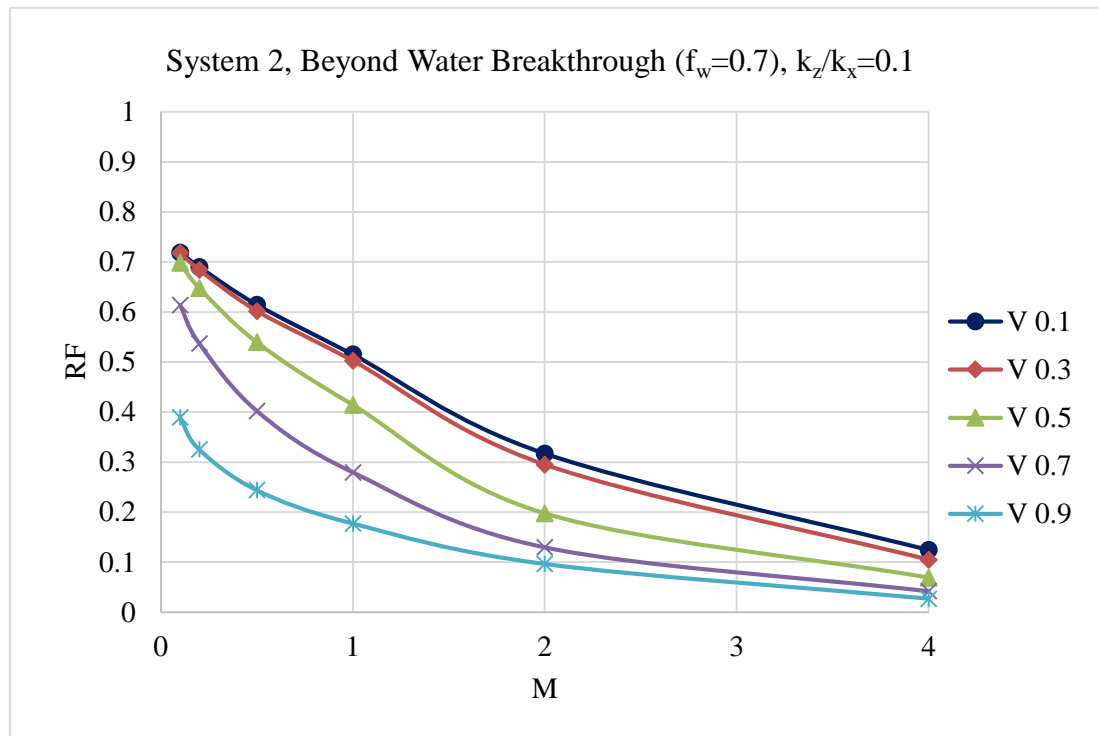


Figure 5.4: Effect of permeability variation on oil recovery factor beyond water breakthrough at $f_w=0.7$

5.3 Effect of Permeability Anisotropy Ratio

The effect of permeability anisotropy ratio was analyzed at and beyond water breakthrough for very favorable and unfavorable mobility ratios. Compared with non-communicating layers, crossflow increases oil recovery at breakthrough for favorable mobility ratios while it results in poorer oil recovery for unfavorable mobility ratios. On the other hand, crossflow holds back the advancement of the front in the low-permeability layers for smaller M , especially for highly heterogeneous reservoirs. This effect is presented in Figures 5.5 and 5.6 for favorable and unfavorable mobility ratios, respectively, for system

2. Beyond breakthrough, crossflow improves oil recovery for all mobility ratios, especially for highly heterogeneous reservoirs. This effect is shown in Figures 5.7 and 5.8 for system 2.

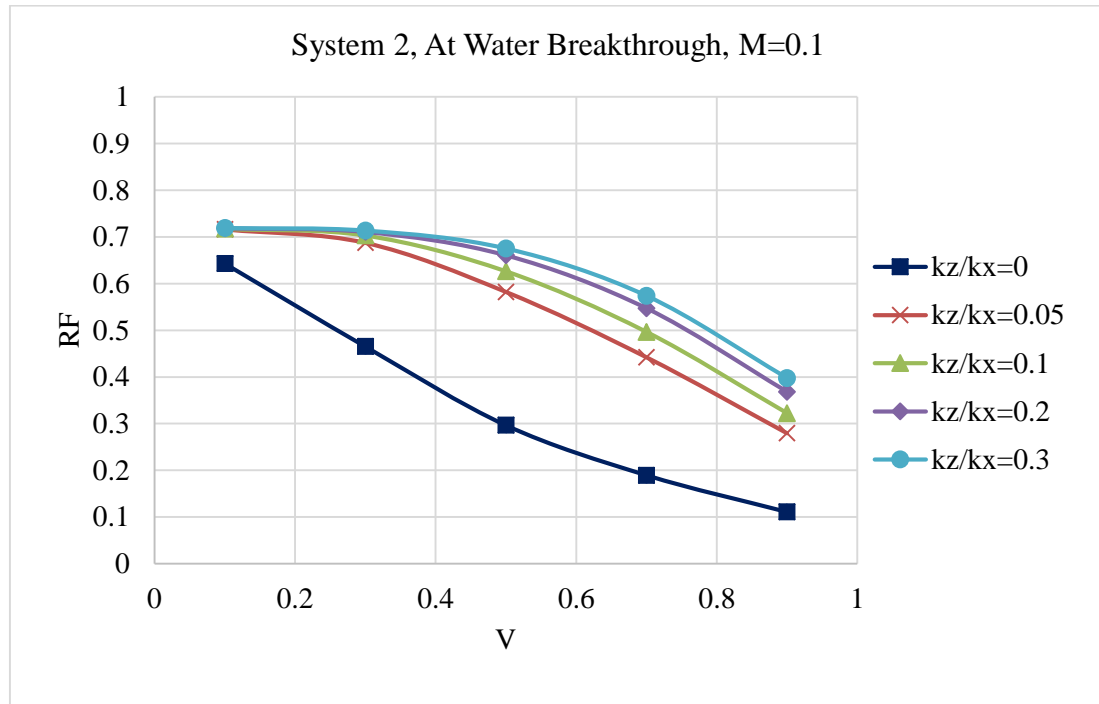


Figure 5.5: Effect of crossflow on oil recovery at water breakthrough for M=0.1

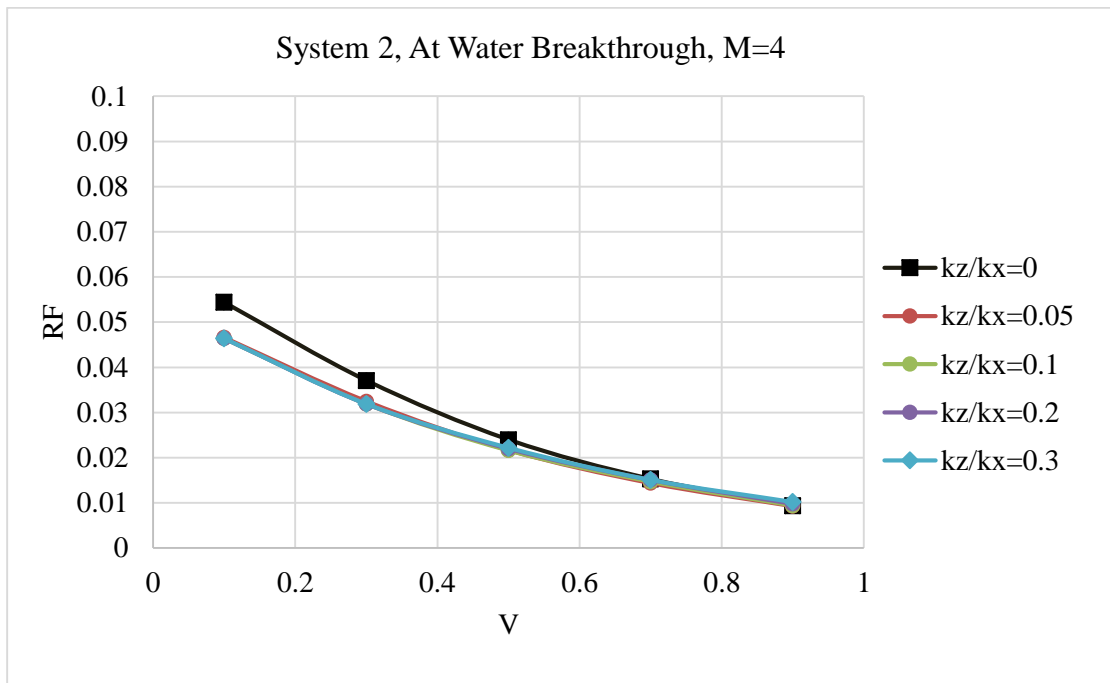


Figure 5.6: Effect of crossflow on oil recovery at water breakthrough for M=4

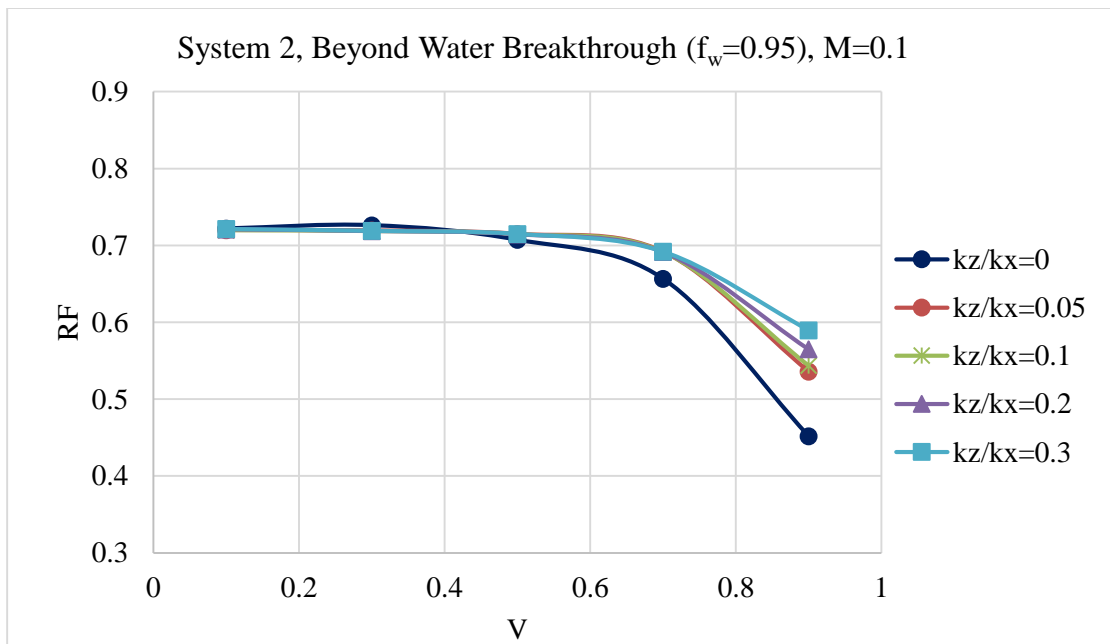


Figure 5.7: Effect of crossflow on oil recovery beyond water breakthrough for M=0.1

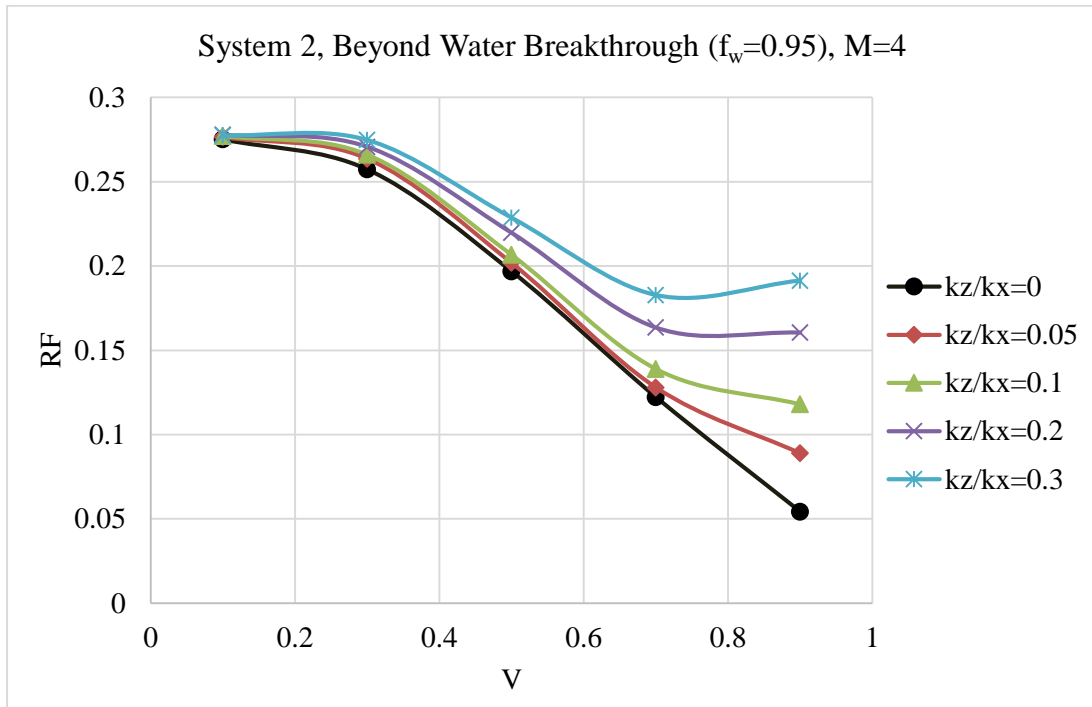


Figure 5.8: Effect of crossflow on oil recovery beyond water breakthrough for $M=4$

5.4 Effect of Wettability

A new parameter was developed in this study to quantify wettability as already discussed in Chapter 1. Three reservoir systems were built with different wettability indicators.

The effect of wettability on oil recovery at breakthrough for favorable and unfavorable mobility ratios is shown in Figures 5.9 and 5.10, respectively. In both cases, it appears that the best recovery is obtained with the neutral-wettability system especially with low-heterogeneity reservoirs. However, inspecting the movable oil recovery (RF_M) reveals that wettability has an insignificant effect on RF_M for low mobility ratios (Figure 5.11) but at high mobility ratios, the neutral-wettability system produces the largest movable oil

recovery especially with low-heterogeneity reservoirs (Figure 5.12). Similar effects were observed with both types of recovery beyond water breakthrough as shown in Figures 5.13 to 5.16.

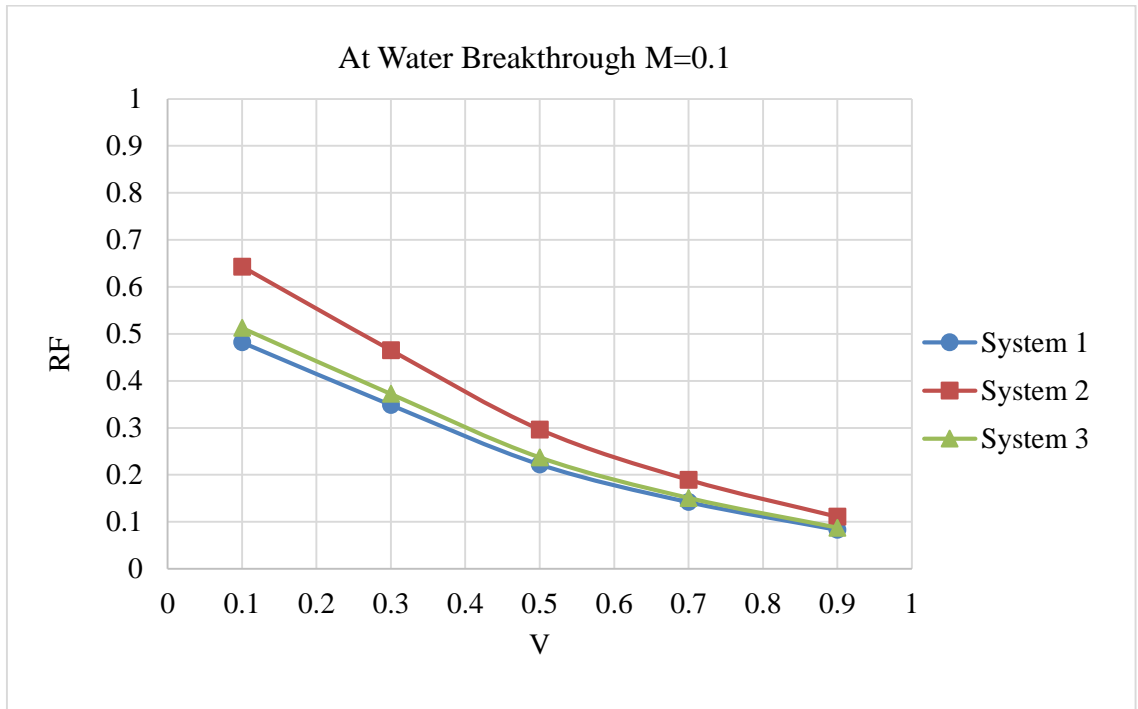


Figure 5.9: Effect of wettability on oil recovery at water breakthrough with M=0.1,

$$k_z/k_x=0$$

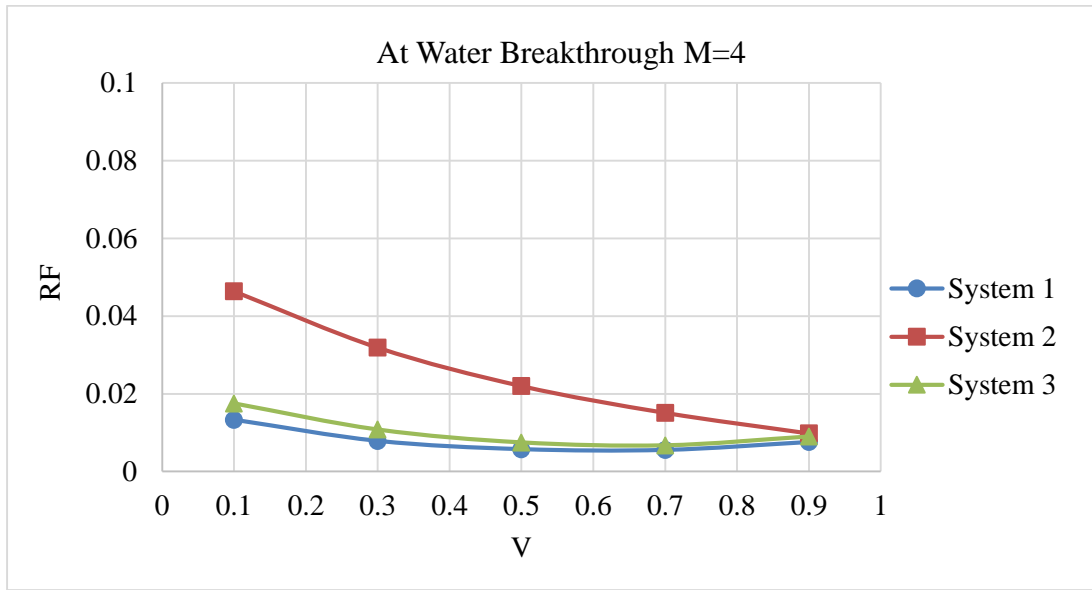


Figure 5.10: Effect of wettability on oil recovery efficiency at water breakthrough with $M=4$, $k_z/k_x=0.2$

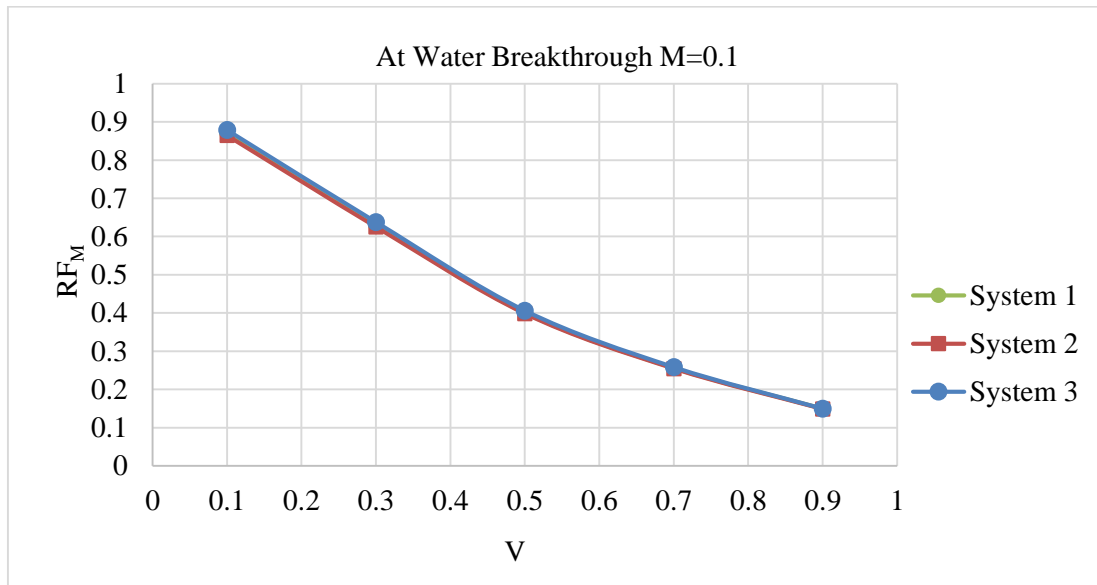


Figure 5.11: Effect of wettability on movable oil recovery efficiency at water breakthrough with $M=0.1$, $k_z/k_x=0$

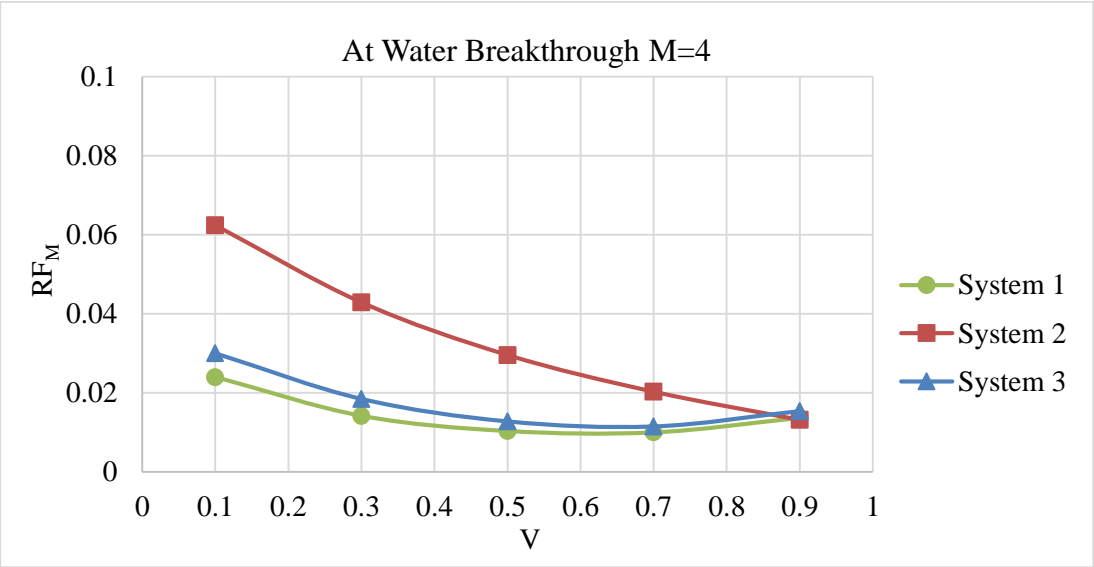


Figure 5.12: Effect of wettability indicator on movable oil recovery efficiency at water breakthrough with $M=4$, $k_z/k_x=0.2$

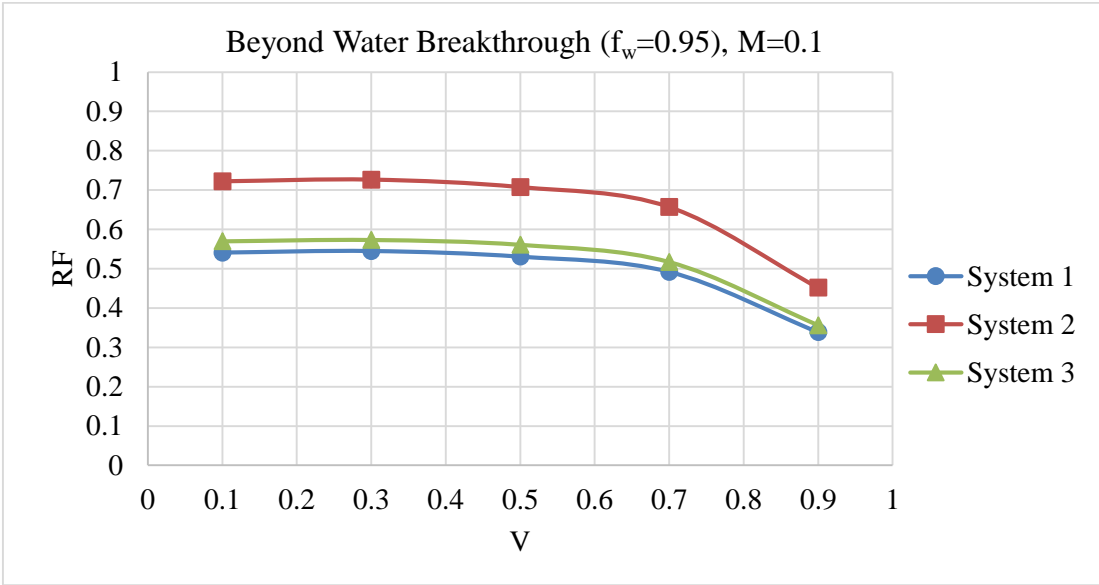


Figure 5.13: Effect of wettability indicator on oil recovery efficiency beyond water breakthrough at $M=0.1$, $k_z/k_x=0$

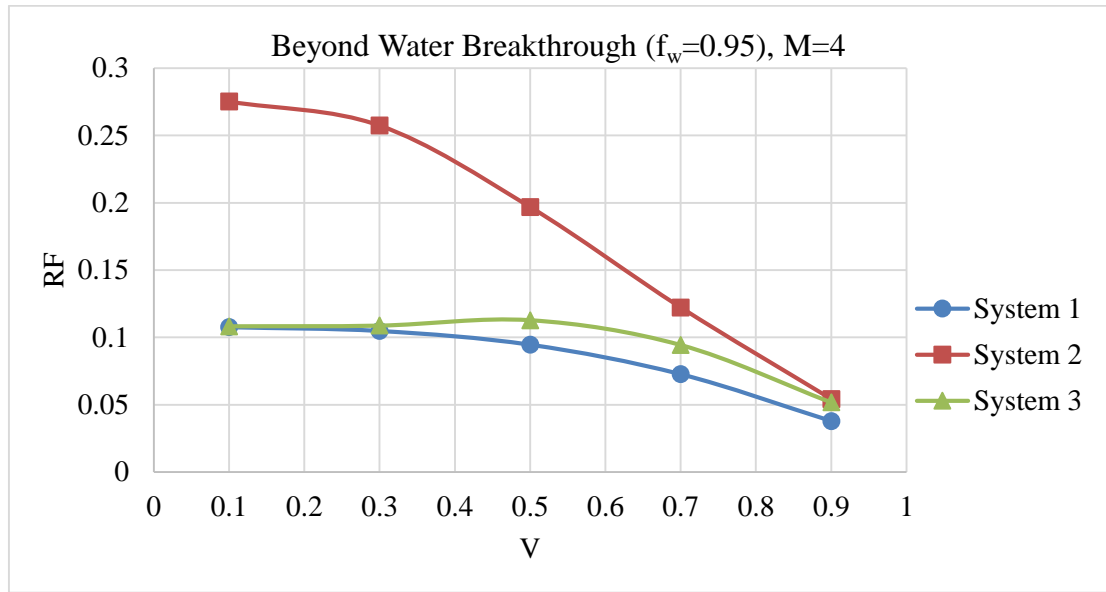


Figure 5.14: Effect of wettability indicator on oil recovery efficiency beyond water breakthrough at $M=4$, $k_z/k_x=0$

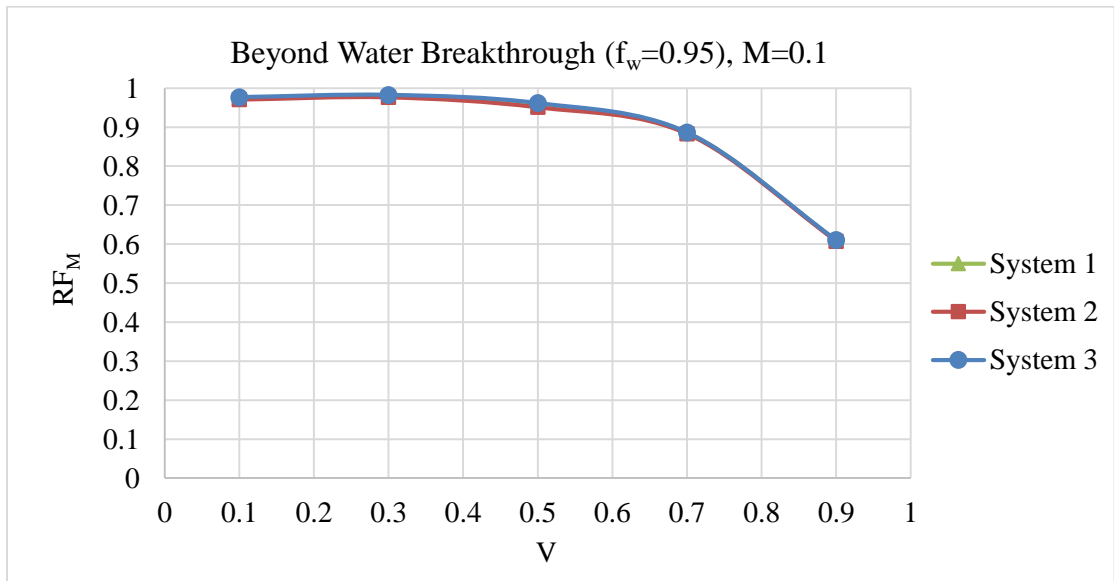


Figure 5.15: Effect of wettability indicator on movable oil recovery efficiency beyond water breakthrough at $M=0.1$, $k_z/k_x=0$

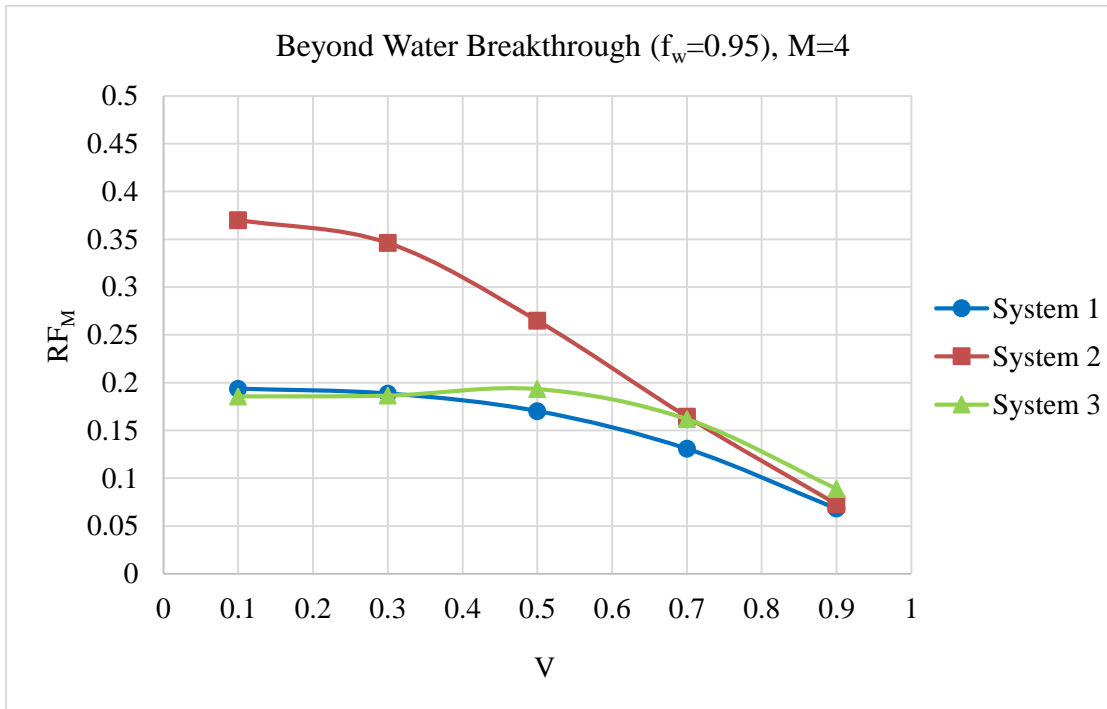


Figure 5.16: Effect of wettability indicator on movable oil recovery efficiency beyond water breakthrough at $M=4$, $k_z/k_x=0$

CHAPTER 6

DEVELOPMENT AND TESTING OF THE

MATHEMATICAL CORRELATION

This chapter presents the new empirical correlation that was developed to fit the simulation results. It also presents the testing of the new correlation and a comparison of its predictions with actual field data.

6.1 Artificial Neural Networks

A correlation refers to any of a wide class of mathematical relationships containing dependence. They are valuable as they can show a predictive relationship which can be used in practice. For many years, petroleum engineers have derived correlations to estimate a number of reservoir rock and fluid properties and to model many reservoir phenomena. There are several statistical tools available to derive a correlation. For example, non-linear regression, artificial neural networks, fuzzy logic, functional networks and support network machine, etc. In this study, Artificial Neural Networks (ANNs) technique was applied on the simulation results to build the new empirical correlation.

ANNs are algorithms used to solve the problem by mimicking the structure and the function of a human nervous system. It is composed of several artificial neurons that are connected together according to a specific network architecture. The aim of ANN is to transform the inputs into meaningful outputs. A typical ANN model is based on a series of three layers (input, hidden and output). Input data is given to the input layer which feeds them to the hidden layer where they are processed and then fed to the output layer. Each layer comprises of a set of neurons which are similar to the computational machines for the layers. The neuron processes each data record based on an activation function. The topology of a basic ANN network is shown in Figure 6.1 consists of 2 input neurons, 5 hidden layer neurons, and one output.

The primary goal of this study was to develop a new empirical correlation that estimates the movable oil recovery factor in terms of permeability variation (V), mobility ratio (M), permeability anisotropy ratio (k_z/k_x), water cut (f_w), and wettability indicator (WI). Input and output variables for the new correlation are listed in Table 6.1.

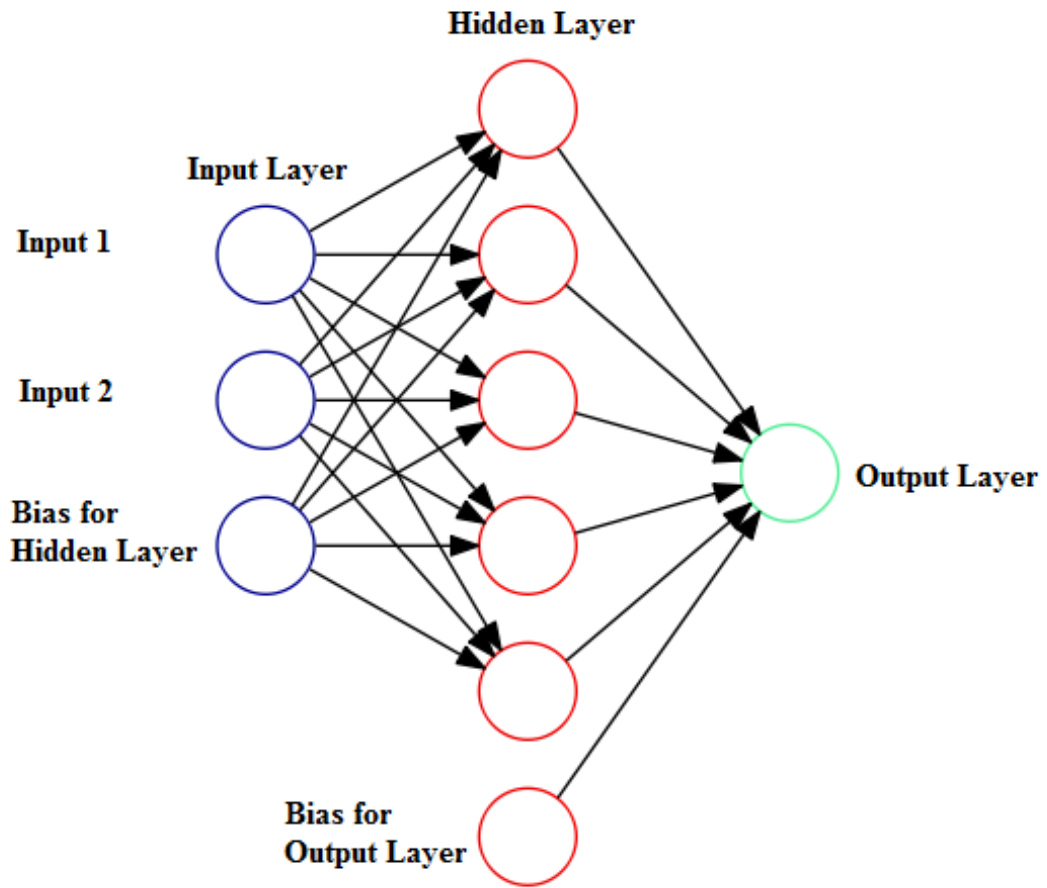


Figure 6.1: Topology of a Basic ANN network

Table 6.1: Dependent and independent variables for the new correlation

Dependent Variable	Independent Variable
RF_M	V
	M
	k_z/k_x
	f_w
	WI

6.2 Correlation Development

Artificial Neural Network (ANN) was applied on the simulated data to develop the proposed correlation. The neural network based model adopted in this study was a feedforward neural network (FFNN). 3500 data points from the simulation runs were used as input to the FFNN for training purposes while the rest of 1500 data points were used to test the model.

The RF_M ANN model consisted of five input neurons (input parameters) which were linked to V , M , α , f_w , WI , one hidden layer and one output neuron (output parameter). The output neuron is the movable oil recovery factor. There were 14 neurons in the hidden layer, which were obtained after the sensitivity runs of a number of neurons. Tan-sigmoid and Linear Transfer functions were used in hidden and output layers respectively. Levenberg-Marquardt back-propagation algorithm was utilized for training of the Neural Network. In order to avoid the local minimum, 2000 multiple realizations with different weights and biases initialization of training were conducted and minimum error realization was selected as the best case. The optimum weights and bias values were obtained for movable oil recovery factor after proper training and are shown in Table 6.3. The network of the new correlation is shown in Figure 6.2 and described mathematically in equations 6.1, 6.2a and 6.2b.

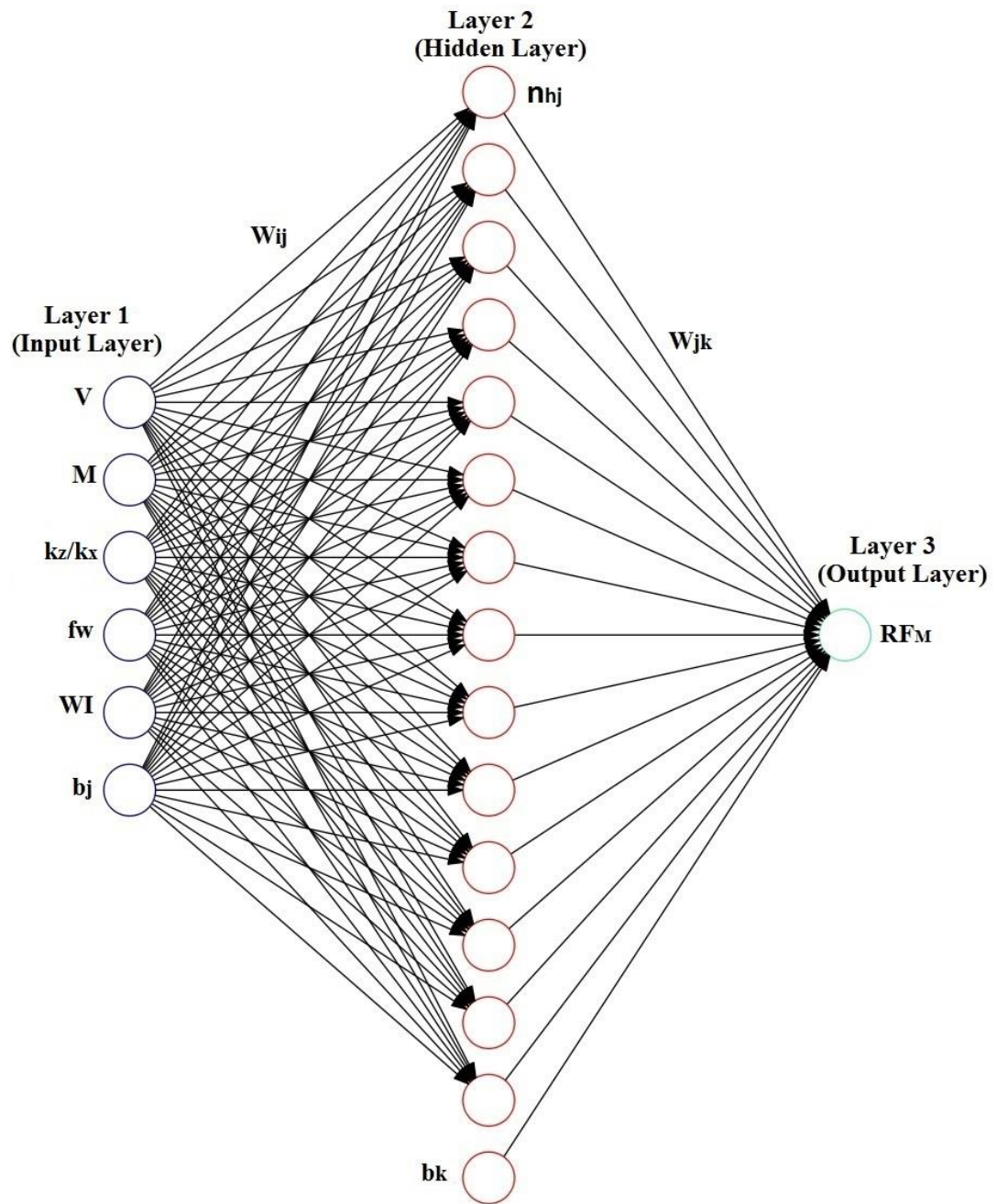


Figure 6.2: Topology of RF_M prediction FFNN-based model

$$(\text{RF}_M)_N = \sum_{j=1}^{N_h} w_{jk} n_{hj} + b_k \quad 6.1$$

$$n_{hj} = f\left(\sum_{i=1}^{N_i} w_{ij} x_i + b_j\right) \quad 6.2a$$

Or

$$n_{hj} = f\left(w_{1j} V_N + w_{2j} M_N + w_{3j} \alpha_N + w_{4j} f_{w_N} + w_{5j} W I_N + b_j\right) \quad 6.2b$$

$$f(x) = \tanh(x) = \frac{2}{1 + e^{-2x}} - 1 \quad 6.3$$

Where,

j = Number of hidden layer neurons

i = Number of input layer neurons

x_i = Input Parameters (Normalized)

b_j = Bias for hidden layer

b_k = Bias for Output layer

W_{ij} = Weights between Input and Hidden Layer

W_{jk} = weights between Hidden and Output Layer

f = Transfer function

N = Subscript 'N' shows normalized parameter

N_h = Total number of neurons in hidden layer

N_i = Total number of inputs

n_{hj} = j th neuron in hidden layer

$(RF_M)_N$ = Normalized output of the output layer

Input parameters were normalized for new correlation and then the output was de-normalized, which is described in the following section.

6.2.1 Input Normalization

The normalization of input parameters was done by the following function:

$$\text{Inputs} = \frac{(y_{\max} - y_{\min})(x - x_{\min})}{(x_{\max} - x_{\min})} + y_{\min} \quad 6.4$$

y_{\min} and y_{\max} are -1 and +1, respectively, in the above equation, while values of x_{\max} and x_{\min} are given in Table 6.2. Normalization equation of each input parameter is given below:

$$V_N = 2.5(V - 0.1) - 1 \quad 6.5a$$

$$M_N = \frac{20}{39}(M - 0.1) - 1 \quad 6.5b$$

$$\alpha_N = \frac{20}{3}\alpha - 1 \quad 6.5c$$

$$fw_N = \frac{40}{19}fw - 1 \quad 6.5d$$

$$WI_N = 0.8(WI - 0.5) - 1 \quad 6.5e$$

6.2.2 Output De-Normalization

The output de-normalization was done by the following function:

$$\text{Output} = \frac{(y_{\max} - y_{\min})(x - x_{\min})}{x_{\max} - x_{\min}} + y_{\min} \quad 6.6$$

x_{\min} and x_{\max} are -1 and +1, respectively, in the above equation, while values of y_{\max} and y_{\min} are given in Table 6.2. De-Normalization equation of the output is given below:

$$\text{RF}_M = 0.48682(\text{RF}_{M_N} + 1) + 0.00933 \quad 6.7$$

The above equation gives the final result of the newly developed ANN based correlation.

Table 6.2: Statistical Description of the Input and Output Data Used for Training

Parameters	Minimum Value	Maximum Value
Output Parameter		
RF _M	0.00933	0.98297
Input Parameter		
V	0.1	0.9
M	0.1	4
α	0	0.3
f _w	0	0.958
WI	0.5	3

Table 6.3: Weights and Bias Values for RF_M Artificial Neural Network Model

Weights between Input Layer and Hidden Layers (w_{ij})					
Hidden Layer Neurons (j)	Input Layer Neurons (i)				
	1	2	3	4	5
1	-0.0287	-0.4573	0.1023	2.2203	-0.0617
2	1.0045	-3.6612	-4.9537	-0.8402	0.0171
3	0.3281	0.7786	-0.0597	-0.5697	4.4795
4	-0.5188	3.5151	-0.0028	0.7087	-3.8602
5	1.0633	-1.2345	0.1102	-0.1091	-0.0071
6	-0.3643	3.3751	-0.0194	0.2064	0.0027
7	-0.8680	1.2776	-0.0689	0.0899	-0.0081
8	0.5681	1.2584	-0.0921	-0.1977	0.0304
9	-0.7817	-0.8879	-0.0534	0.7074	-0.0077
10	0.6062	0.7747	0.1241	-0.8013	-0.0072
11	-1.1626	3.6055	5.1372	0.9160	-0.0265
12	-0.5266	-0.7621	-0.1762	0.9159	0.0130
13	-0.2983	-0.9337	0.0447	0.5549	-3.7984
14	-0.0548	-0.6913	0.1030	2.2167	-0.0650
Bias Values for Hidden Layer Neurons (b_j)		Weights between Hidden Layer and Output Layers (w_{jk})			
Hidden Layer Neurons (j)	Bias (b_j)	Hidden Layer Neurons (j)		Output One Neuron	
1	-3.2785	1		6.4945	
2	-9.8858	2		-7.8405	
3	-3.9017	3		1.7436	
4	-8.6694	4		-0.4930	
5	-2.7530	5		6.4079	
6	5.0365	6		-7.2144	
7	3.1122	7		18.4542	

8	1.2574	8	-1.5411
9	-1.3804	9	-5.1601
10	1.1276	10	-8.9059
11	10.1931	11	-7.2916
12	-1.0360	12	-4.0158
13	3.0948	13	1.7324
14	-3.44023	14	-5.8550
Bias Values for Output Layer Neuron (b_k)			
Output Layer Neuron		Bias Value (b_k)	
1		-4.9495	

Mean Absolute Percentage Error (MAPE) and coefficient of determination (R^2) are statistical tools to determine the accuracy of data. MAPE is defined mathematically in Eq. 6.8.

$$MAPE = \frac{100}{n} \sum_{i=1}^n \left| \frac{Actual_i - Predicted_i}{Actual_i} \right| \quad 6.8$$

Scatter plots were made between simulated and new correlation results for seen (training) and unseen (testing) data as shown in Figures 6.3 and 6.4 respectively. Both scatter diagrams show coefficient of determination, R^2 above 0.99, which indicates that the developed empirical model is a strong positive correlation. Also, MAPE for both training and testing data is 6.75% and 7.08% respectively as shown in table 6.4. Further correlation testing and comparison with the field data is presented in the next section.

Table 6.4: Accuracy measurement of training and testing data

Data Type	MAPE, %	R ²
Training (Seen)	6.75	0.9973
Testing (Unseen)	7.08	0.997

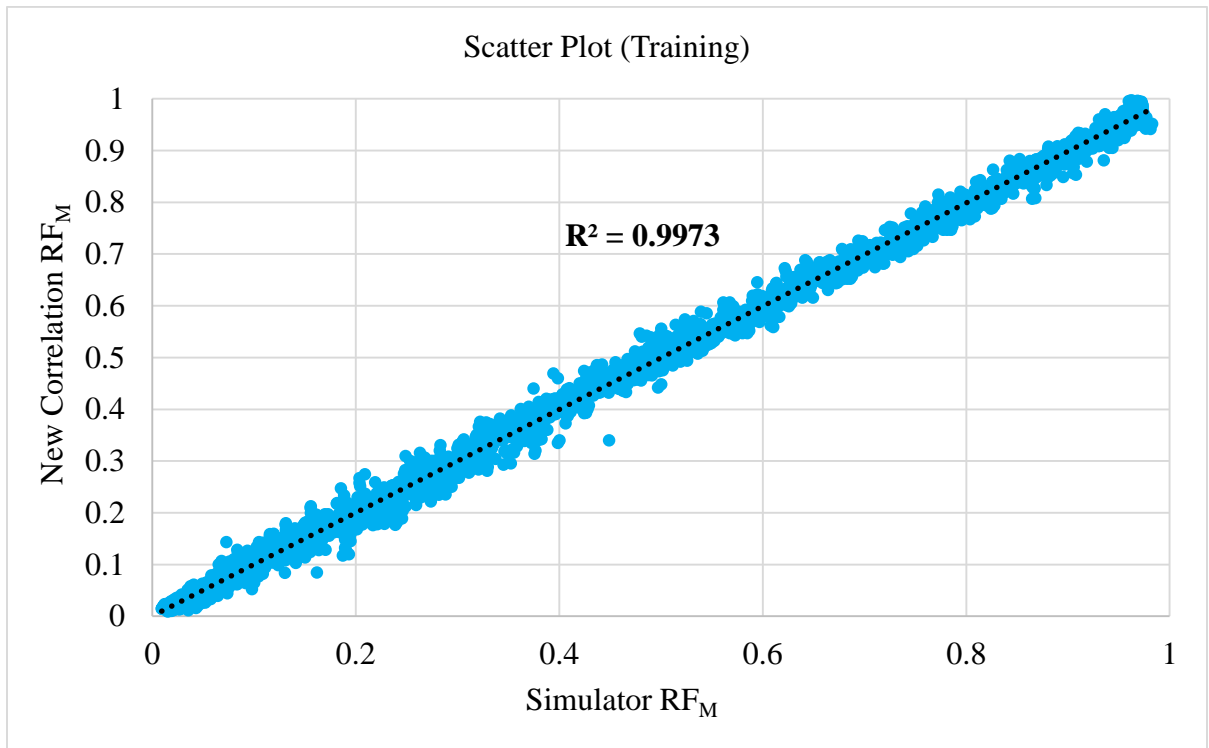


Figure 6.3: Scatter plot for training data

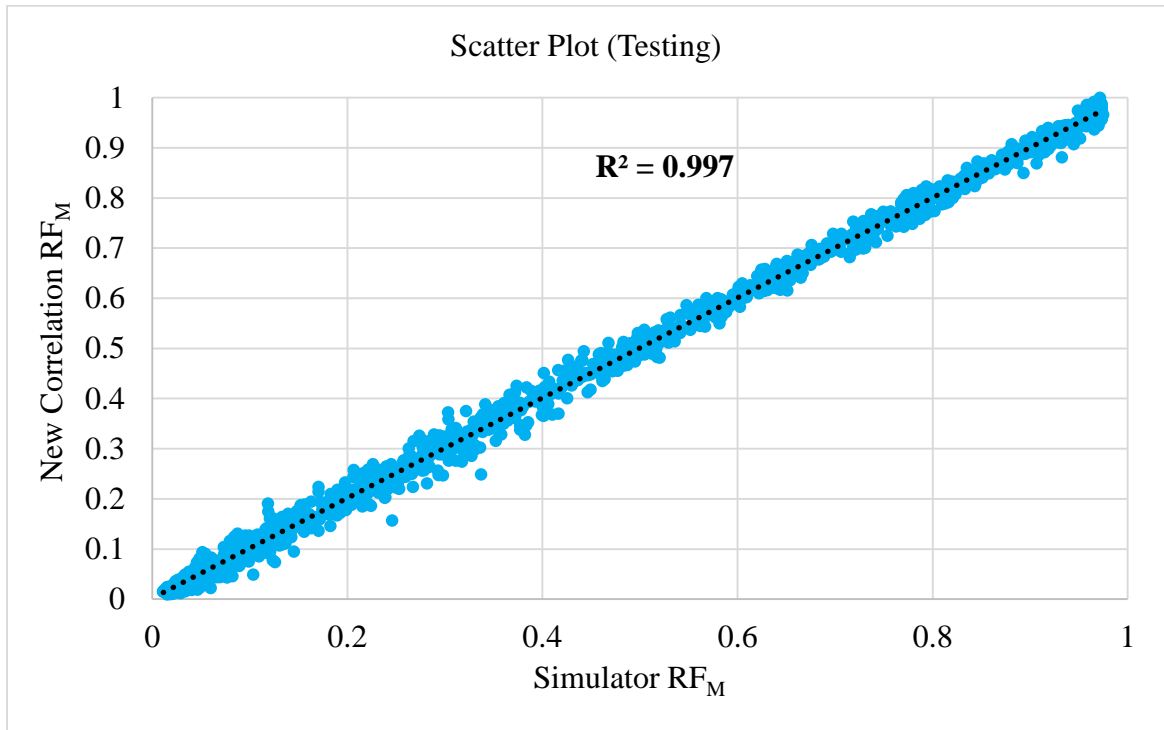


Figure 6.4: Scatter plot for testing data

6.3 Correlation Testing

The newly developed correlation was tested for several mobility ratios and two different wettability systems. These systems were not simulated before. Table 6.5 lists the parameters used in testing the new correlation.

Table 6.5: New correlation testing parameters

	V	M	k_z/k_x	WI
Case 1	0.5	0.7	0.15	0.8
		1		
		4		
Case 2	0.4	0.7	0.25	1.51
		1		
		4		

6.3.1 Case 1: Wettability Indicator=0.8

Figure 6.5 shows the relative permeability curves of the system with WI of 0.8 while Figure 6.6 shows the fractional flow curves at several mobility ratios. The simulation results were compared with the new correlation predictions for different mobility ratios as illustrated in Figure 6.7, which shows an excellent match.

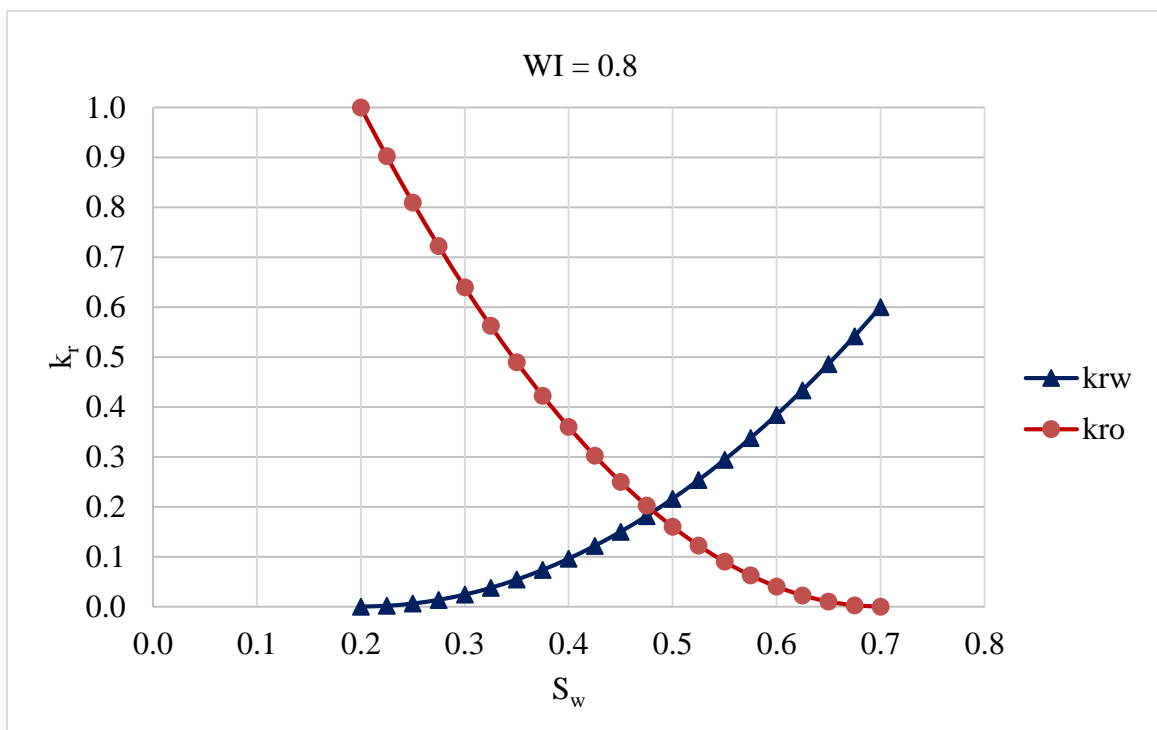


Figure 6.5: Relative permeability curves for case 1

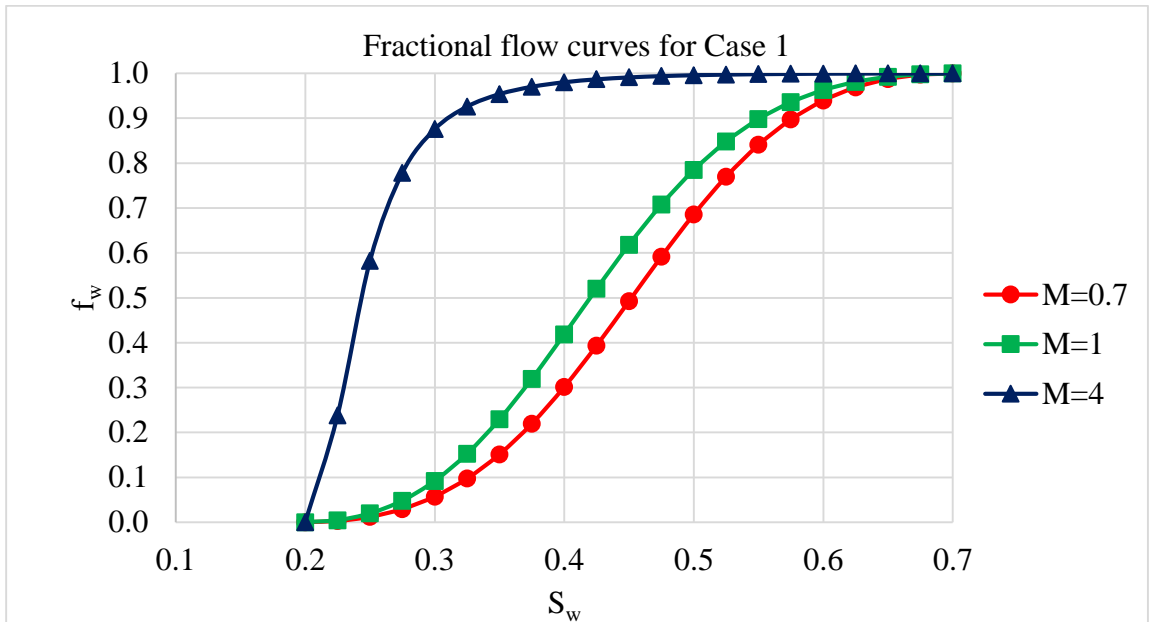


Figure 6.6: Fractional flow curve for case 1

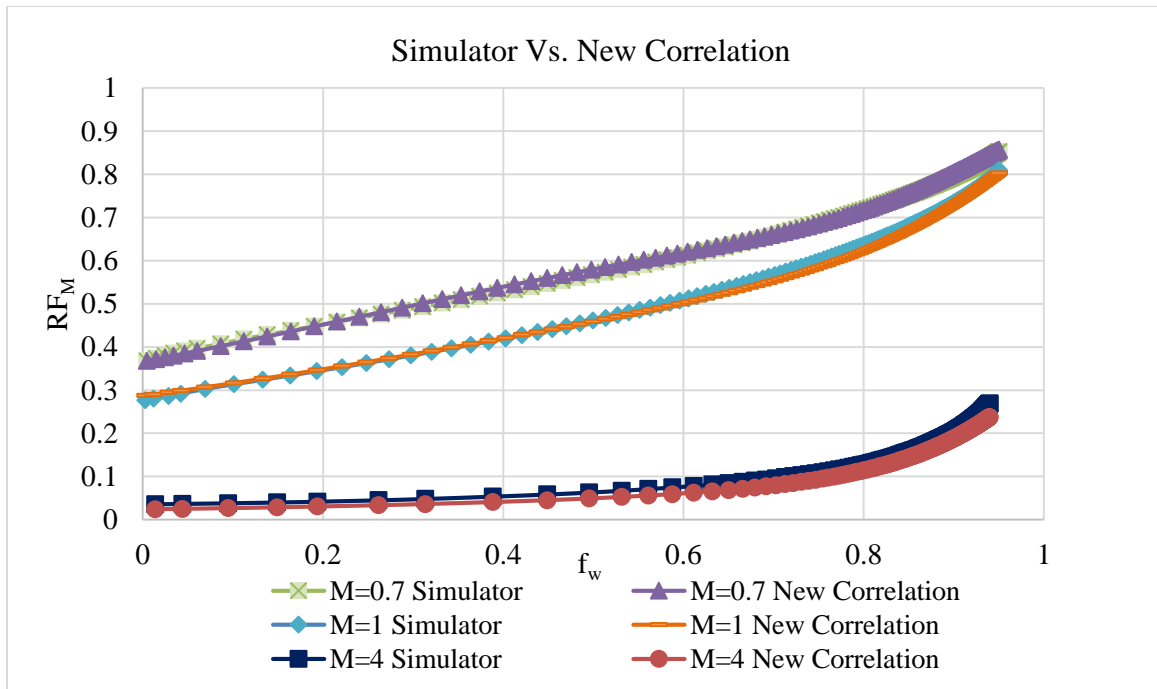


Figure 6.7: Comparison between simulator and new correlation at several M

6.3.2 Case 2: Wettability Indicator=1.51

Figure 6.8 shows the relative permeability curves of the system with WI of 1.51 while Figure 6.9 shows the fractional flow curves at several mobility ratios. Comparison between simulator and new correlation shows excellent match at different mobility ratios as shown in Figure 6.10.

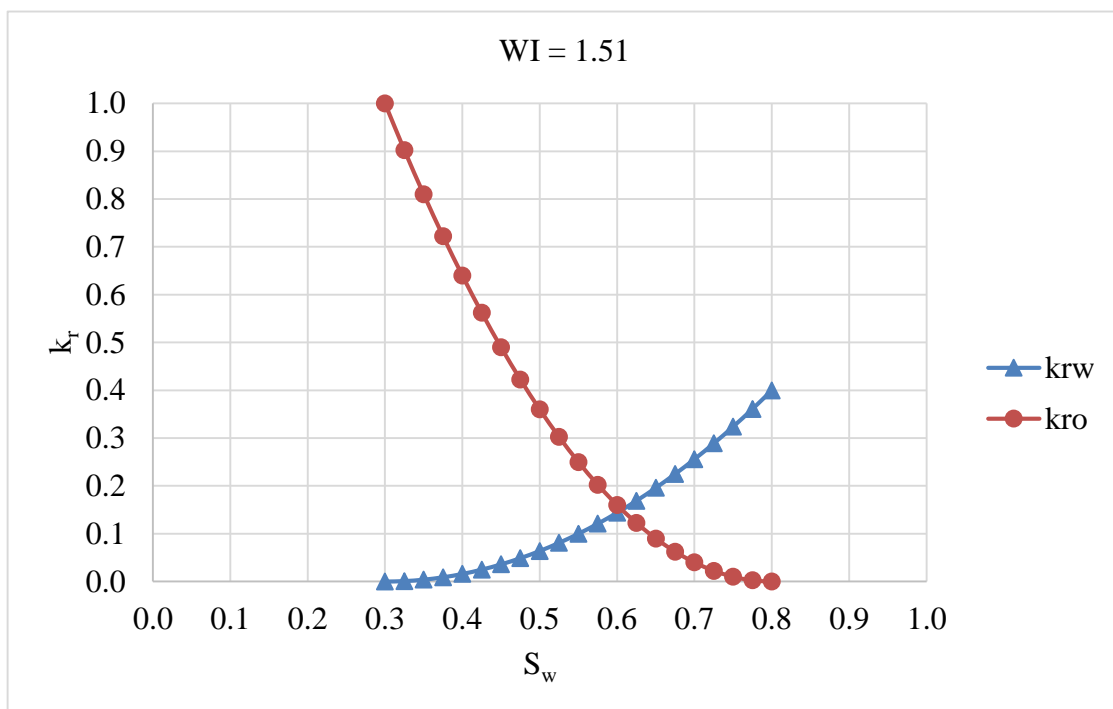


Figure 6.8: Relative permeability curves for case 2

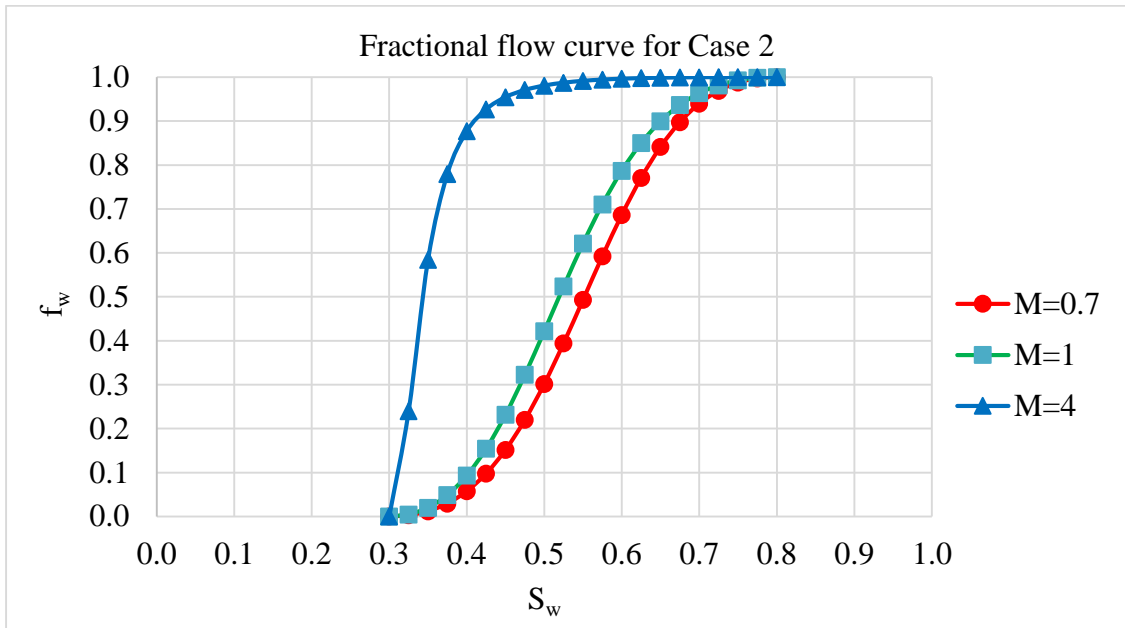


Figure 6.9: Fractional flow curves for several M

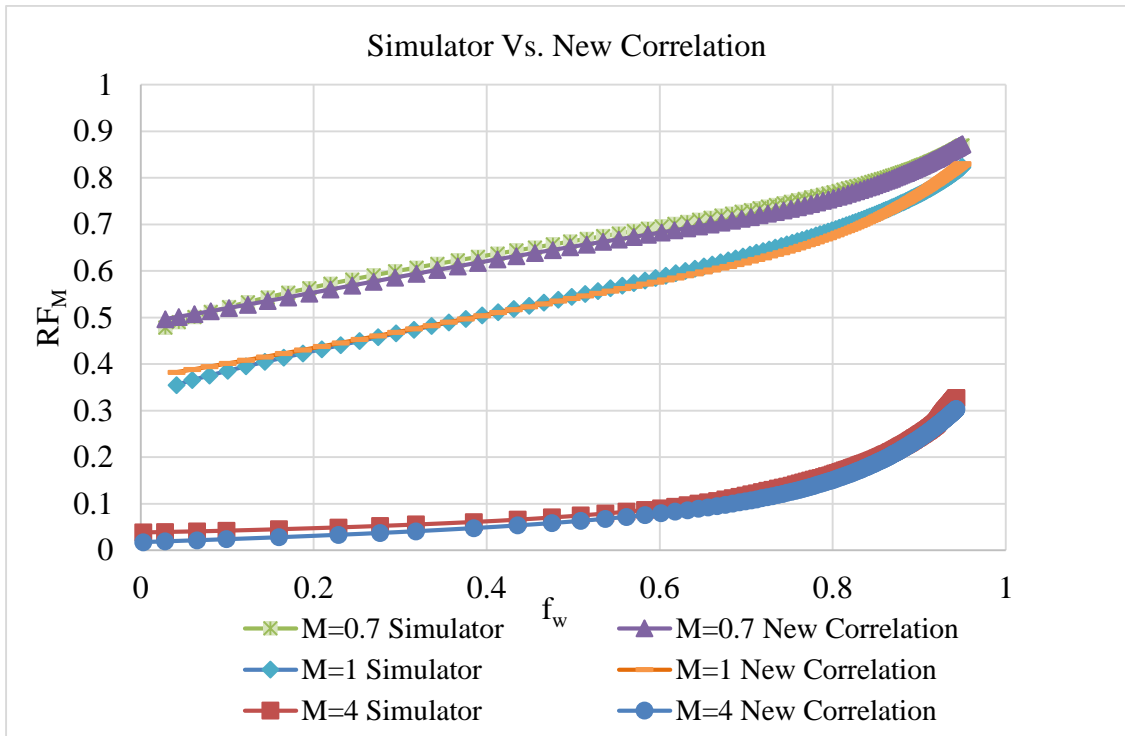


Figure 6.10: Comparison between simulator and new correlation at several M

6.3.3 Wettability Indicator Testing

The correlation was further tested for seven cases involving five new wettability systems at random values of V , M , α and water cuts as detailed in Table 6.6. Figure 6.11 shows relative permeability curves for five new systems. Fractional flow curves for those cases are shown in Figure 6.12. Scatter plot between simulator vs. the developed new correlation is shown in Figure 6.13, which confirms the high quality of the new correlation ($R^2 > 0.99$).

Table 6.6: New correlation testing parameters (with several values of WI)

Cases	V	M	k_z/k_x	WI
1	0.5	2	0	0.6
2	0.7	0.2	0.2	0.7
3	0.5	4	0.15	0.8
4	0.5	4	0.1	1
5	0.4	0.7	0.25	1.51
6	0.3	0.5	0	2.26
7	0.9	1	0.3	2.73

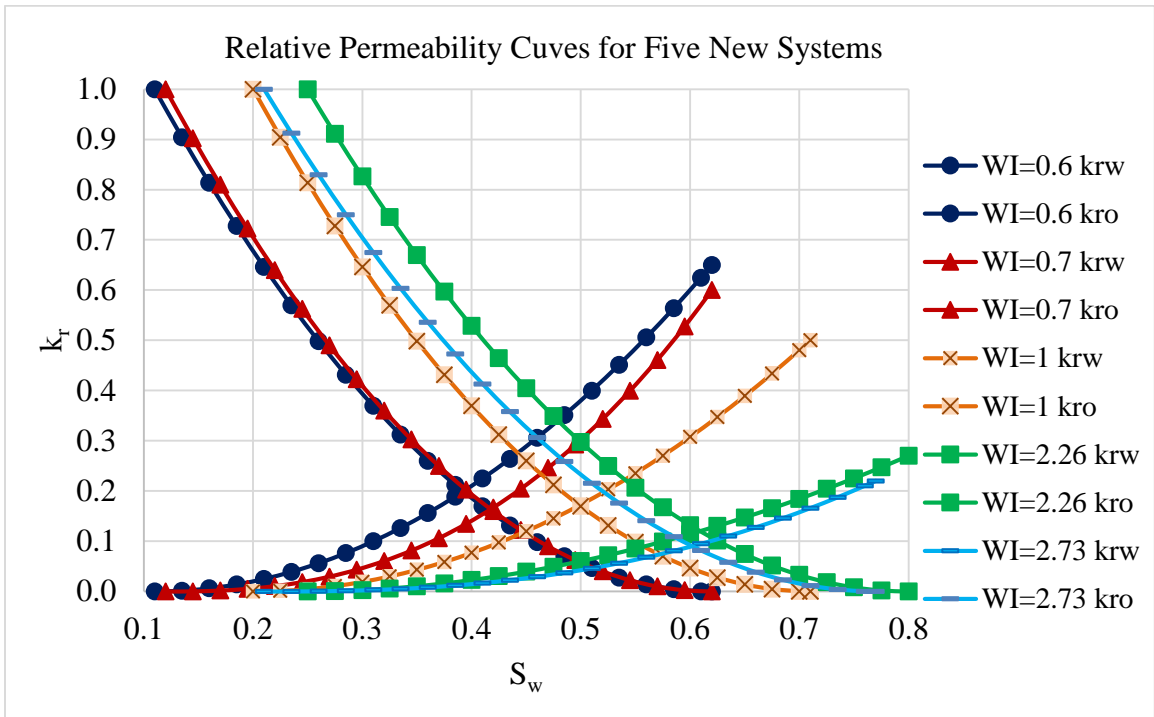


Figure 6.11: Relative permeability curves for 5 other systems

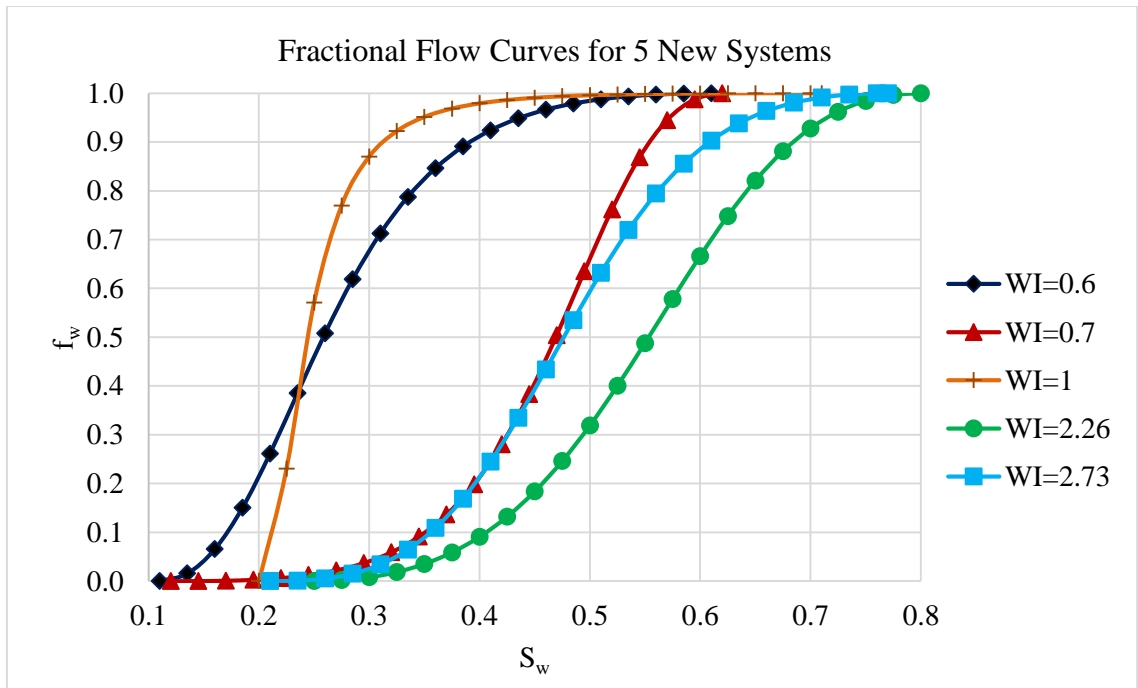


Figure 6.12: Fractional flow curves for 5 new systems

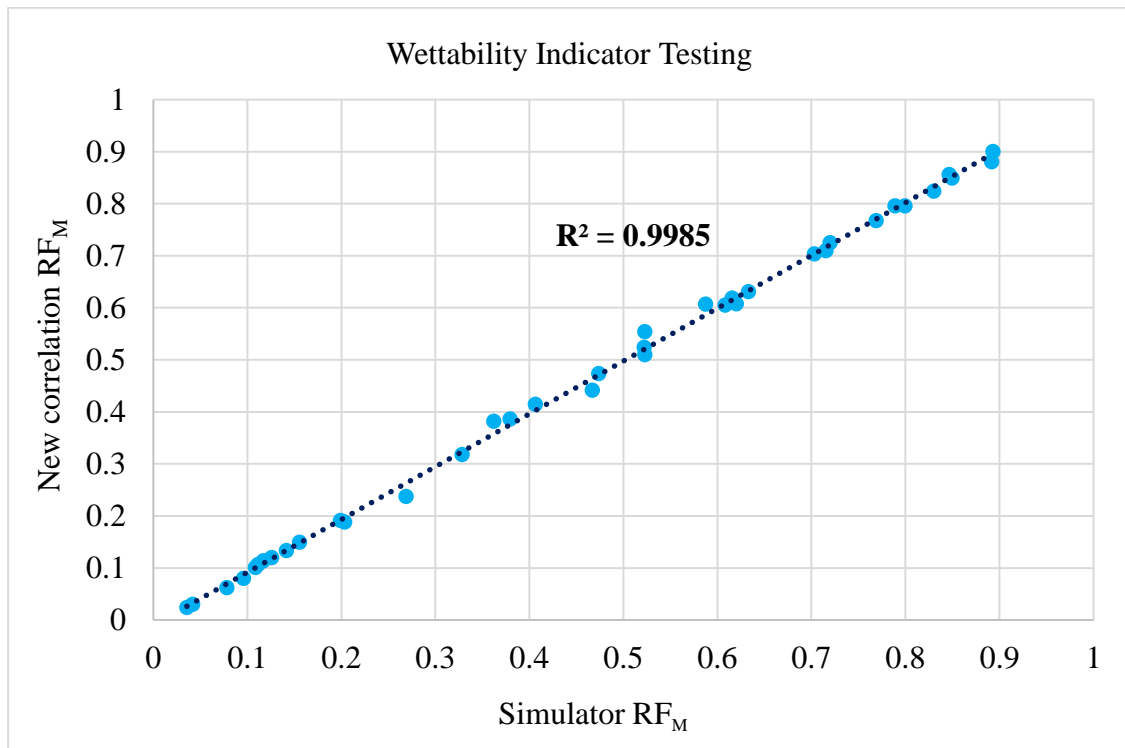


Figure 6.13: Scatter plot for WI testing between simulator vs. new correlation

6.4 Comparison with Field Data

Two different field cases (Espinel, 2010) were tested with the newly developed correlation. This field data belongs to infill wells with no primary production.

6.4.1 Case 1: Field A

Field A is a highly heterogeneous reservoir with water wet rock that is flooded at a mobility ratio 0.439. Reservoir properties are presented in Table 6.7. Relative permeability and fractional flow curves for the reservoir are shown in Figures 6.34 and 6.35, respectively.

Comparison between actual field performance and the newly developed correlation shows a good match as presented in Figure 6.16. The new correlation matched the data perfectly up to $RF_M = 82\%$. At that point, the well was apparently worked over to reduce water production (notice sudden drop in WOR). The initial deviation between the new correlation and Field A data upto $WOR = 0.2$ is due to the fact that water breakthrough in real fields may occur before the waterflood water from the injector. The early water breakthrough may be as a result of formation water or water coming from aquifer.

Table 6.7: Data for Field A

Data for Field A	
Parameter	Value
Initial water saturation, S_{wi}	0.38
Residual oil saturation, S_{or}	0.23
Initial gas saturation, S_{gi}	0.01
Water viscosity, μ_w , cP	0.9
Oil viscosity, μ_o , cP	1.2
Oil formation volume factor, B_o , RB/STB	1.15
Water formation volume factor, B_w , RB/STB	1
End-point oil relative perm, $(k_{ro})_{S_{wi}}$	0.96865
End-point water relative perm, $(k_{rw})_{S_{or}}$	0.551
Corey's oil exponent, n_o	3.017
Corey's water exponent, n_w	1.8045
Permeability variation coefficient, V	0.8
Anisotropy ratio, k_z/k_x	0.1
Oil density, lb/ft ³	49.1
Water density, lb/ft ³	62.42

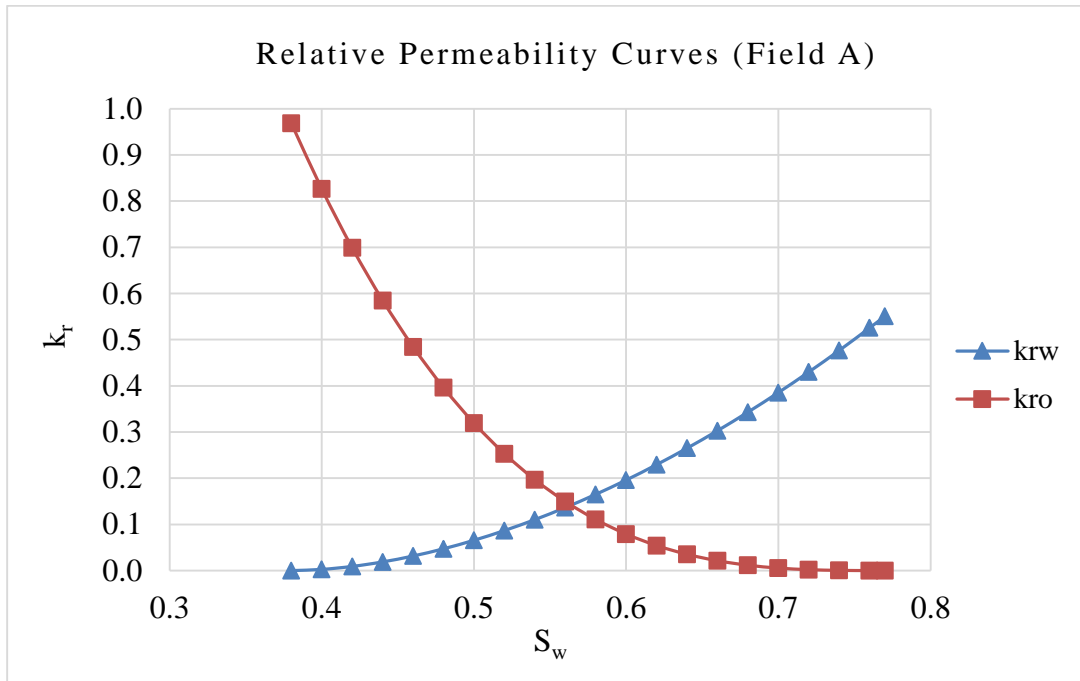


Figure 6.14: Relative permeability curves for field A

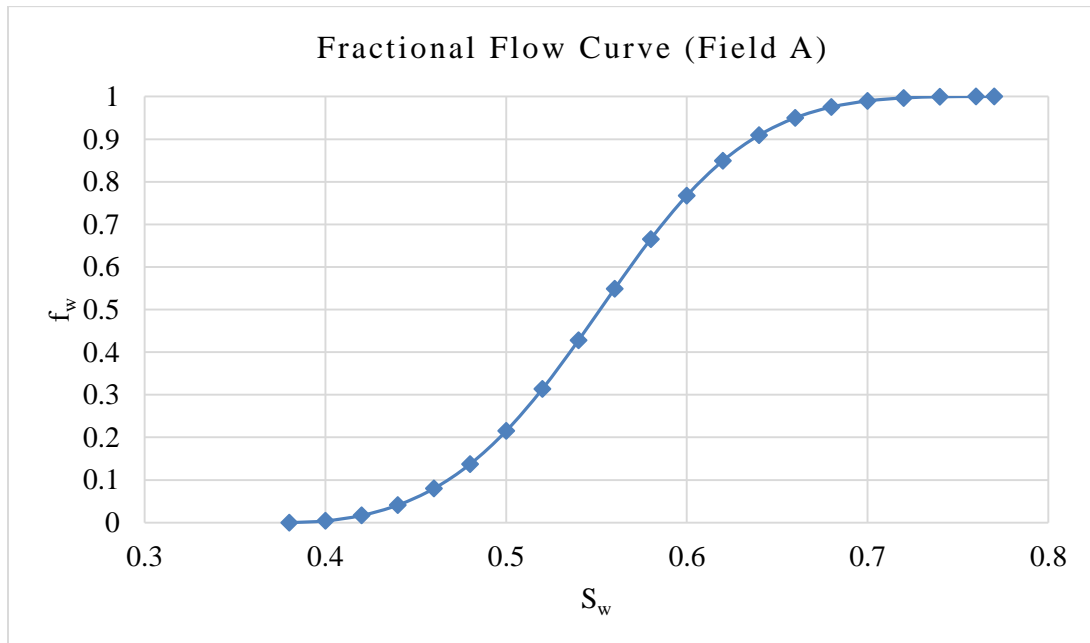


Figure 6.15: Fractional flow curve for field A

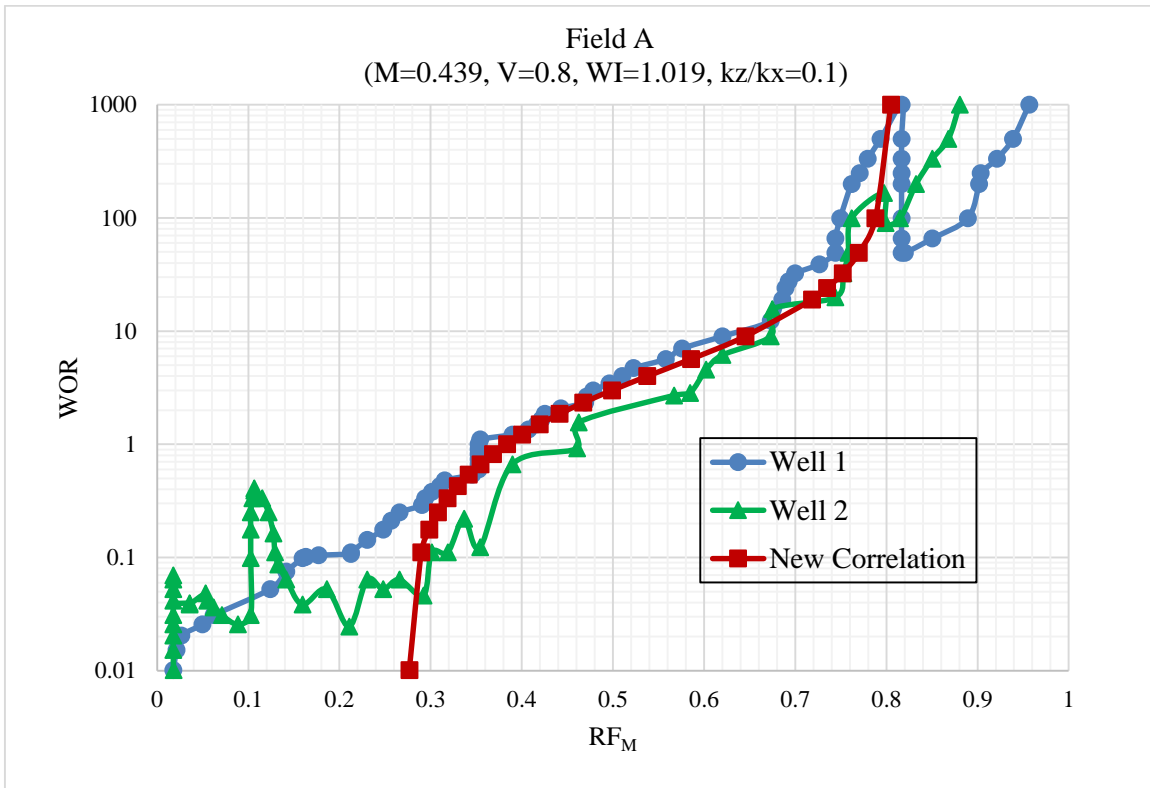


Figure 6.16: Comparison of water flood performance of two different wells from Field A with the new correlation

6.4.2 Case 2: Field B

Field B is a reservoir with high heterogeneity and neutral wet rock with mobility ratio 0.94. Reservoir properties for field B are presented in Table 6.8. Relative permeability and fractional flow curves for field B are shown in Figures 6.37 and 6.38, respectively. Comparison between actual performance of field B and the prediction of the newly developed correlation also shows a good match as presented in Figure 6.39. The ultimate values of movable oil recovery factor are 63% and 67% for field and new correlation

respectively. The new correlation followed the data trend very well. The initial deviation between the new correlation and Field B data upto WOR = 0.02 is due to the fact that water breakthrough in real fields may occur before the waterflood water from the injector. The early water breakthrough may be as a result of formation water or water coming from aquifer.

Table 6.8: Data for Field B

Data for Field B	
Parameter	Value
Initial water saturation, S_{wi}	0.17
Residual oil saturation, S_{or}	0.25
Initial gas saturation, S_{gi}	0
Water viscosity, μ_w , cP	0.25
Oil viscosity, μ_o , cP	2.54
Oil formation volume factor, B_o , RB/STB	1.108
Water formation volume factor, B_w , RB/STB	1
End-point oil relative perm, $(k_{ro})_{S_{wi}}$	1.0
End-point water relative perm, $(k_{rw})_{S_{or}}$	0.25
Corey's oil exponent, n_o	3.0
Corey's water exponent, n_w	2.0
Permeability variation coefficient, V	0.8
Anisotropy ratio, k_z/k_x	0.1
Oil density, lb/ft ³	49.1
Water density, lb/ft ³	62.42

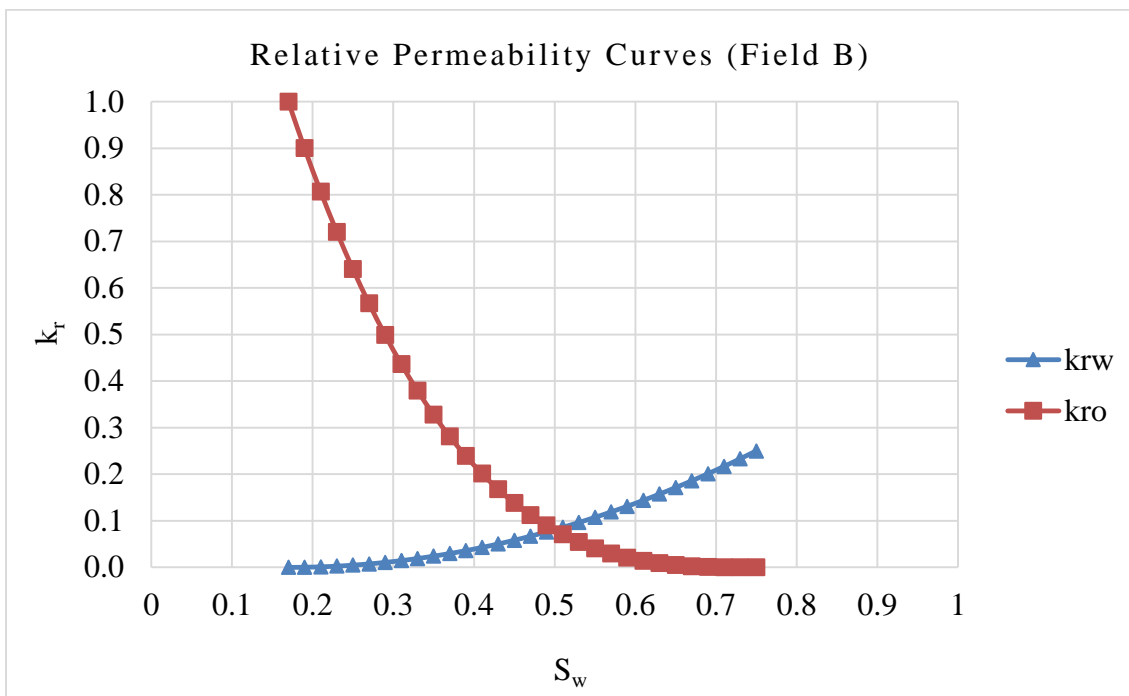


Figure 6.17: Relative permeability curves for field B

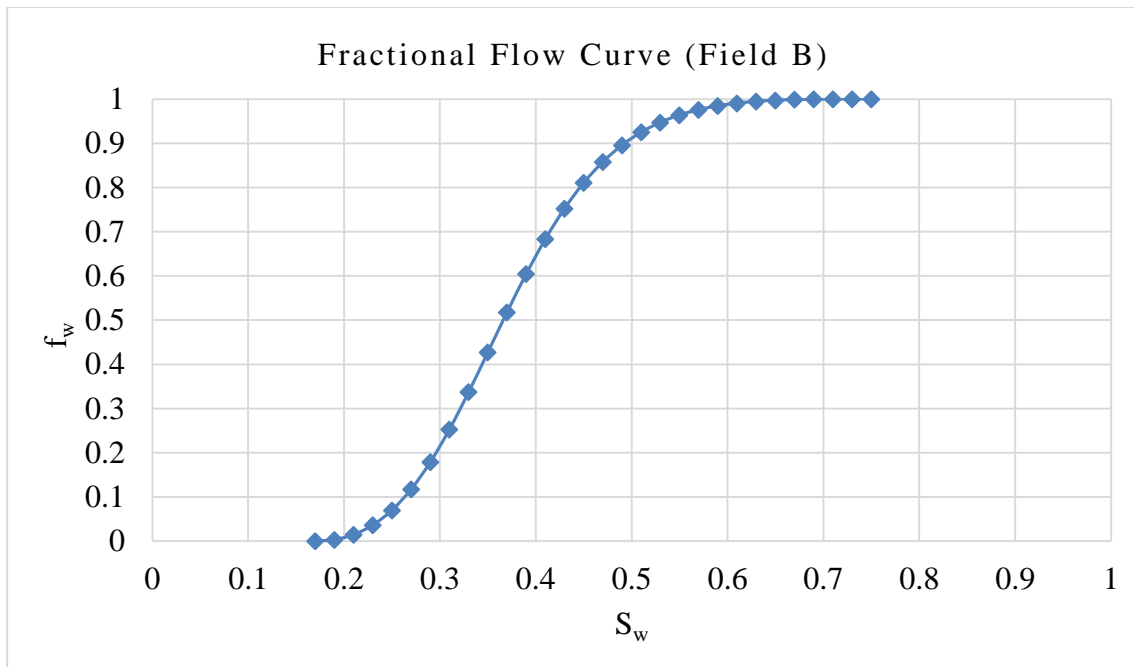


Figure 6.18: Fractional flow curve for field B

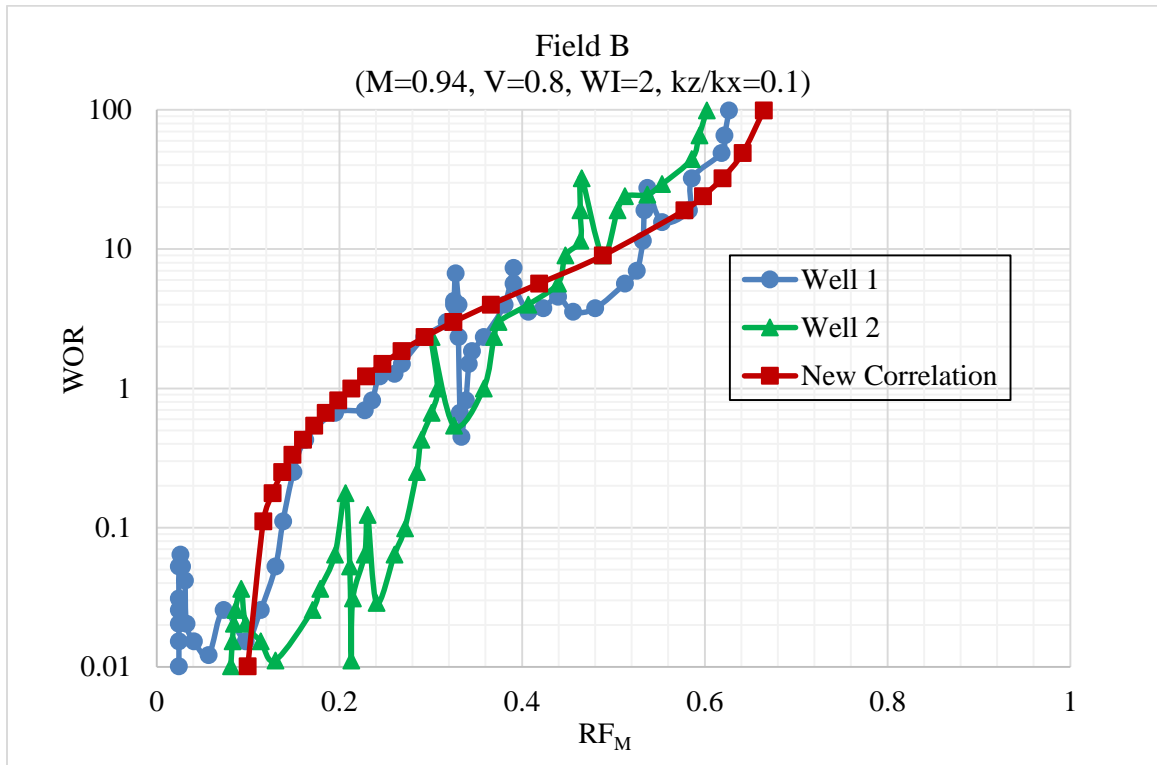


Figure 6.19: Comparison of water flood performance of two different wells from Field B with the new correlation

6.5 Comparison with Craig-Geffen-Morse Method

The Craig, Geffen and Morse's (CGM) method, described in Chapter 2, applies to 5-spot water flooding in homogenous reservoirs. To further test the predictions of the new correlation developed in this study against the CGM predictions, system 2 with a mobility ratio of 1.062 was selected. The recovery factor with no crossflow at three different water cuts were predicted by using new correlation at $V = 0$, which represents a homogeneous reservoir. Figure 6.20 shows the fractional-flow curve for this system at $M = 1.062$.

Because of the difference in definitions, the corresponding value of M by the CGM's method is 1. Figure 6.21 compares recovery predictions of the new correlation for a homogeneous system with the CGM estimates. The maximum relative error between the two predictions is 4.28%.

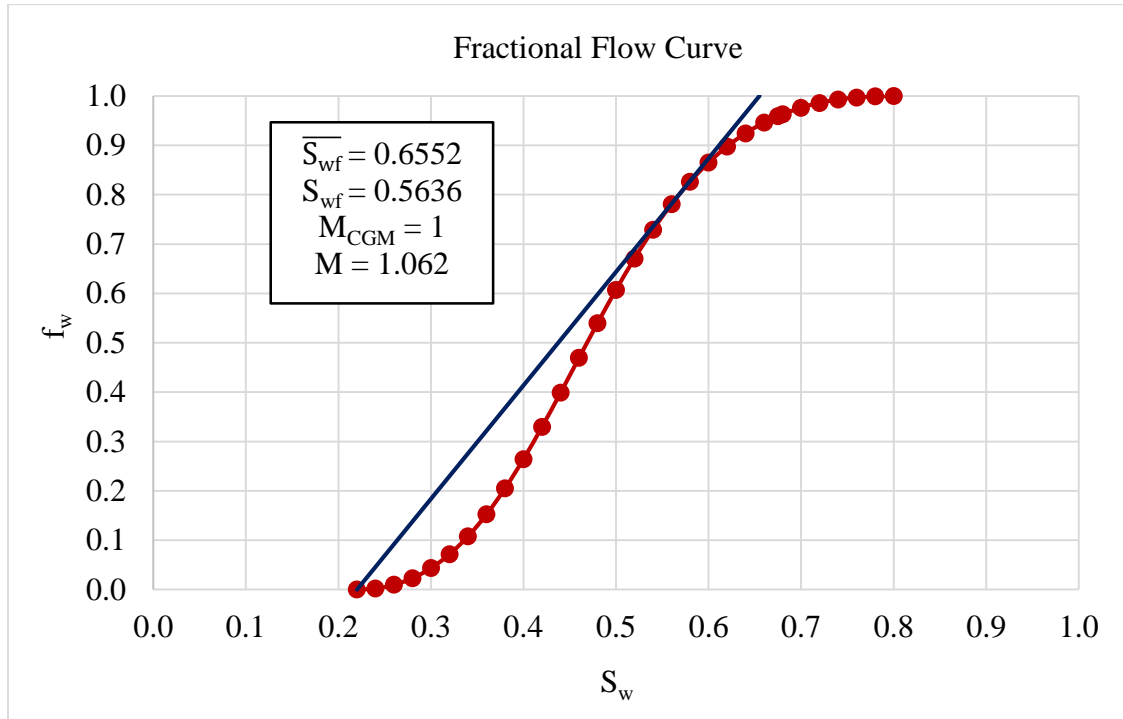


Figure 6.20 Fractional flow curve for System 2 at M=1.062

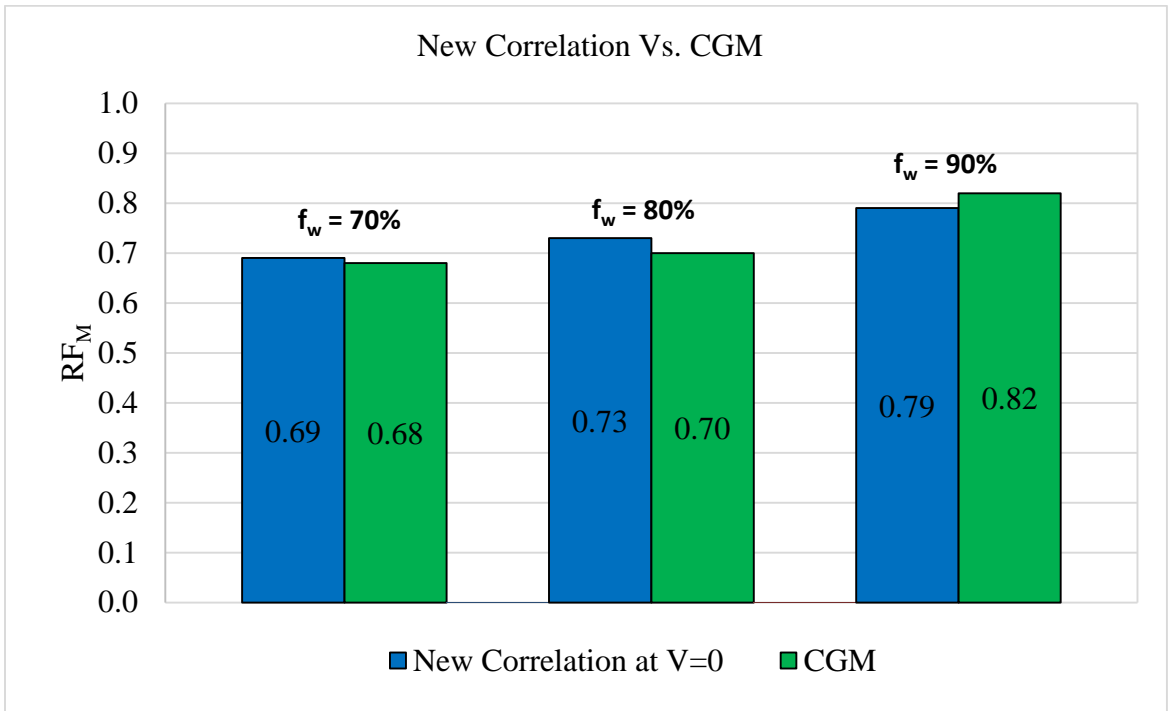


Figure 6.21: Comparison of new correlation with the CGM Method

CHAPTER 7

CONCLUSIONS AND RECOMMENDATIONS

This research work was conducted to analyze the performance of a five-spot, water-flooding pattern in both communicating and non-communicating stratified reservoirs. Conclusions and some recommendations from this study are presented in this chapter.

7.1 Conclusions

Conclusions drawn from this study are:

- 1- Based on numerical simulation results, a new empirical correlation has been developed to predict the performance of a 5-spot water flood in a stratified reservoir.
- 2- The new correlation predicts the movable oil recovery in terms of the flood's mobility ratio, the reservoir's permeability variation and permeability anisotropy ratio, rock wettability and production water cut.
- 3- The new correlation was developed using artificial neural networks with optimum number of weights and biases.
- 4- A new parameter called the 'wettability indicator' has been introduced to quantify rock wettability from the relative permeability curves.
- 5- The new correlation was able to match actual field data with good accuracy.

7.2 Recommendations for Future Work

Recommendations for the future work are:

1. The density ratio in this study was taken as 1, which nullifies the gravity crossflow. This work can be extended for several density ratios to encounter the crossflows due to gravity.
2. Capillary pressure effects were neglected in this research. Future work can include capillary pressure, especially for very low permeability reservoirs.
3. Experiments could be run using rock blocks of various wettabilities to test the new correlation.
4. Lorenz coefficient (L) should be considered for reservoir heterogeneity quantification for the future work instead of Dykstra-Parsons permeability variation coefficient because L also considers random distribution of porosity.
5. The new correlation should also be tested with more field data.

References

- Craig, F., Geffen, T., and Morse, R., "Oil Recovery Performance of Pattern Gas or Water Injection Operations from Model Tests," JPT, Vol. 204, pp. 7-15, Jan. 1955.
- Craig, F.F., "Effect of Reservoir Description on Performance Predictions," JPT, pp. 1239-1245, Oct. 1970.
- de Souza, A., and Brigham, W., "A Study on Dykstra-Parsons Curves," TR29, Stanford University Petroleum Research Institute, Palo Alto, California, 1981.
- Dykstra, H., and Parsons, R., "The Prediction of Oil Recovery by Water Flood," in Secondary Recovery of Oil in the United States, 2nd edition, Washington, DC, American Petroleum Institute, pp. 160-174, 1950.
- El-Khatib, N., "Effect of Gravity on Waterflooding Performance of Stratified Reservoirs," paper SPE 81465 presented at the SPE 13th Middle East Oil Show & Conference, Bahrain, April 2003.
- El-Khatib, N., "The Effect of Crossflow on Waterflooding of Stratified Reservoirs," SPE Journal of Reservoir Engineering, pp. 291-302, April 1985.
- El-Khatib, N., "The Modification of the Dykstra-Parsons Method for Inclined Stratified Reservoirs," SPE Journal, pp. 1029-1040, Dec. 2012.
- El-Khatib, N., "Waterflooding Performance of Communicating Stratified Reservoirs with Log-Normal Permeability Distribution," SPE Journal of Reservoir Evaluation & Engineering, Vol. 2, No. 6, pp. 542-549, Dec. 1999.
- Espinel, A.L., "Generalized Correlations to Estimate Oil Recovery and Pore Volumes Injected in Waterflooding Projects," PhD dissertation, Texas A&M University, College Station, Texas, Dec. 2010.
- Espinel, A.L., and Barrufet, M.A., "A Generalized Semi-Analytical and Statistical Model to Estimate Oil and Water Production, Pore Volume Injected, and Ultimate Recovery in Mature Waterflooding Projects," paper SPE 122749 presented at the SPE Latin American and Caribbean Petroleum Engineering Conference, Cartagena, Colombia, June 2009.
- Fassihi, M.R., "New Correlations for Calculation of Vertical Coverage and Areal Sweep Efficiency," SPE Journal of Reservoir Engineering, pp. 604-606, Nov. 1986.
- Felsenthal, M., Cobb, T.R., and Heuer, G.J., "A Comparison of Waterflood Evaluation Methods," paper SPE 332 presented at the SPE 5th Secondary Recovery Symposium, Wichita Falls, Texas, May 1962.
- Fettke, C.R., "Bradford Oil Field, Pennsylvania and New York," Pennsylvania Geological Survey, 4th Series, M-21, 1938.

Goddin, C.S., Craig, F.F., Wilkes, J.O., and Tek, M.R., "A Numerical Study of Waterflood Performance in a Stratified System with Crossflow," paper SPE 1223 presented at the SPE Annual Fall Meeting, Denver, Colorado, June 1966.

Guerrero, E. T., and Earlougher, R. C., "Analysis and Comparison of Five Methods Used to Predict Water-flood Reserves and Performance," paper API-61-078 presented at the Spring Meeting of the Mid-Continent District, Division of Production, Tulsa, Oklahoma, April 1961.

Hirasaki, G.J., "Properties of Log-Normal Permeability Distribution for Stratified Reservoirs," SPE 13416-MS, Jan. 1984.

History of Petroleum Engineering, API, Dallas, Texas, 1961.

Johnson, C., "Prediction of Oil Recovery by Water Flood - A Simplified Graphical Treatment of the Dykstra-Parsons Method," Trans. AIME, Vol. 207, pp. 345-346, 1956.

McGuire, M.J., "The Inclusion of Viscous Cross Flow in a Simple Dykstra Parson Model," SPE 2382-MS, 1968.

Mobarak, S., "Waterflooding Performance Using Dykstra-Parsons as Compared with Numerical Model Performance," JPT, pp. 113-115, Jan. 1975.

Osman, M.E., "Waterflooding Performance and Pressure Analysis of Heterogeneous Reservoirs," paper SPE 9656-MS presented at the 2nd Middle East Oil Technical Conference, Manama, Bahrain, March 1981.

Pande, K.K., Ramey, H.J., Brigham, W.E., and Orr, F.M., "Frontal Advance Theory for Flow in Heterogeneous Porous Media," paper SPE 16344 presented at the SPE California Regional Meeting, April 1987.

Tiab, D., "Extension of the Dykstra-Parsons Method to Layered-Composite Reservoirs," paper SPE 15020 presented at the Permian Basin CM & Gas Recovery Conference in Midland, Texas, March 1986.

Warner, G.E., "Waterflooding a Highly Stratified Reservoir," paper SPE 2106 presented at the 8th Secondary Recovery Symposium in Wichita Falls, Texas, May 1968.

APPENDIX

I. Simulation Results for System 1 (WI=0.5)

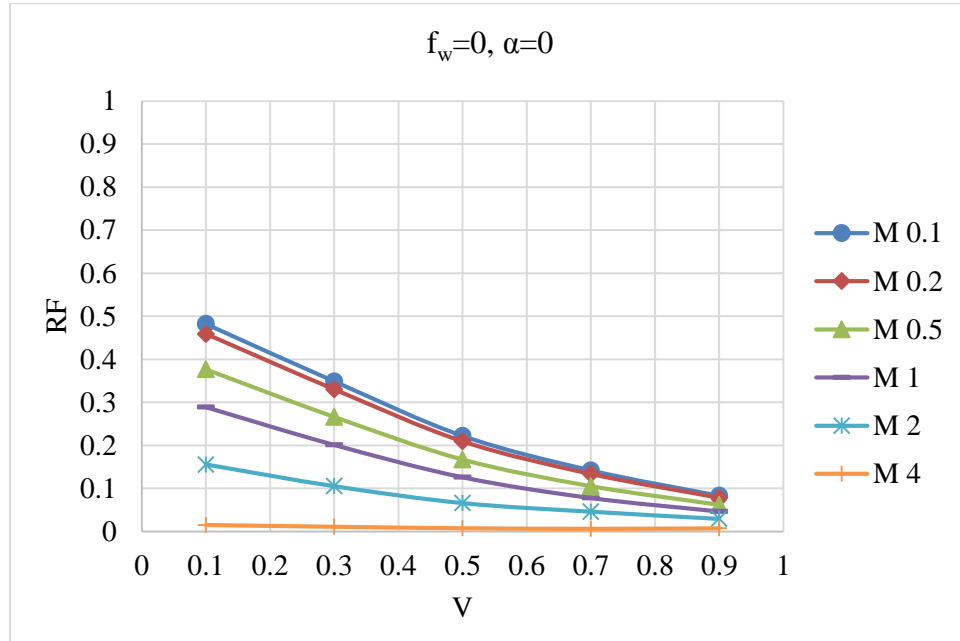


Figure A.1: Recovery factors at breakthrough without crossflow ($\alpha=0$) for system 1

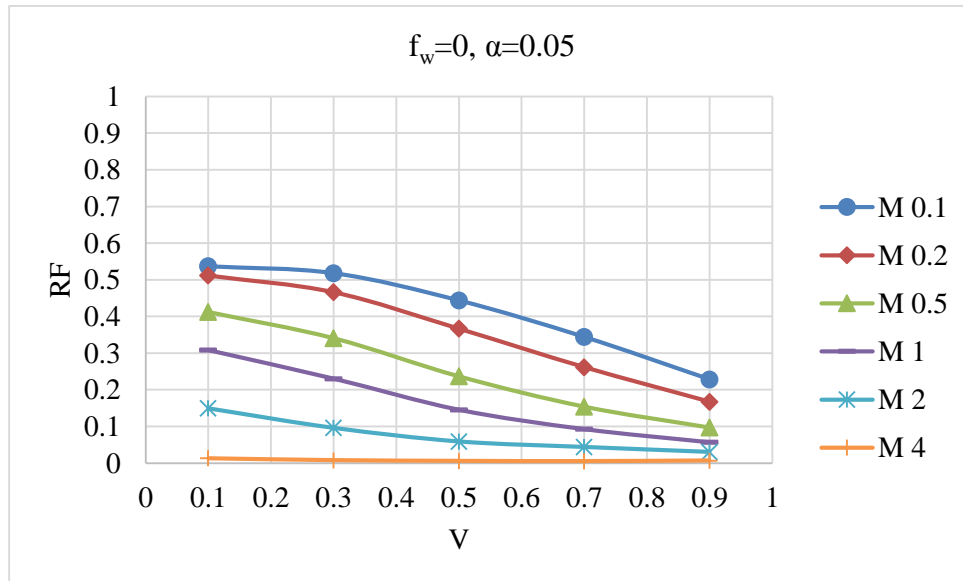


Figure A.2: Recovery factors at breakthrough with crossflow ($\alpha=0.05$) for system 1

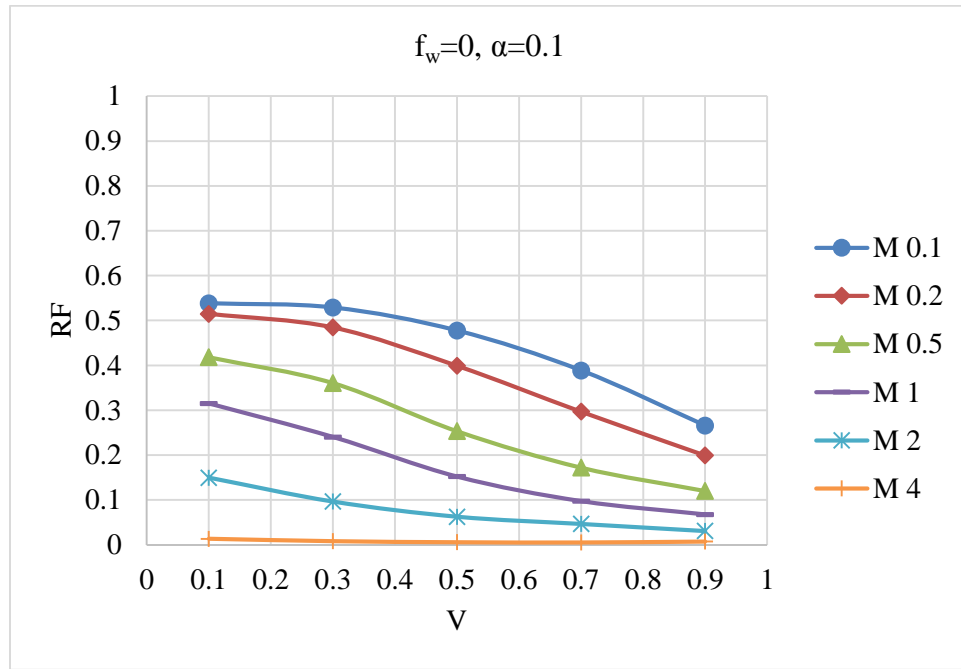


Figure A.3: Recovery factors at breakthrough with crossflow ($\alpha=0.1$) for system 1

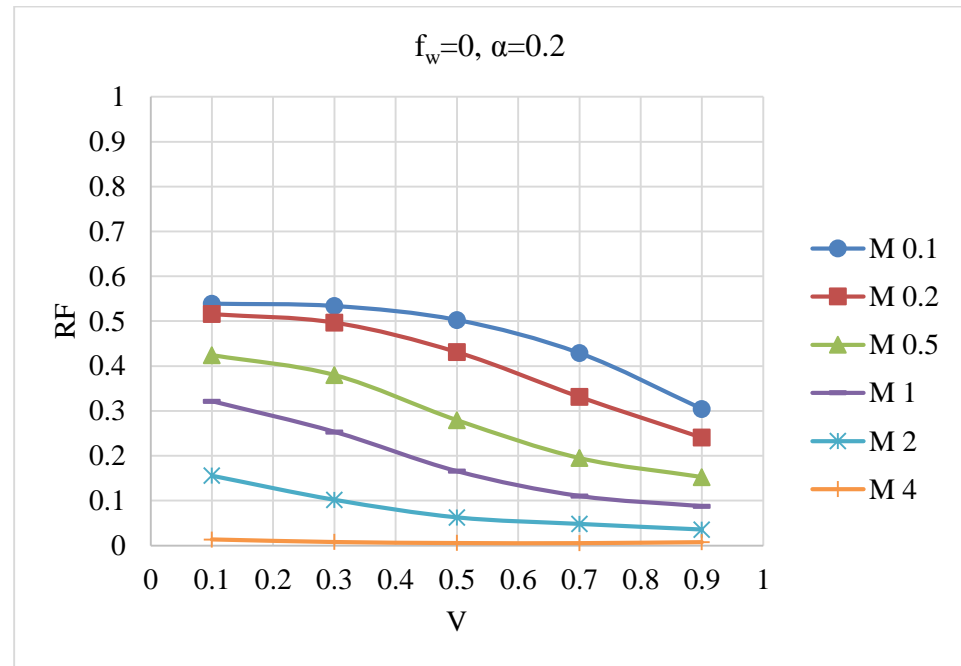


Figure A.4: Recovery factors at breakthrough with crossflow ($\alpha=0.2$) for system 1

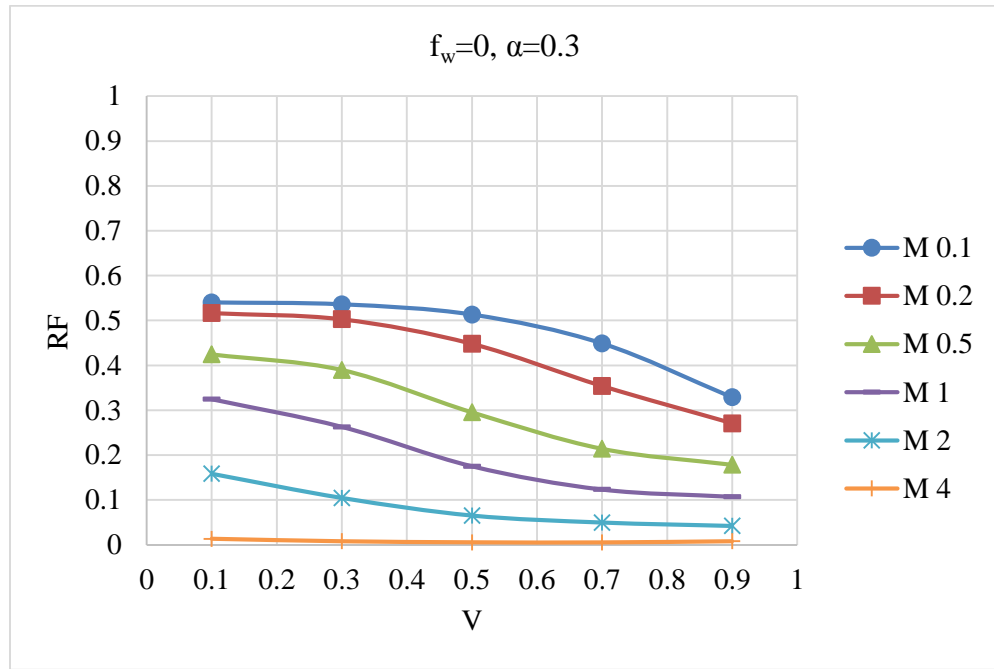


Figure A.5: Recovery factors at breakthrough with crossflow ($\alpha=0.3$) for system 1

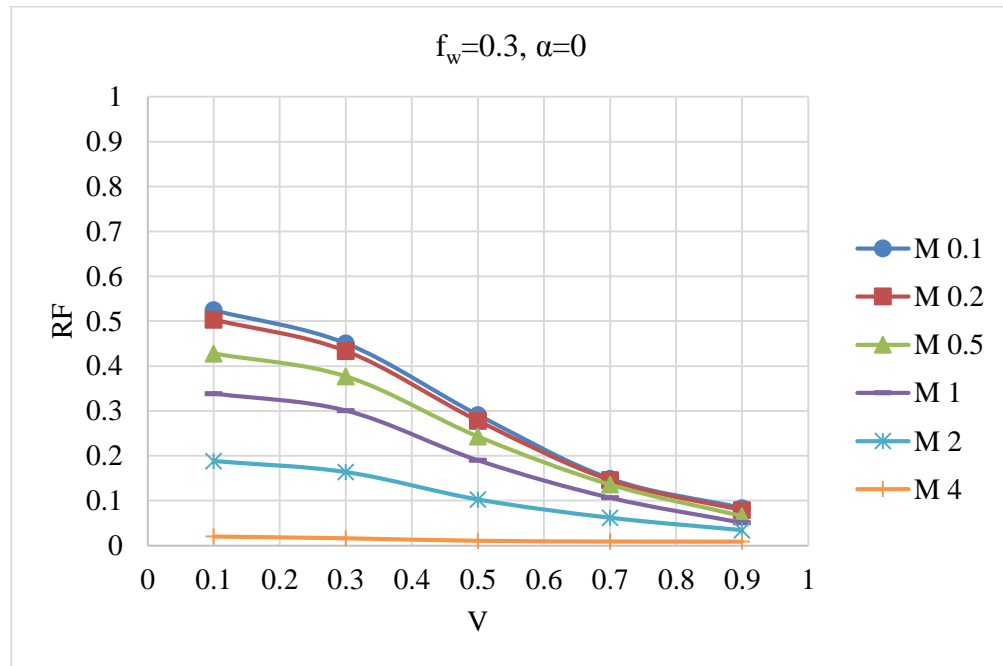


Figure A.6: Recovery factors after breakthrough ($f_w=0.3$) without crossflow ($\alpha=0$) for

system 1

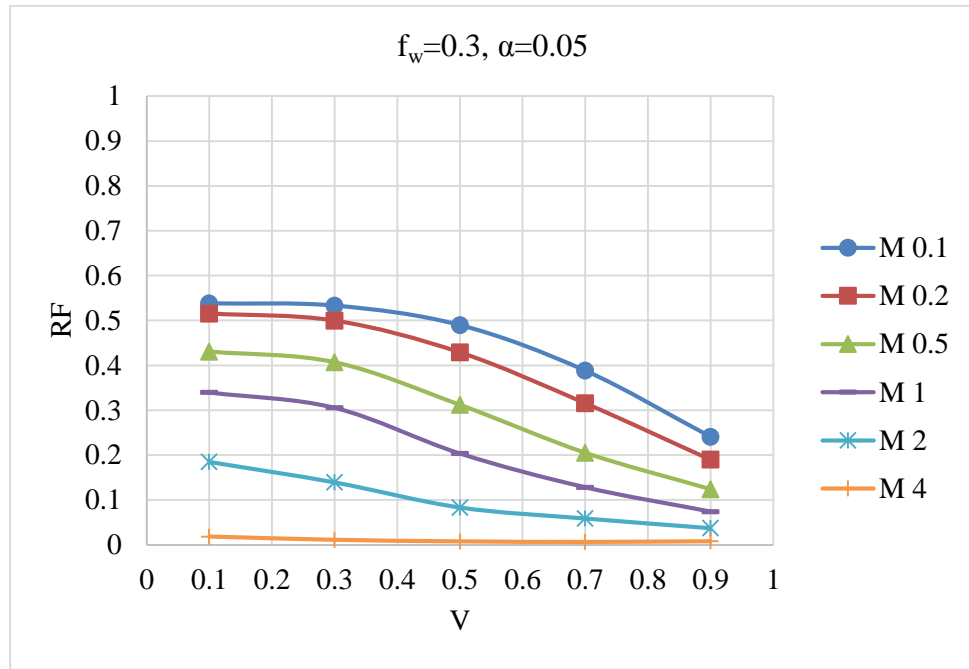


Figure A.7: Recovery factors after breakthrough ($f_w=0.3$) with crossflow ($\alpha=0.05$) for system 1

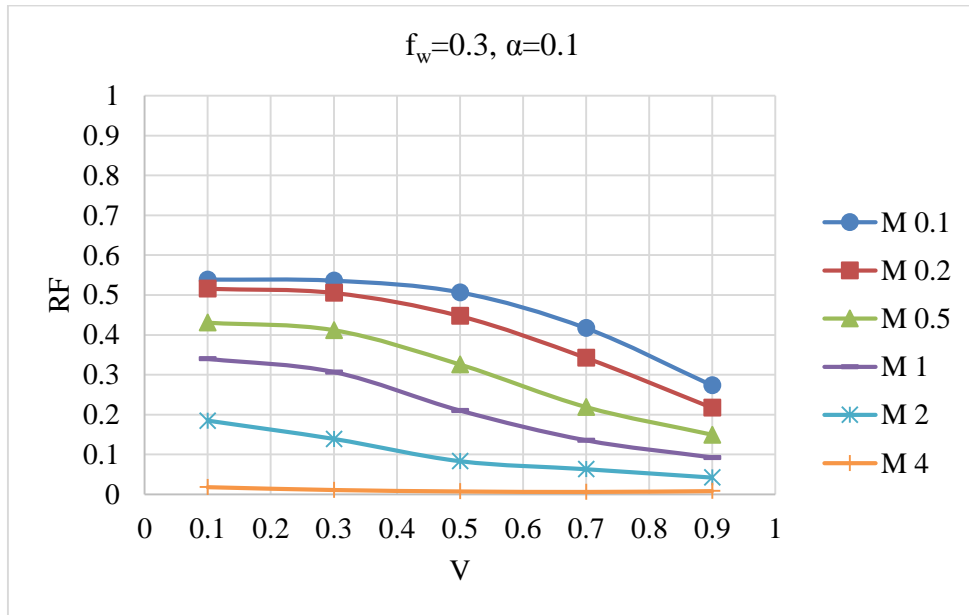


Figure A.8: Recovery factors after breakthrough ($f_w=0.3$) with crossflow ($\alpha=0.1$) for system 1

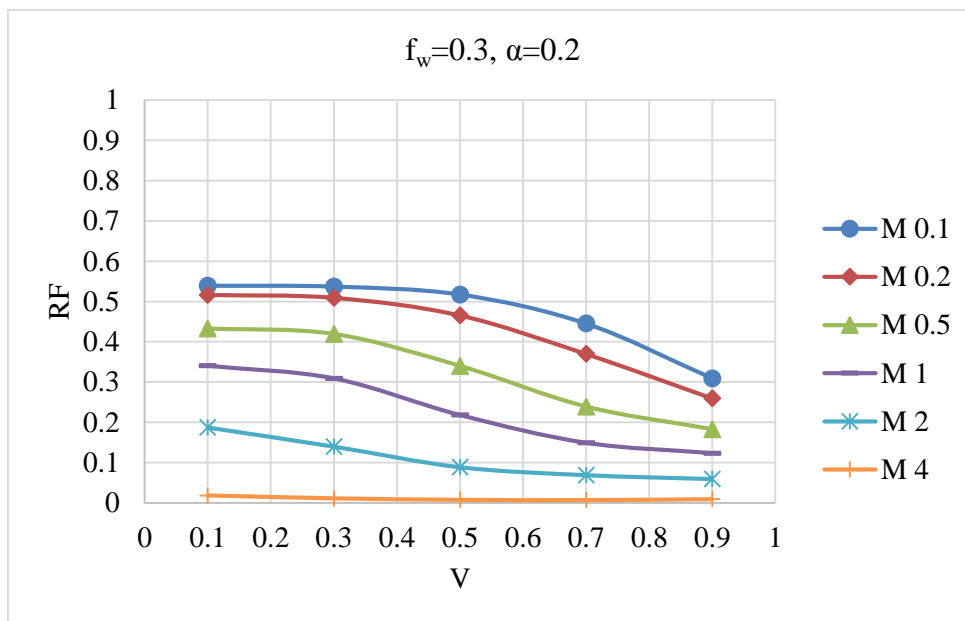


Figure A.9: Recovery factors after breakthrough ($f_w=0.3$) with crossflow ($\alpha=0.2$) for system 1

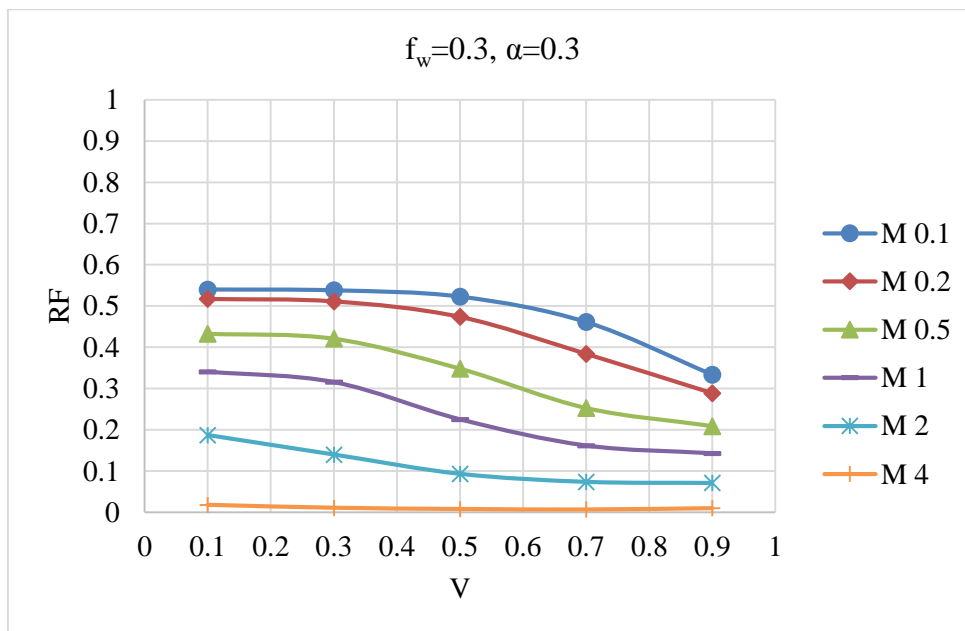


Figure A.10: Recovery factors after breakthrough ($f_w=0.3$) with crossflow ($\alpha=0.3$) for system 1

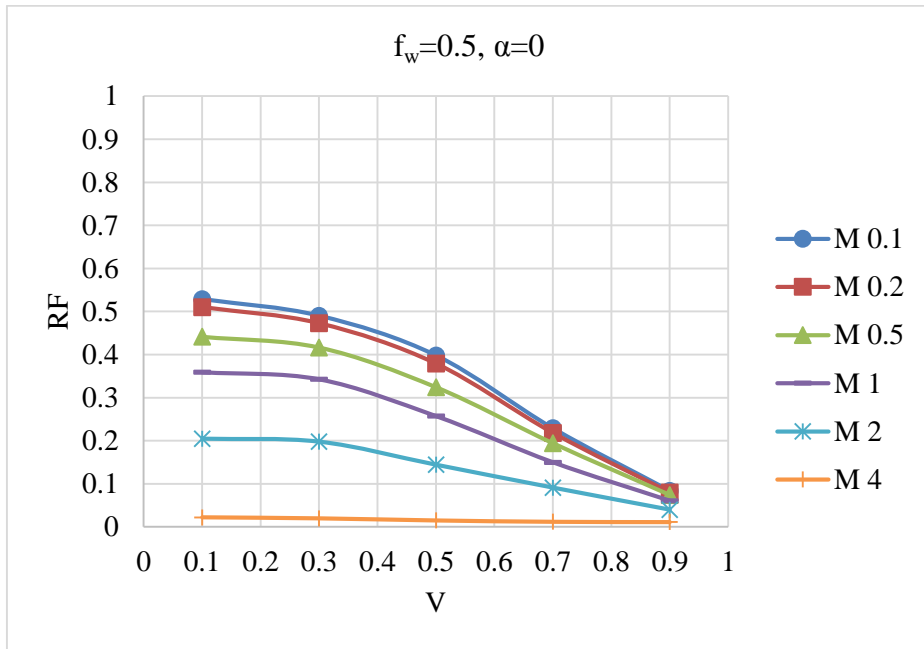


Figure A.11: Recovery factors after breakthrough ($f_w=0.5$) without crossflow ($\alpha=0$)
for system 1

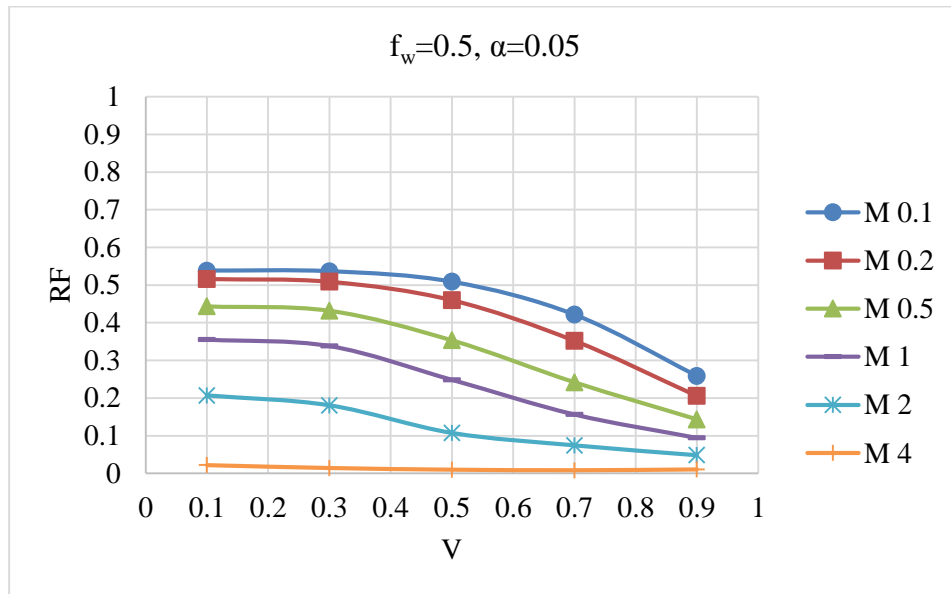


Figure A.12: Recovery factors after breakthrough ($f_w=0.5$) with crossflow ($\alpha=0.05$)
for system 1

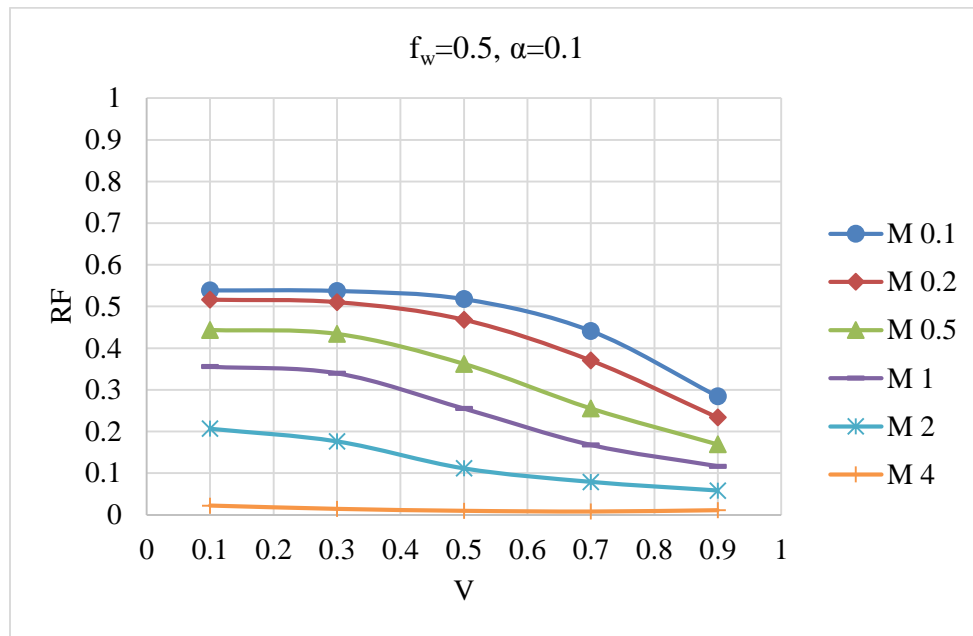


Figure A.13: Recovery factors after breakthrough ($f_w=0.5$) with crossflow ($\alpha=0.1$) for

system 1

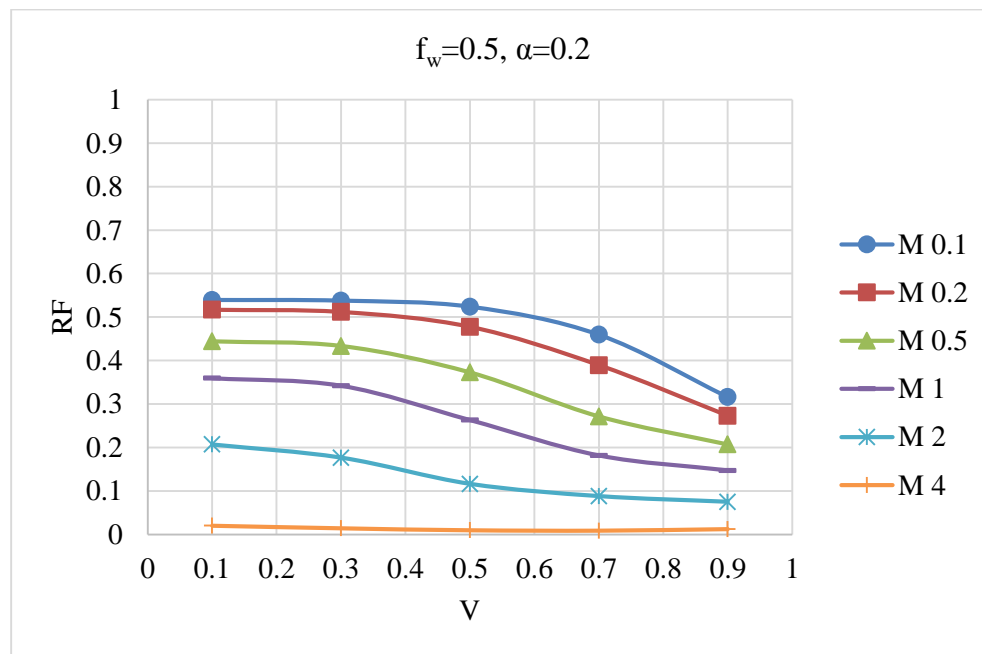


Figure A.14: Recovery factors after breakthrough ($f_w=0.5$) with crossflow ($\alpha=0.2$) for

system 1

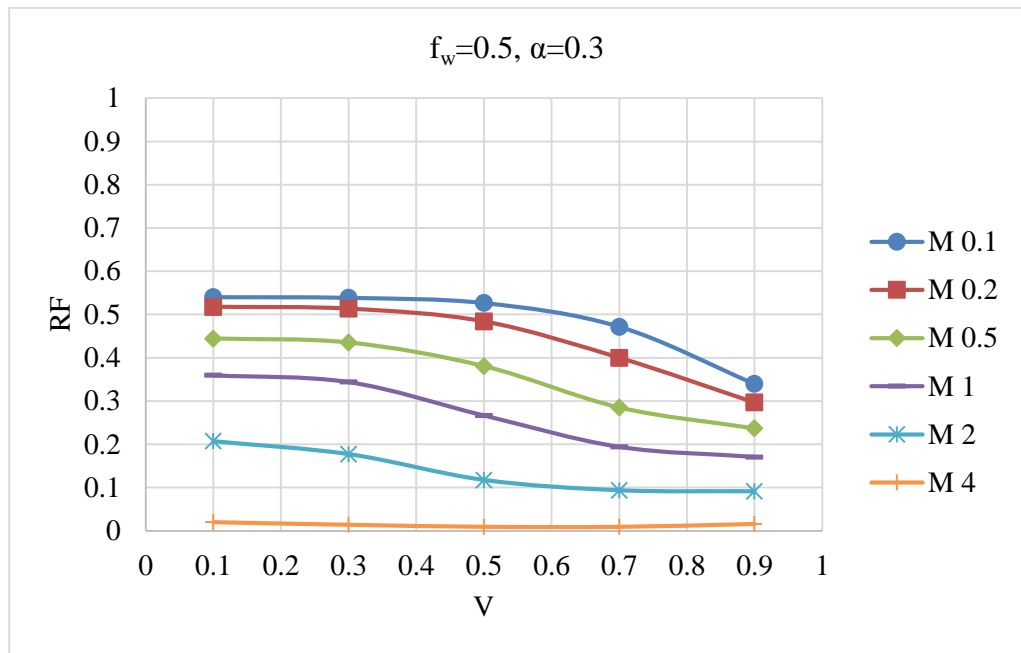


Figure A.15: Recovery factors after breakthrough ($f_w=0.5$) with crossflow ($\alpha=0.3$) for system 1

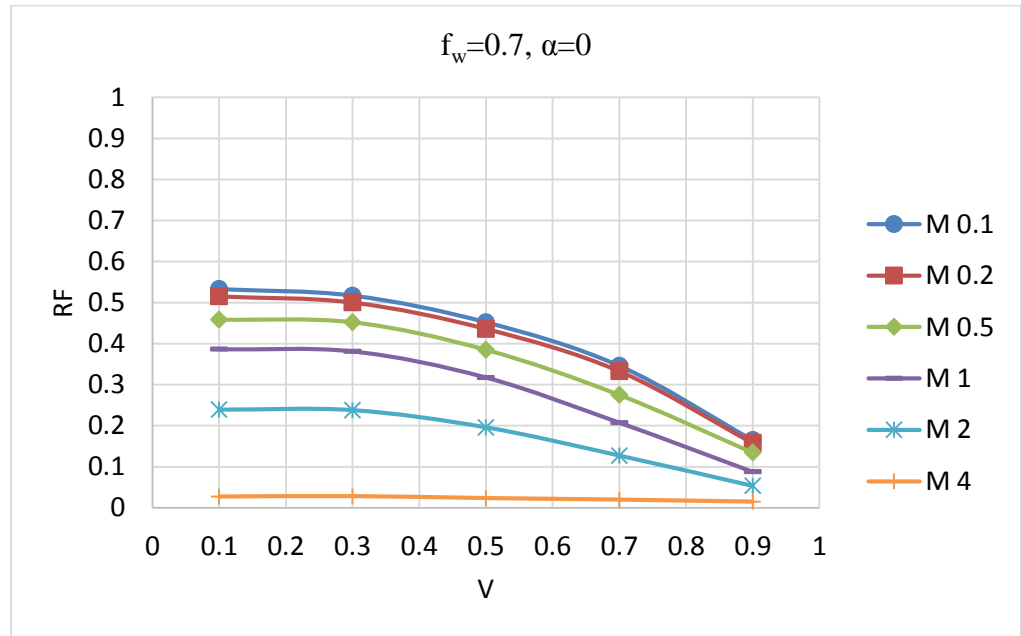


Figure A.16: Recovery factors after breakthrough ($f_w=0.7$) without crossflow ($\alpha=0$) for system 1

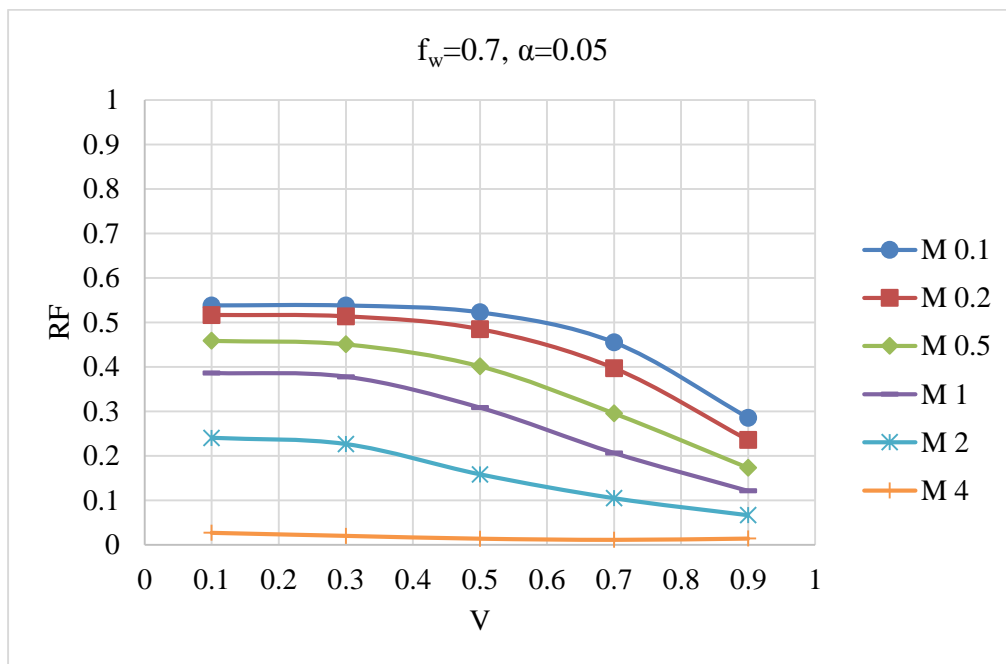


Figure A.17: Recovery factors after breakthrough ($f_w=0.7$) with crossflow ($\alpha=0.05$)

for system 1

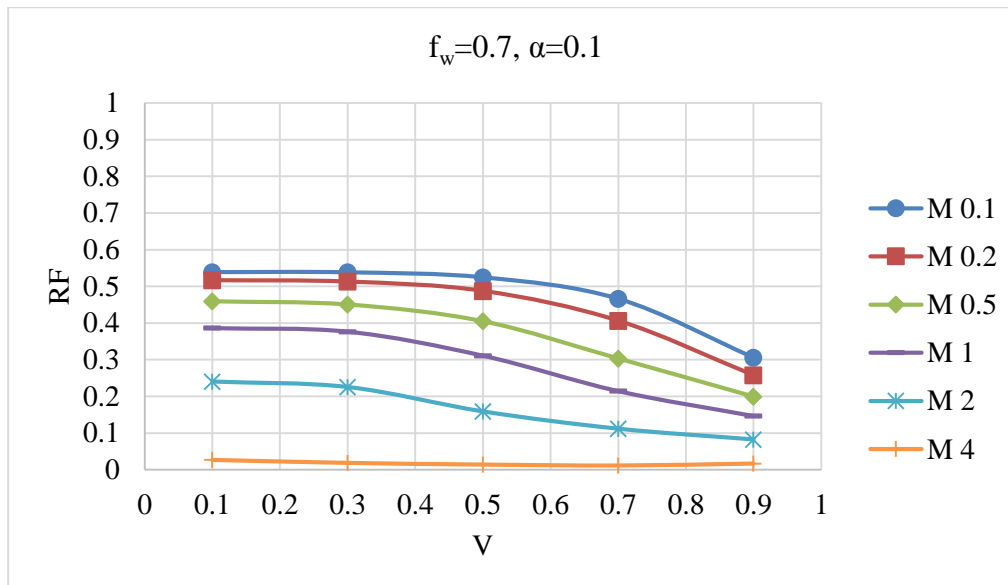


Figure A.18: Recovery factors after breakthrough ($f_w=0.7$) with crossflow ($\alpha=0.1$) for

system 1

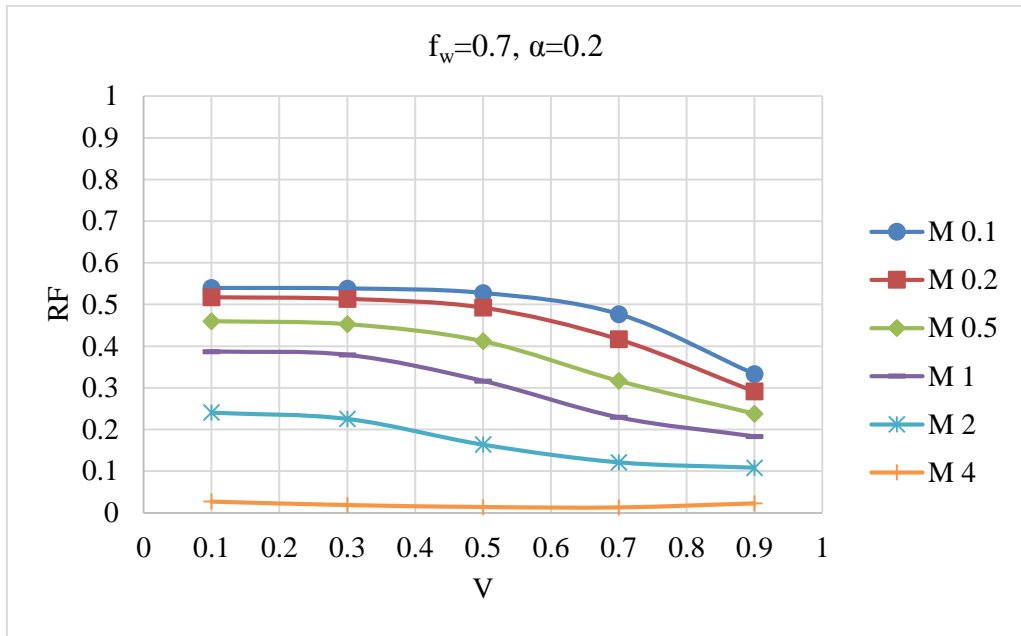


Figure A. 19: Recovery factors after breakthrough ($f_w=0.7$) with crossflow ($\alpha=0.2$) for system 1

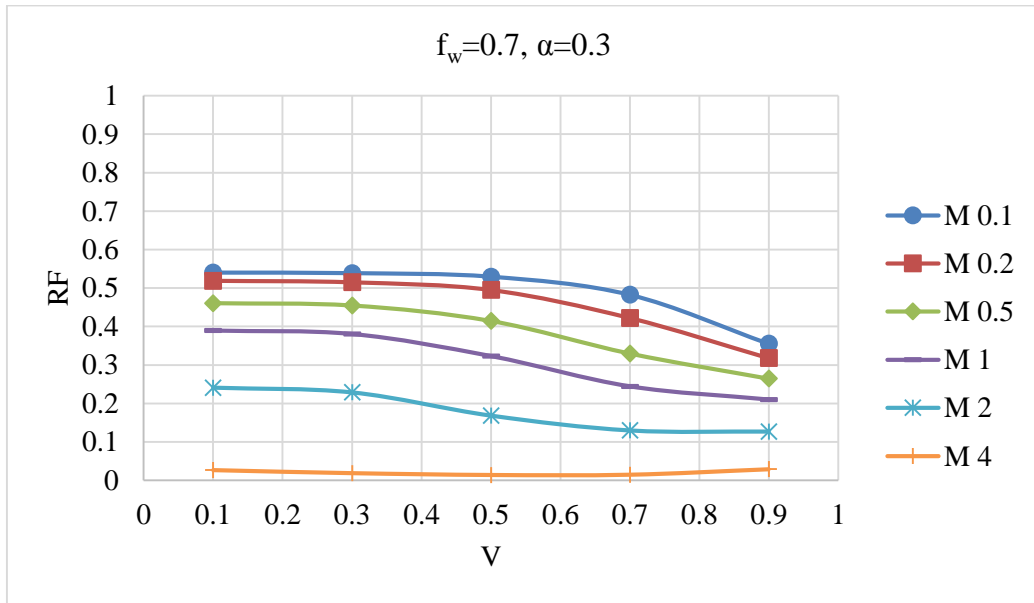


Figure A.20: Recovery factors after breakthrough ($f_w=0.7$) with crossflow ($\alpha=0.3$) for system 1

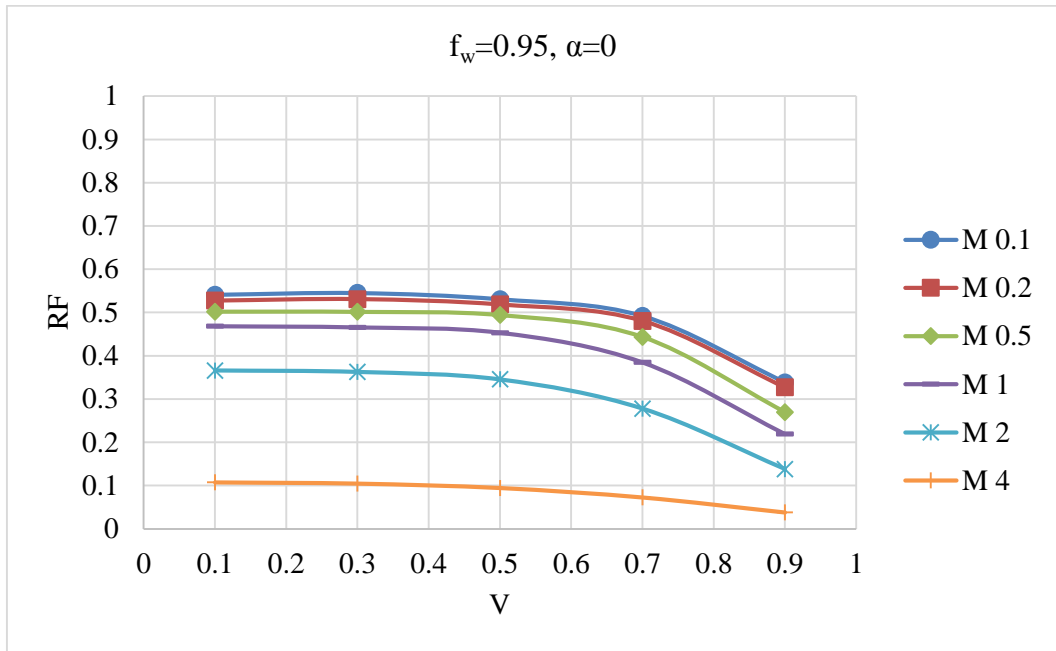


Figure A.21: Recovery factors after breakthrough ($f_w=0.95$) without crossflow ($\alpha=0$) for system 1

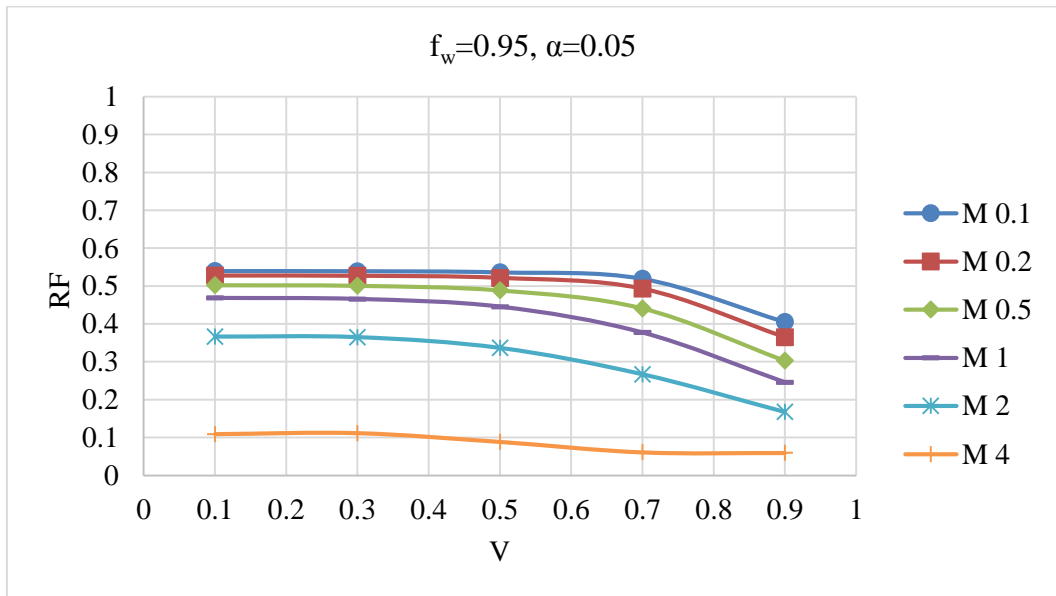


Figure A.22: Recovery factors after breakthrough ($f_w=0.95$) with crossflow ($\alpha=0.05$) for system 1

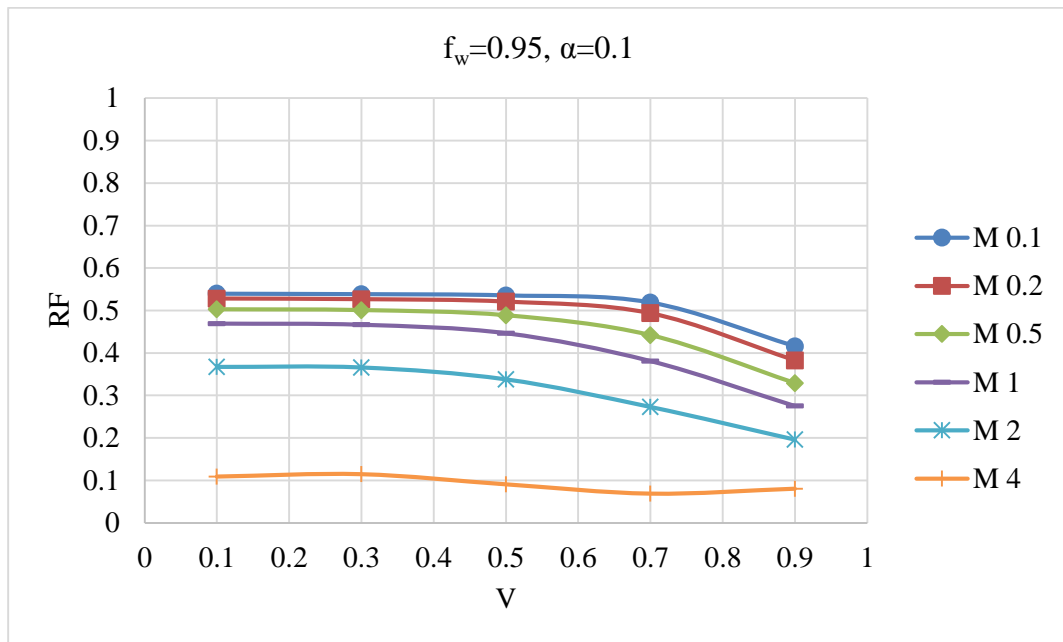


Figure A.23: Recovery factors after breakthrough ($f_w=0.95$) with crossflow ($\alpha=0.1$)
for system 1

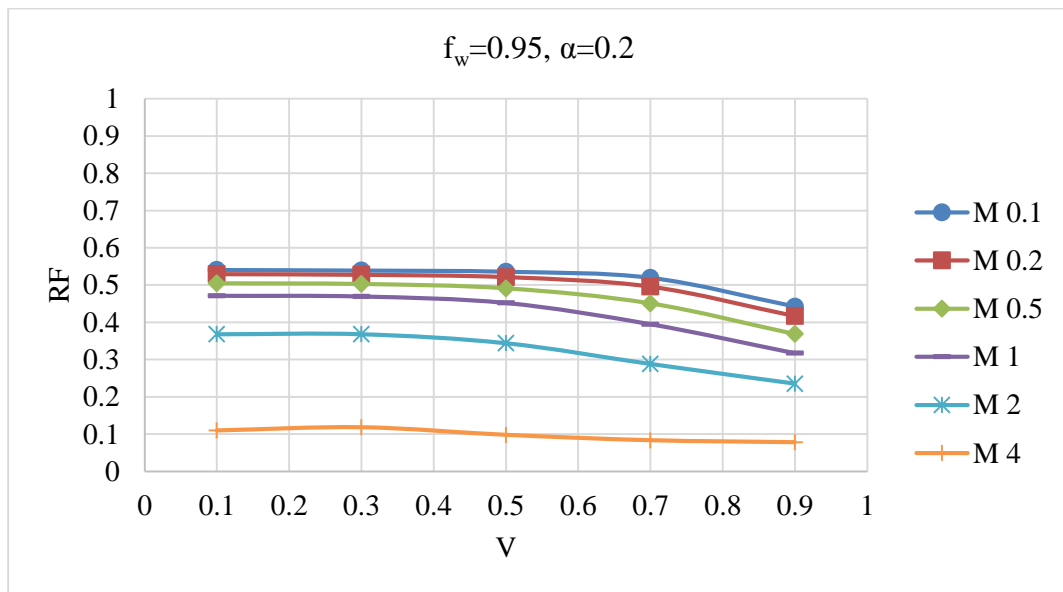


Figure A.24: Recovery factors after breakthrough ($f_w=0.95$) with crossflow ($\alpha=0.2$)
for system 1

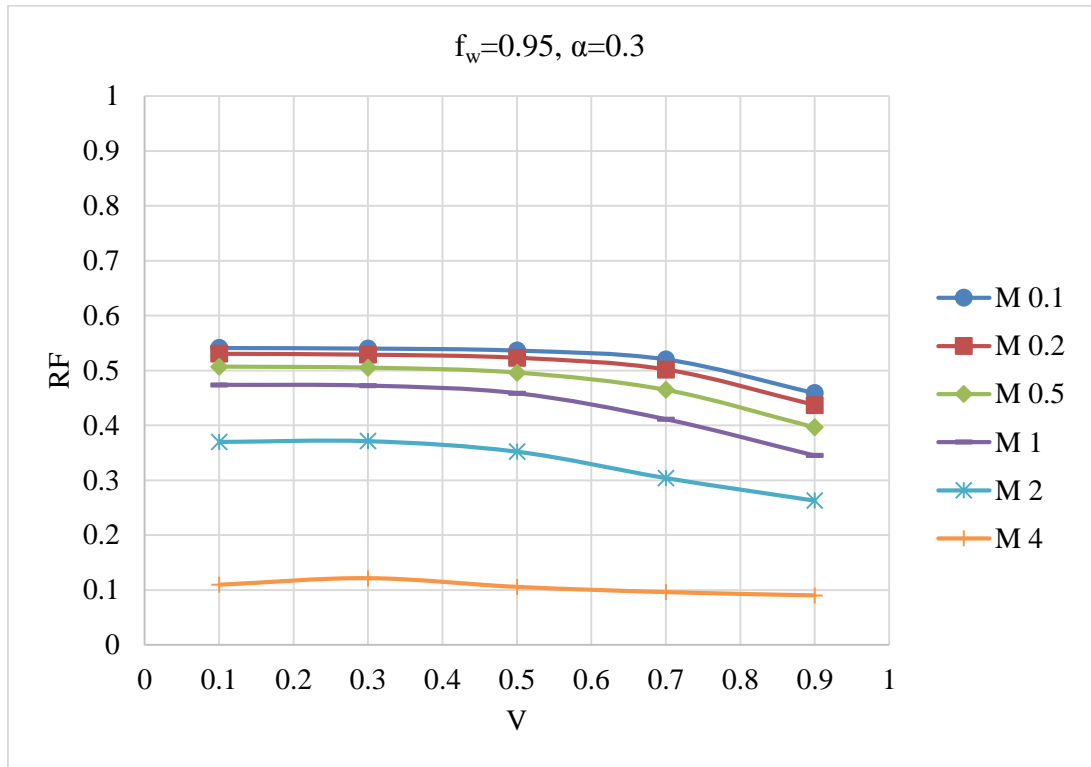


Figure A.25: Recovery factors after breakthrough ($f_w=0.95$) with crossflow ($\alpha=0.3$)
for system 1

II. Simulation Results for System 2 (WI=1.12)

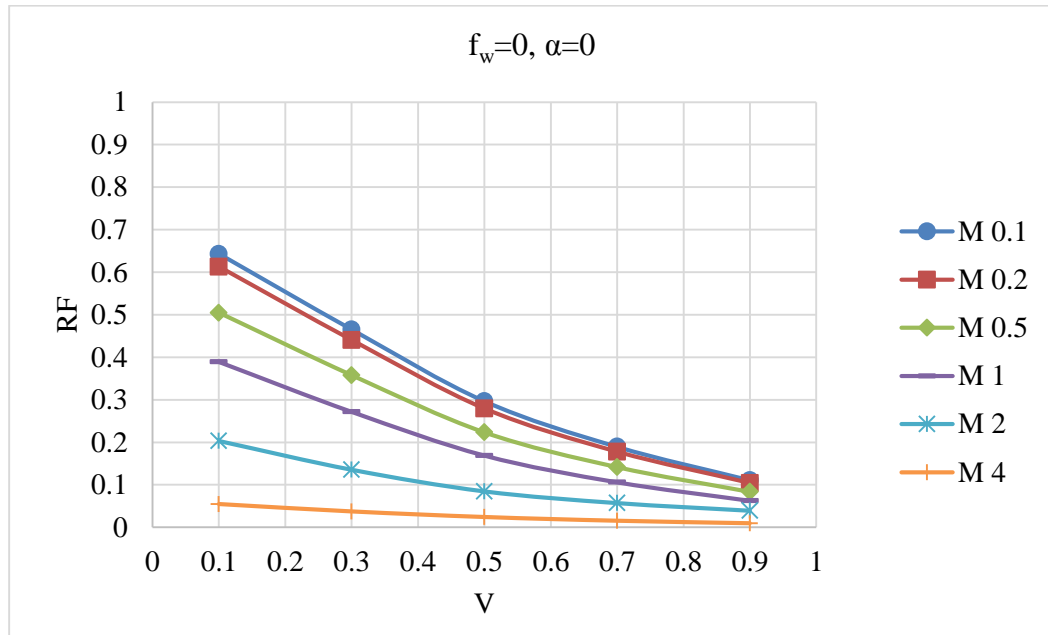


Figure A.26: Recovery factors at breakthrough without crossflow ($\alpha=0$) for system 2

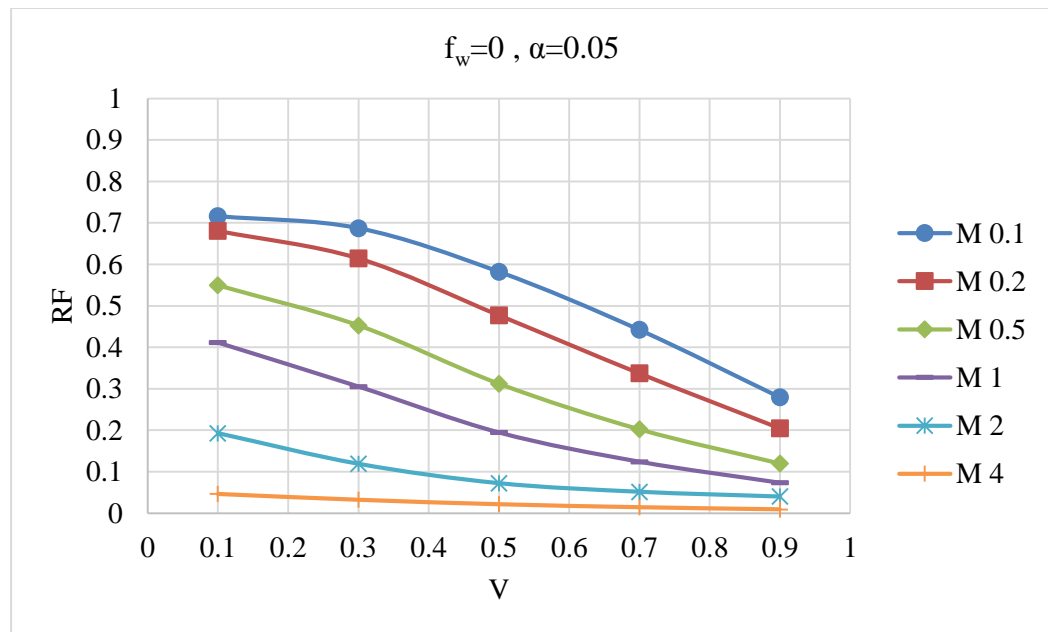


Figure A.27: Recovery factors at breakthrough with crossflow ($\alpha=0.05$) for system 2

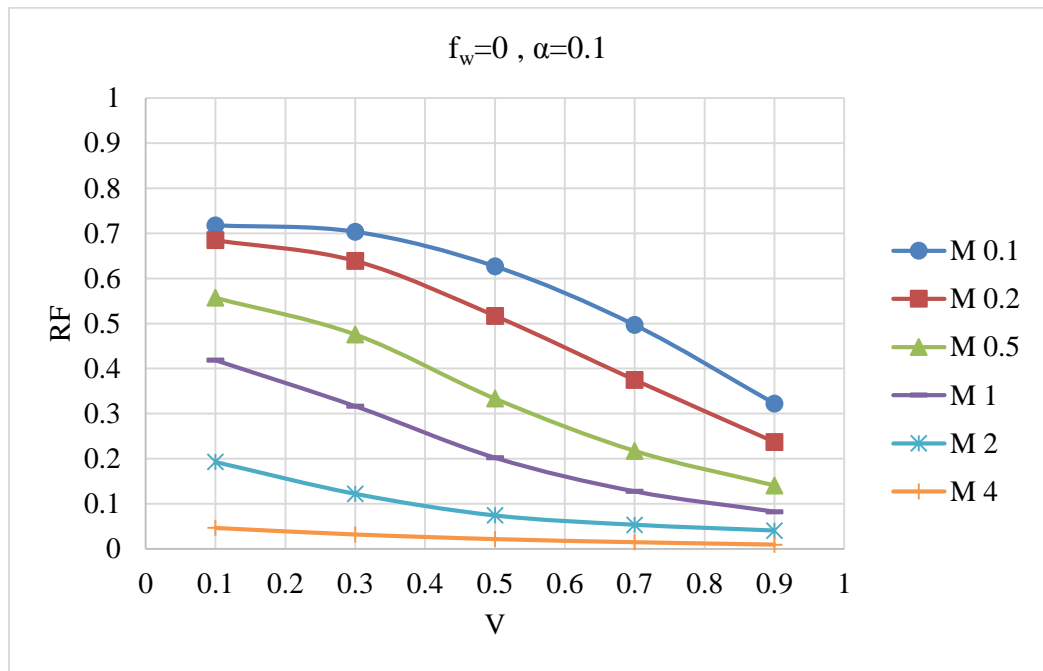


Figure A.28: Recovery factors at breakthrough with crossflow ($\alpha=0.1$) for system 2

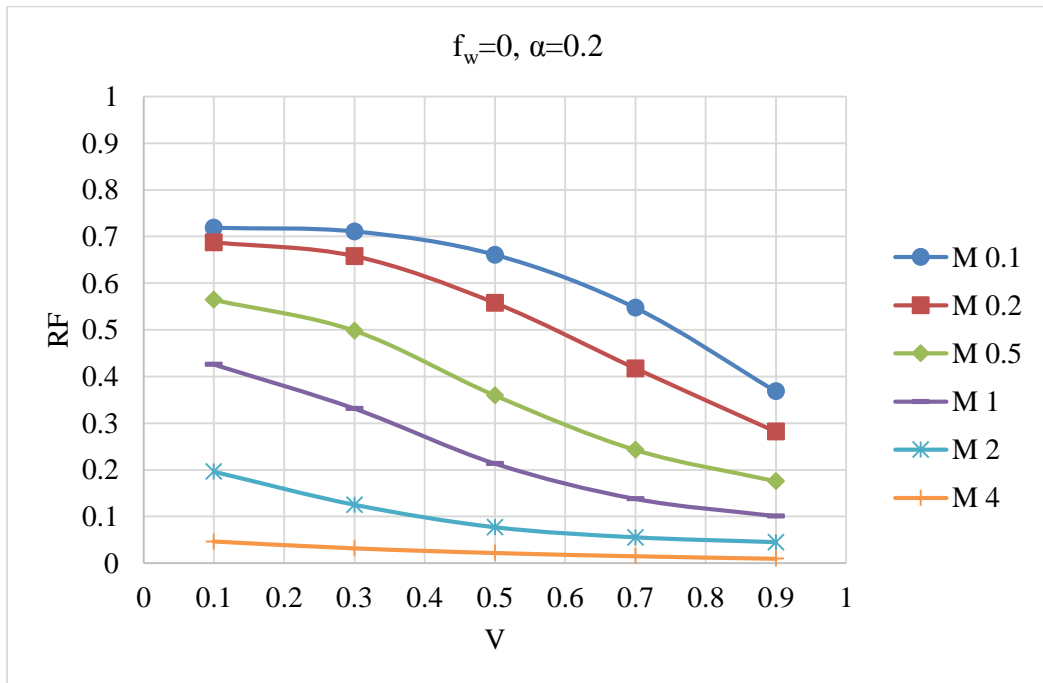


Figure A.29: Recovery factors at breakthrough with crossflow ($\alpha=0.2$) for system 2

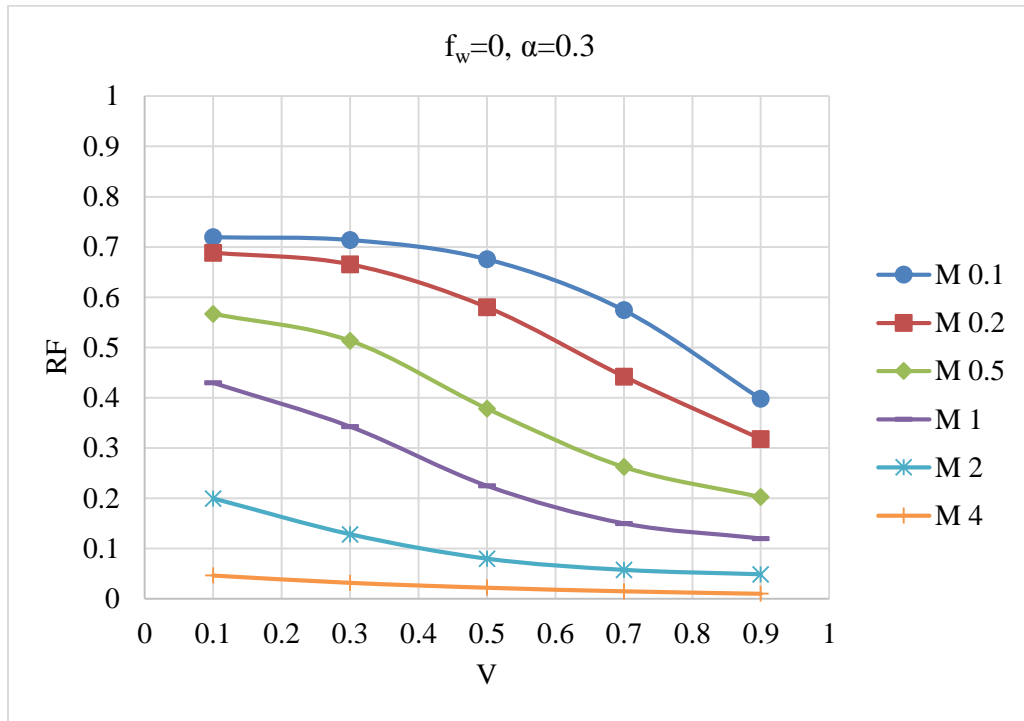


Figure A.30: Recovery factors at breakthrough with crossflow ($\alpha=0.3$) for system 2

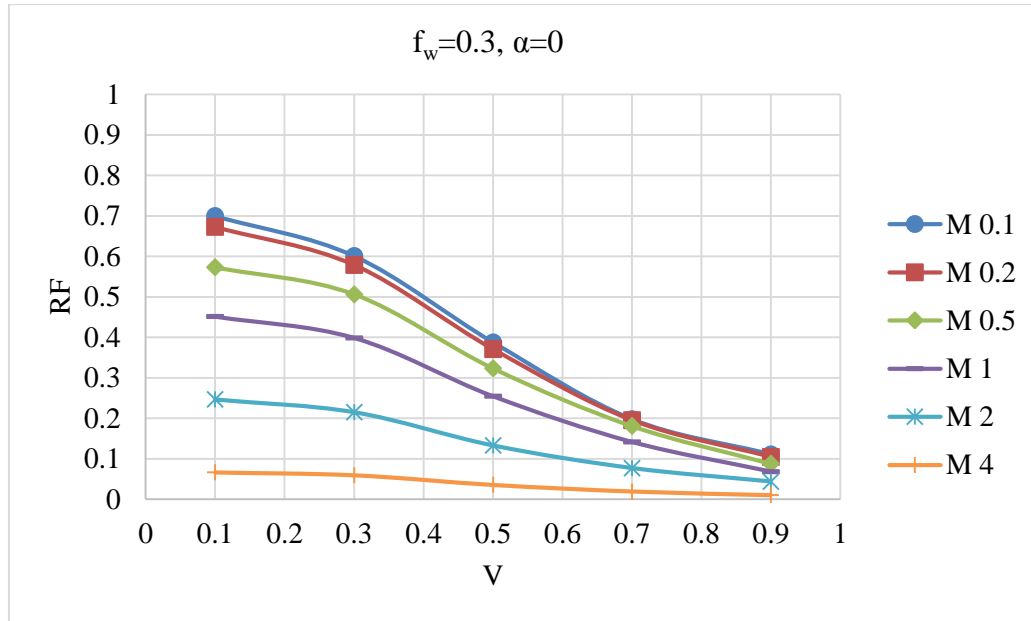


Figure A.31: Recovery factors after breakthrough ($f_w=0.3$) without crossflow ($\alpha=0$) for system 2

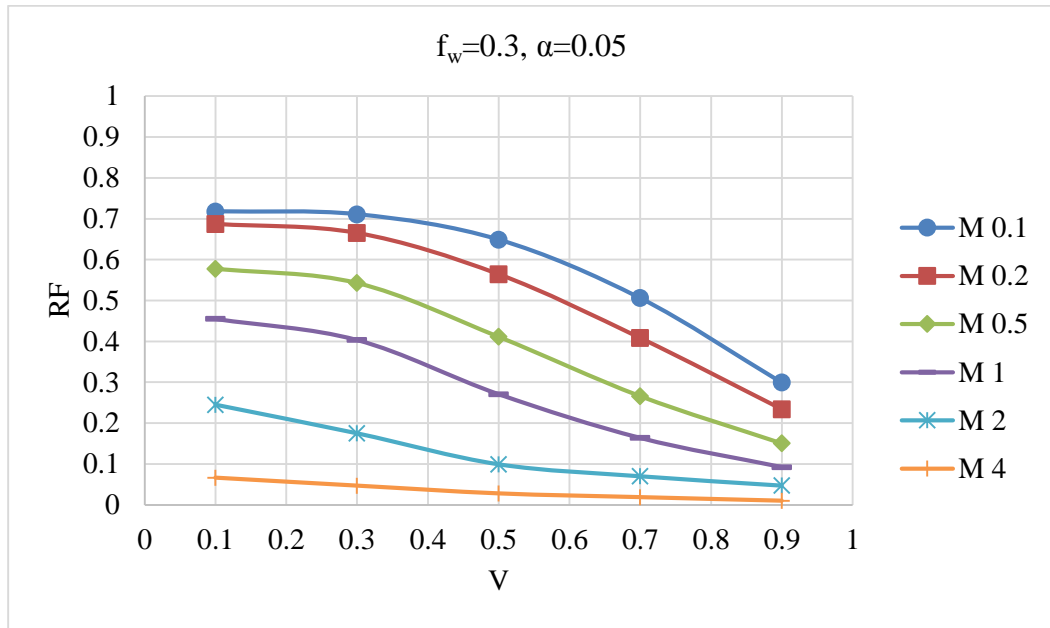


Figure A.32: Recovery factors after breakthrough ($f_w=0.3$) with crossflow ($\alpha=0.05$)
for system 2

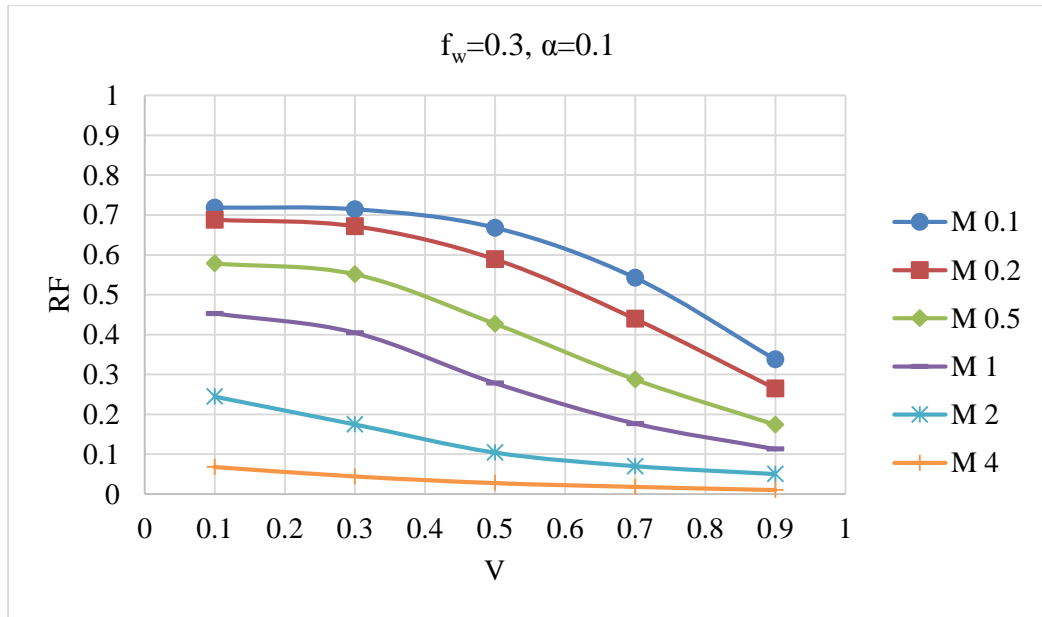


Figure A.33: Recovery factors after breakthrough ($f_w=0.3$) with crossflow ($\alpha=0.1$) for
system 2

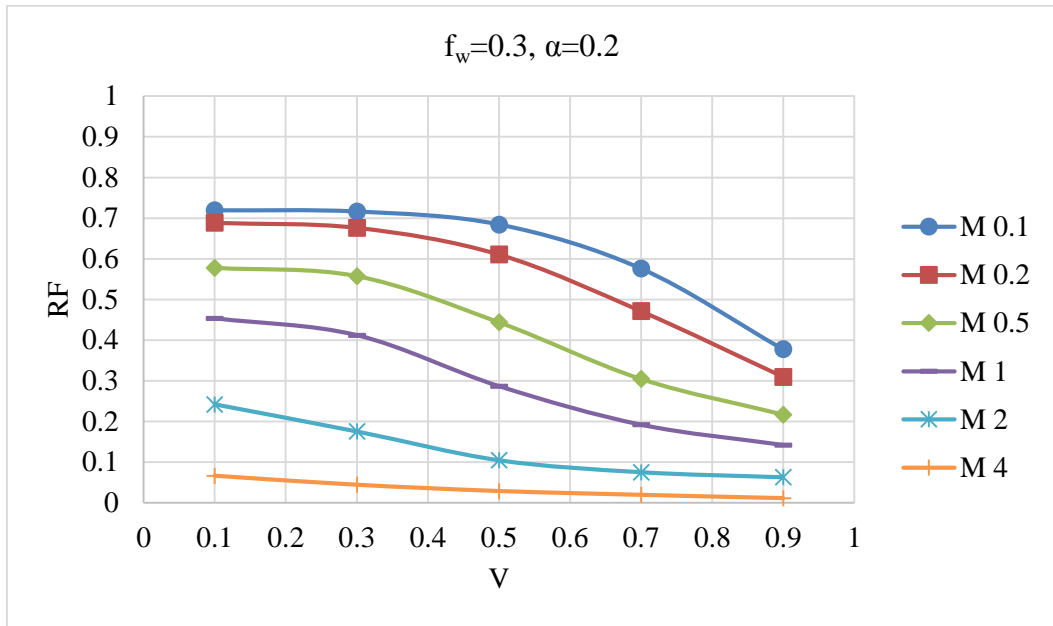


Figure A.34: Recovery factors after breakthrough ($f_w=0.3$) with crossflow ($\alpha=0.2$) for system 2

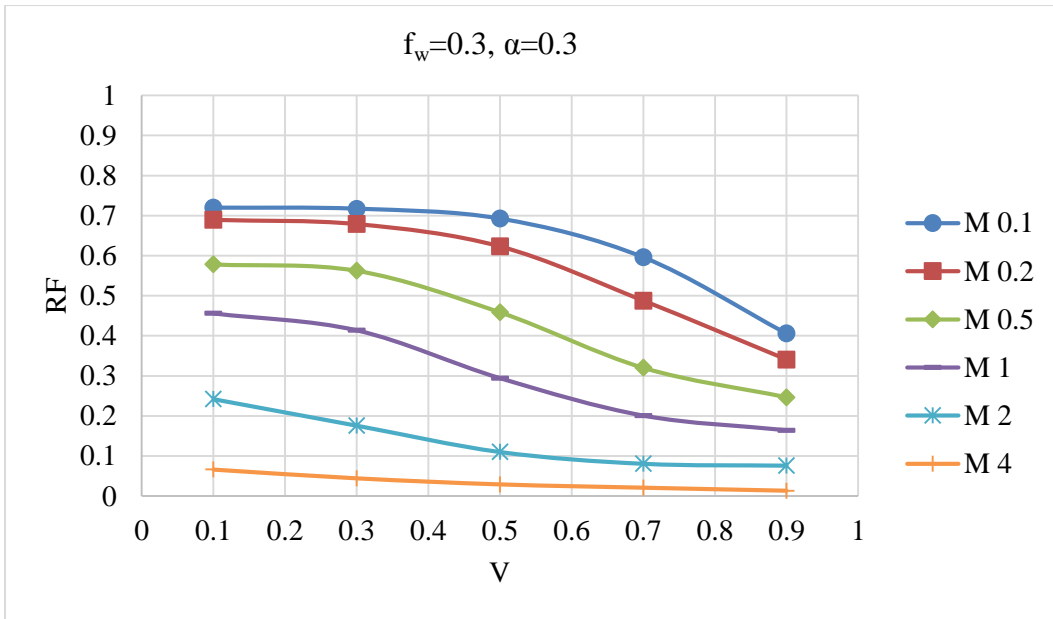


Figure A.35: Recovery factors after breakthrough ($f_w=0.3$) with crossflow ($\alpha=0.3$) for system 2

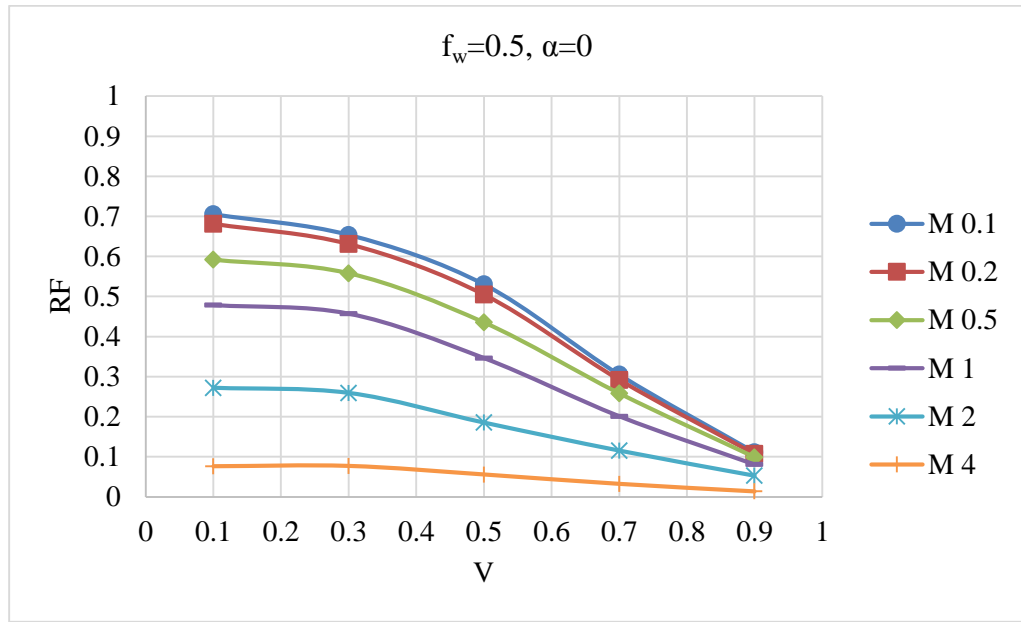


Figure A.36: Recovery factors after breakthrough ($f_w=0.5$) without crossflow ($\alpha=0$)
for system 2

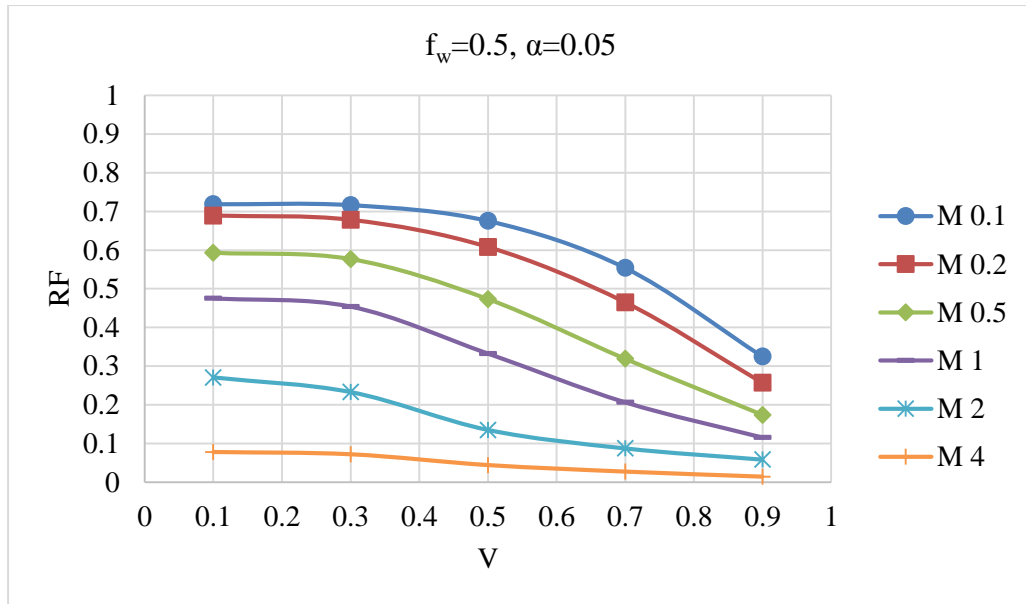


Figure A.37: Recovery factors after breakthrough ($f_w=0.5$) with crossflow ($\alpha=0.05$)
for system 2

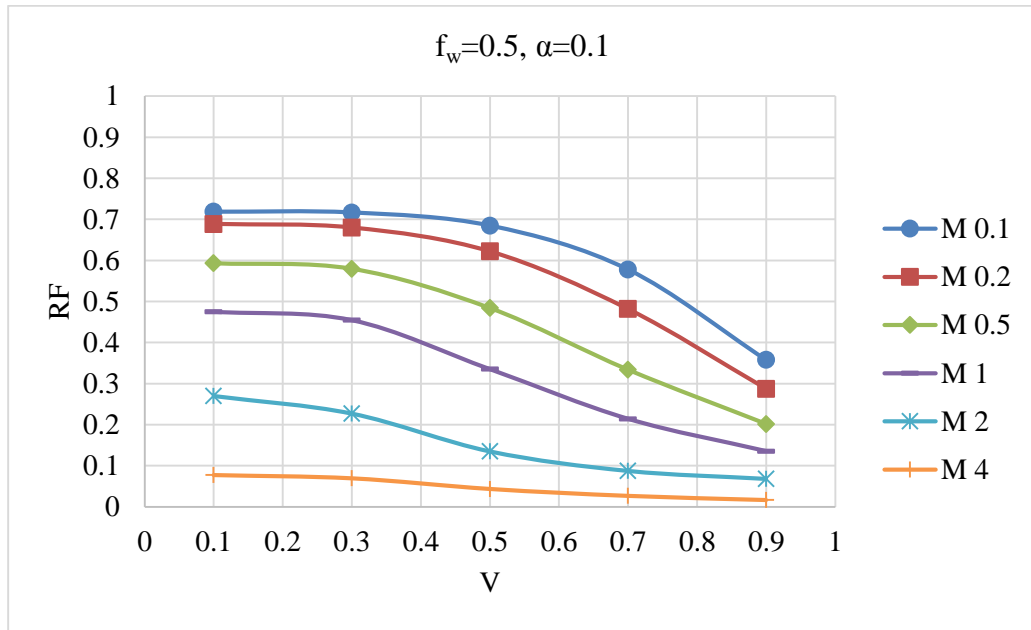


Figure A.38: Recovery factors after breakthrough ($f_w = 0.5$) with crossflow ($\alpha=0.1$) for system 2

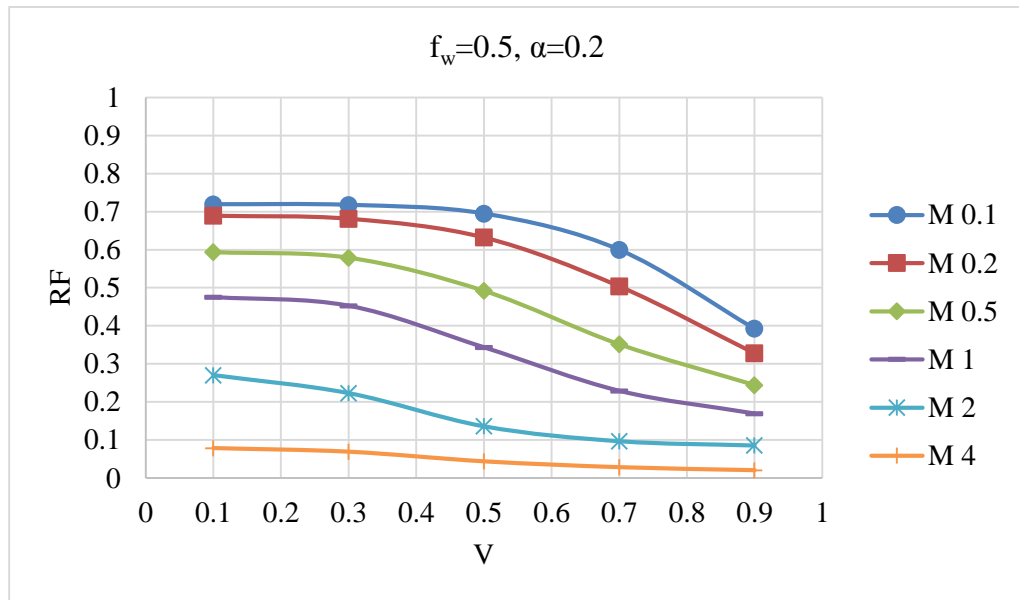


Figure A.39: Recovery factors after breakthrough ($f_w=0.5$) with crossflow ($\alpha=0.2$) for system 2

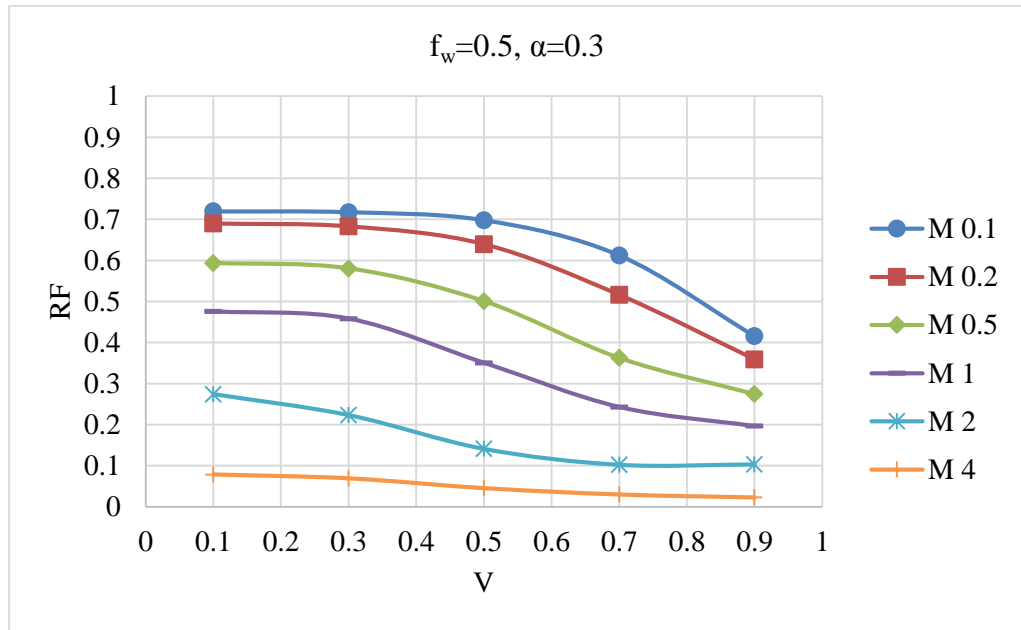


Figure A.40: Recovery factors after breakthrough ($f_w=0.5$) with crossflow ($\alpha=0.3$) for system 2

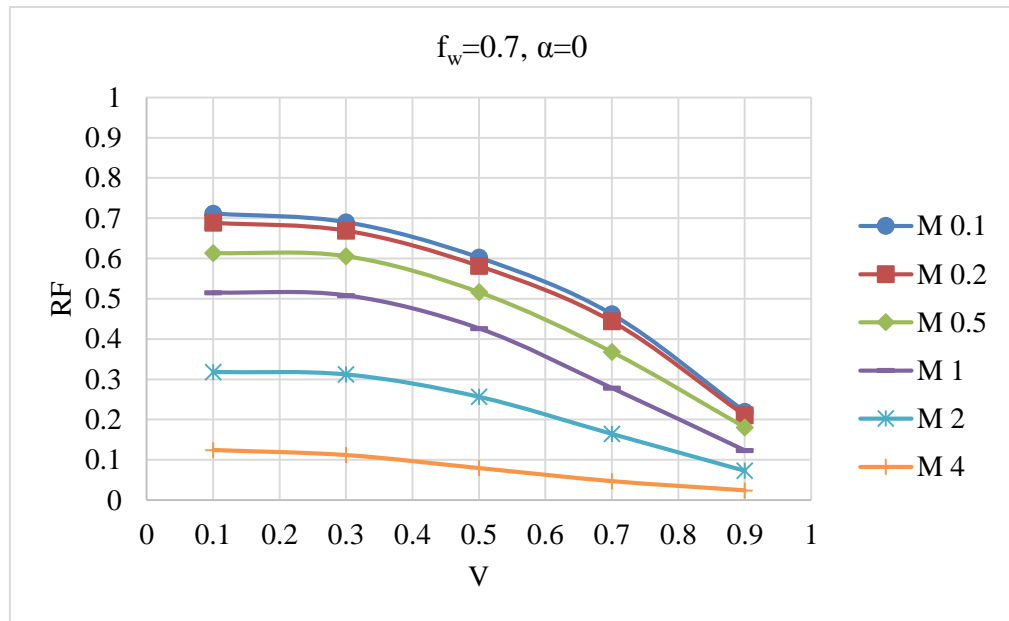


Figure A.41: Recovery factors after breakthrough ($f_w=0.7$) without crossflow ($\alpha=0$) for system 2

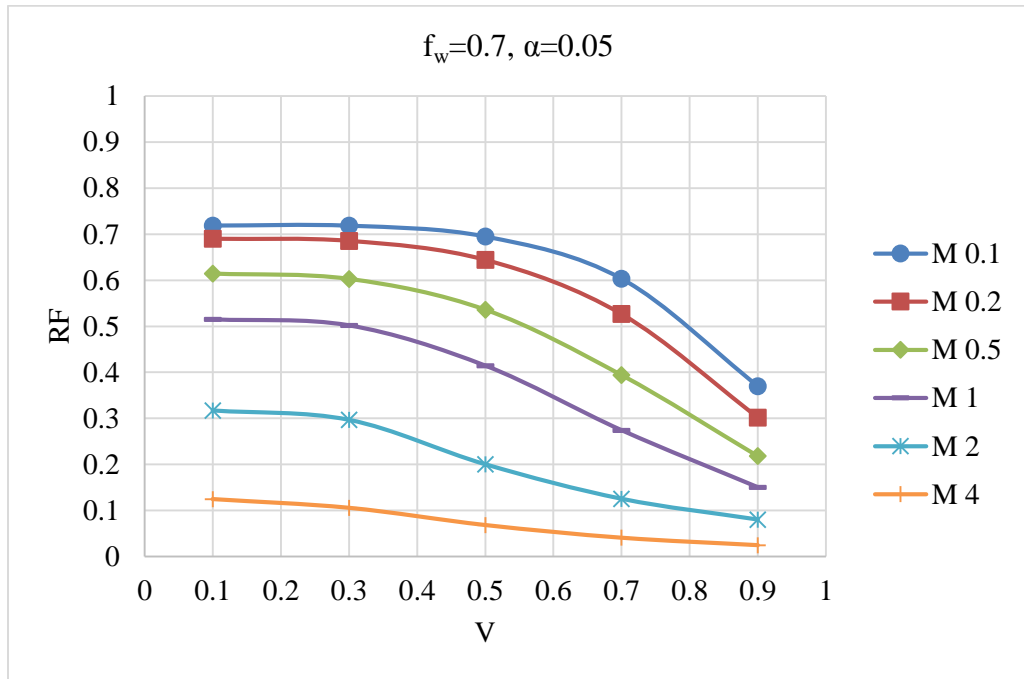


Figure A.42: Recovery factors after breakthrough ($f_w=0.7$) with crossflow ($\alpha=0.05$)

for system 2

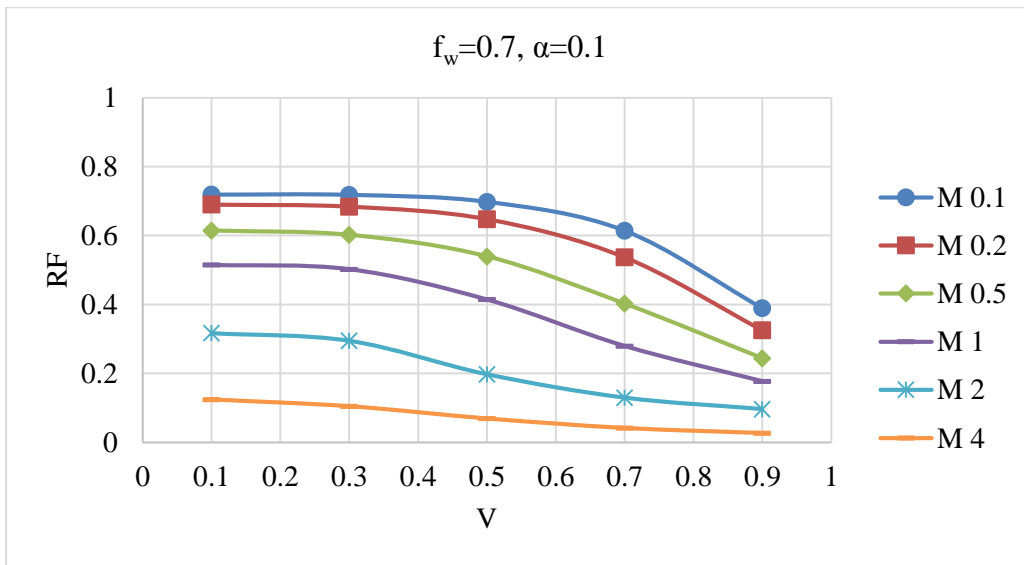


Figure A.43: Recovery factors after breakthrough ($f_w=0.7$) with crossflow ($\alpha=0.1$) for

system 2

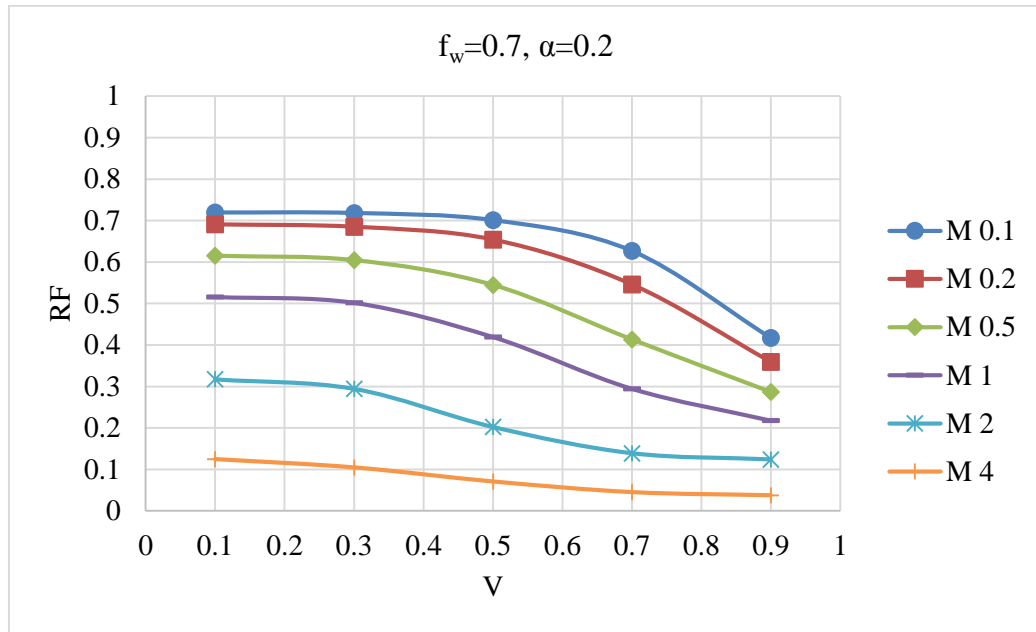


Figure A.44: Recovery factors after breakthrough ($f_w=0.7$) with crossflow ($\alpha=0.2$) for system 2

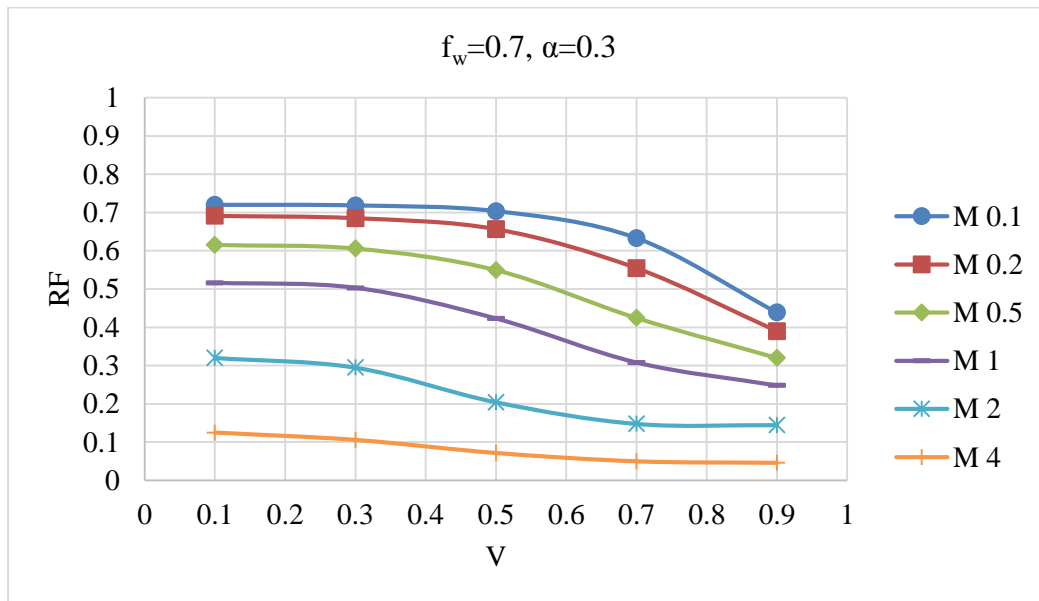


Figure A.45: Recovery factors after breakthrough ($f_w=0.7$) with crossflow ($\alpha=0.3$) for system 2

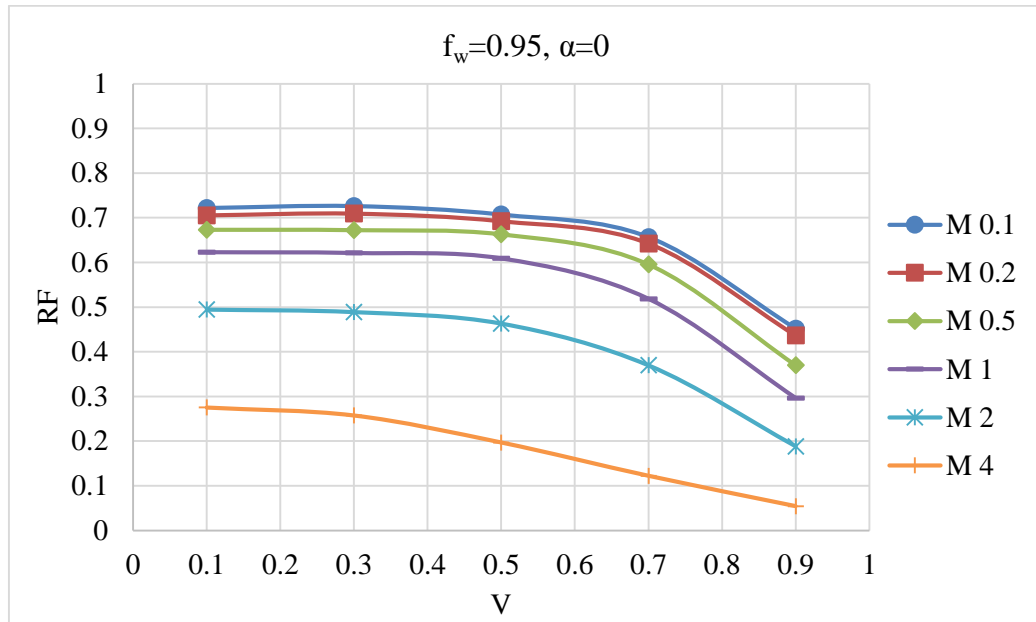


Figure A.46: Recovery factors after breakthrough ($f_w=0.95$) without crossflow ($\alpha=0$)
for system 2

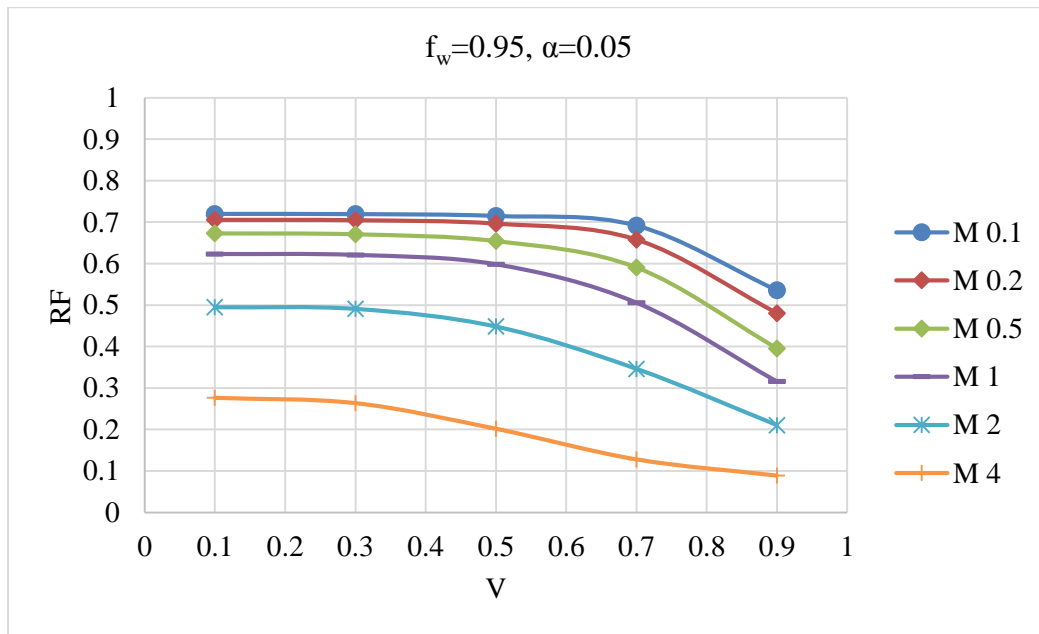


Figure A.47: Recovery factors after breakthrough ($f_w=0.95$) with crossflow ($\alpha=0.05$)
for system 2

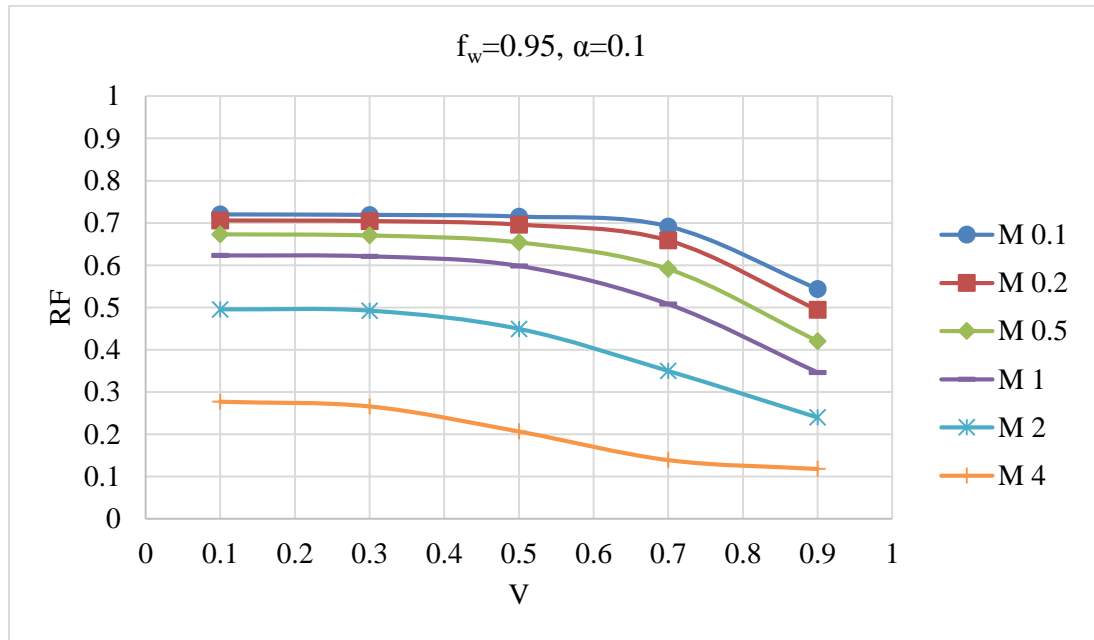


Figure A.48: Recovery factors after breakthrough ($f_w=0.95$) with crossflow ($\alpha=0.1$)
for system 2

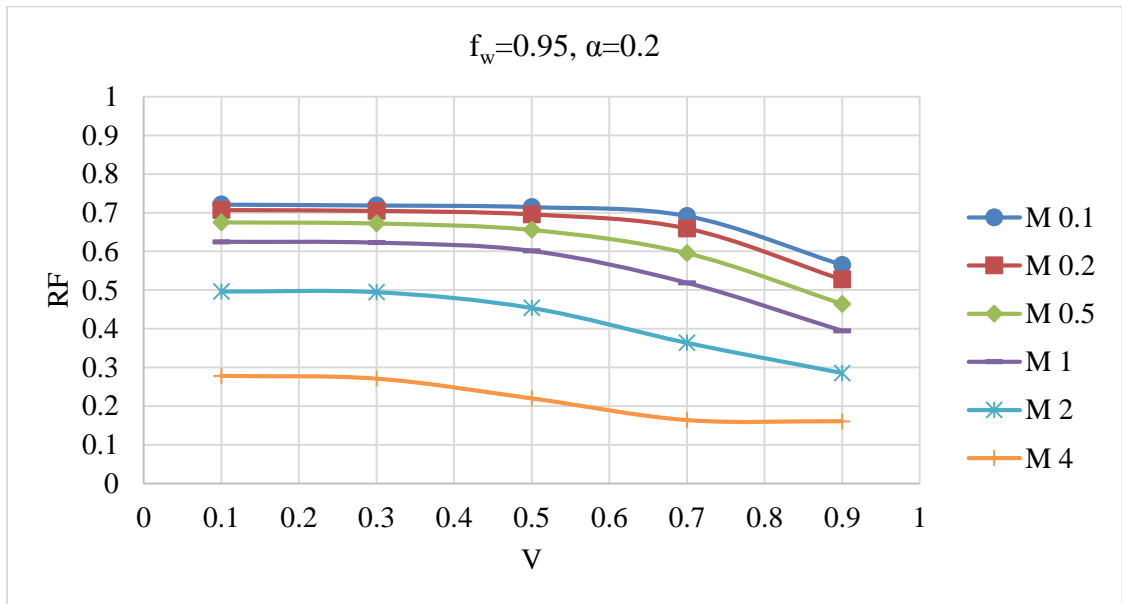


Figure A.49: Recovery factors after breakthrough ($f_w=0.95$) with crossflow ($\alpha=0.2$)
for system 2

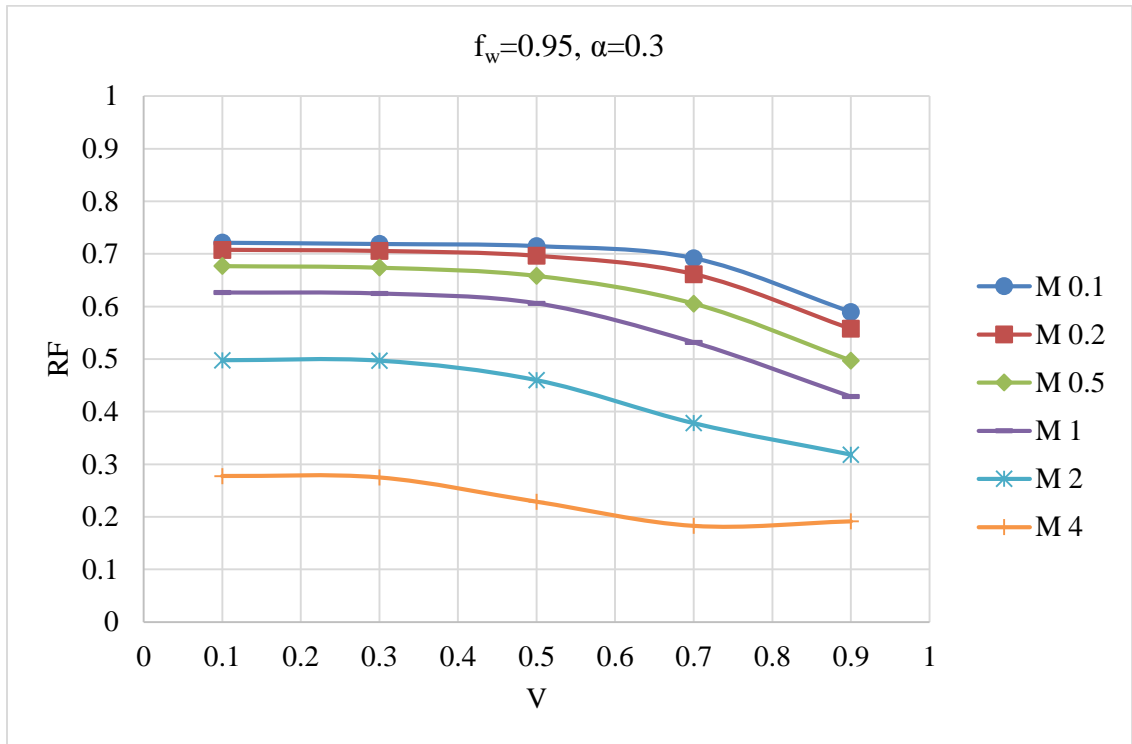


Figure A.50: Recovery factors after breakthrough ($f_w=0.95$) with crossflow ($\alpha=0.3$)
for system 2

III. Simulation Results for System 3 (WI=3)

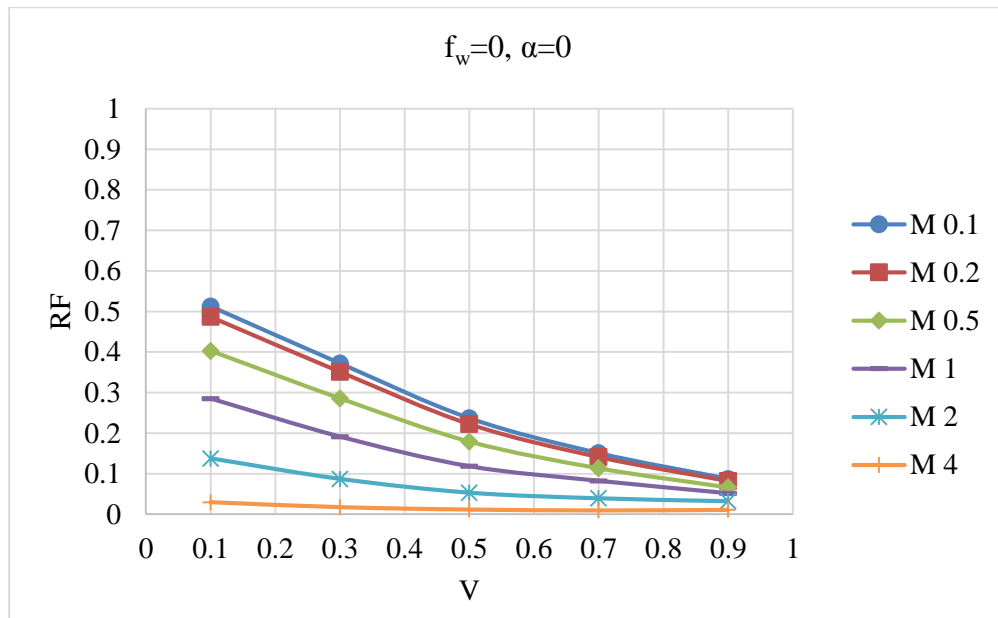


Figure A.51: Recovery factors at breakthrough without crossflow ($\alpha=0$) for system 3

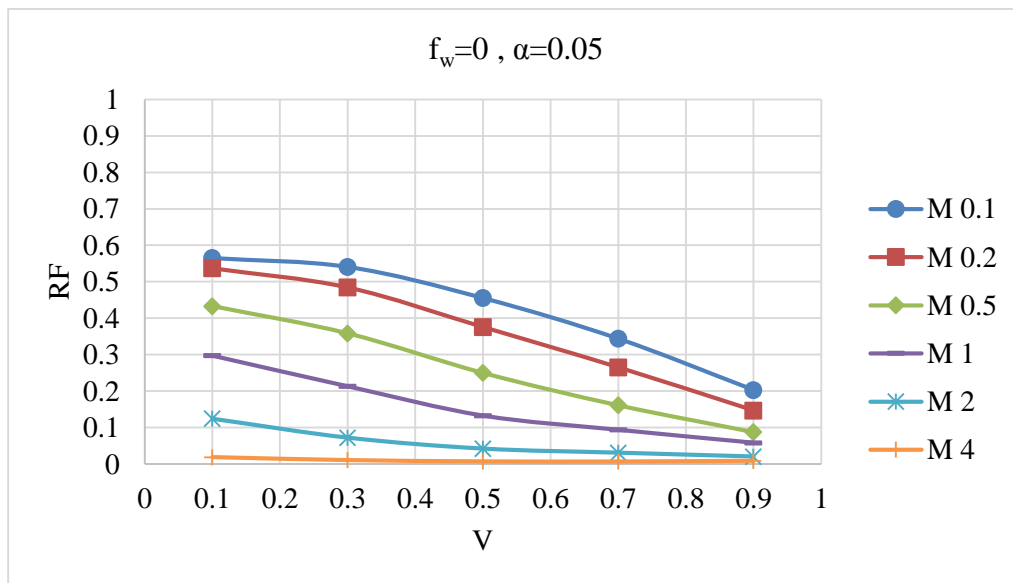


Figure A.52 Recovery factors at breakthrough with crossflow ($\alpha=0.05$) for system 3

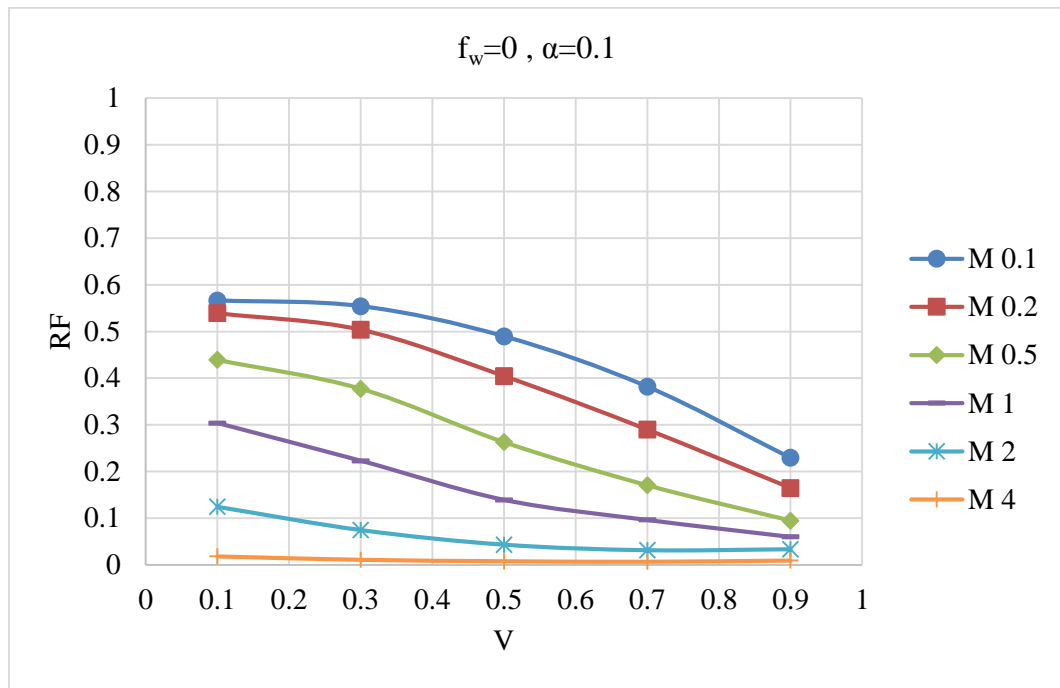


Figure A.53: Recovery factors at breakthrough with crossflow ($\alpha=0.1$) for system 3

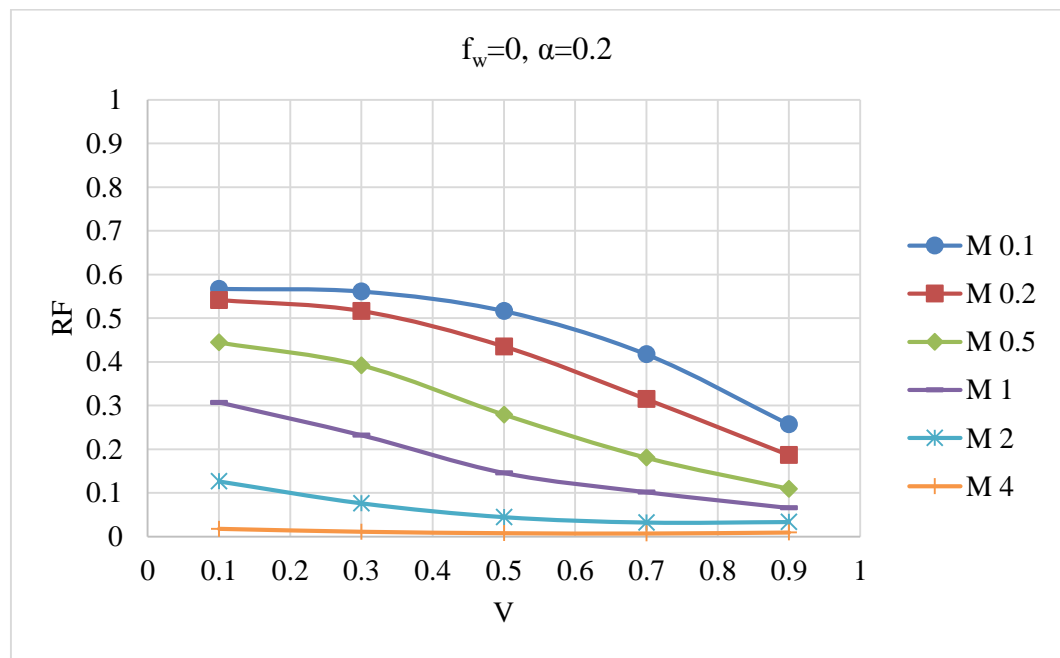


Figure A.54: Recovery factors at breakthrough with crossflow ($\alpha=0.2$) for system 3

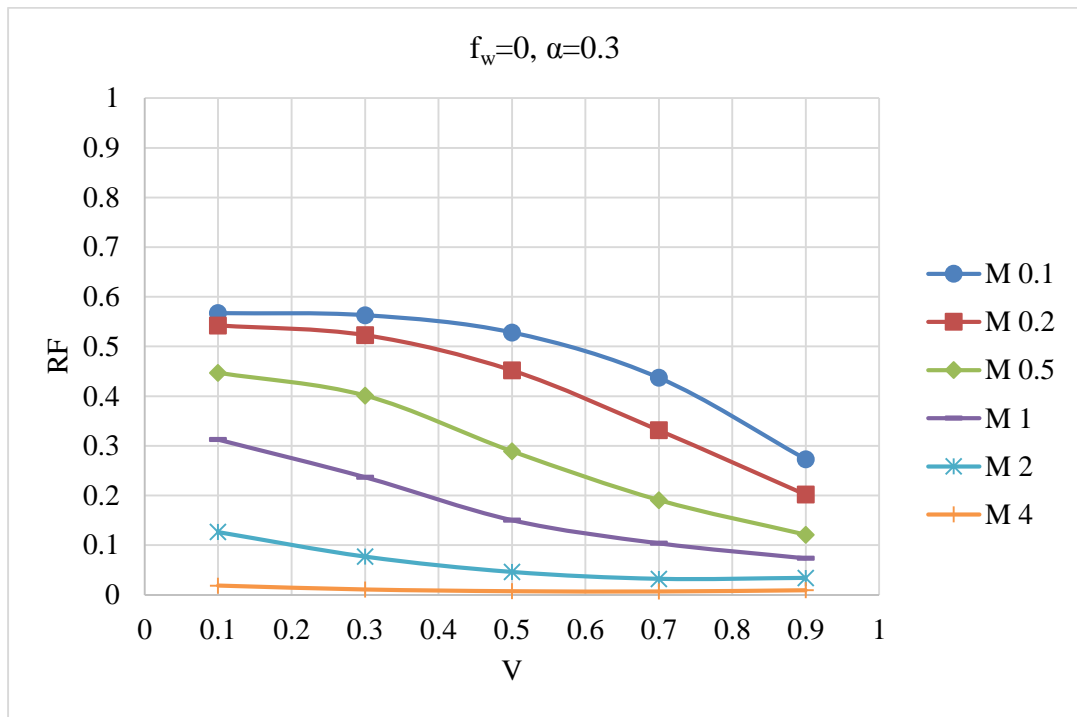


Figure A.55: Recovery factors at breakthrough with crossflow ($\alpha=0.3$) for system 3

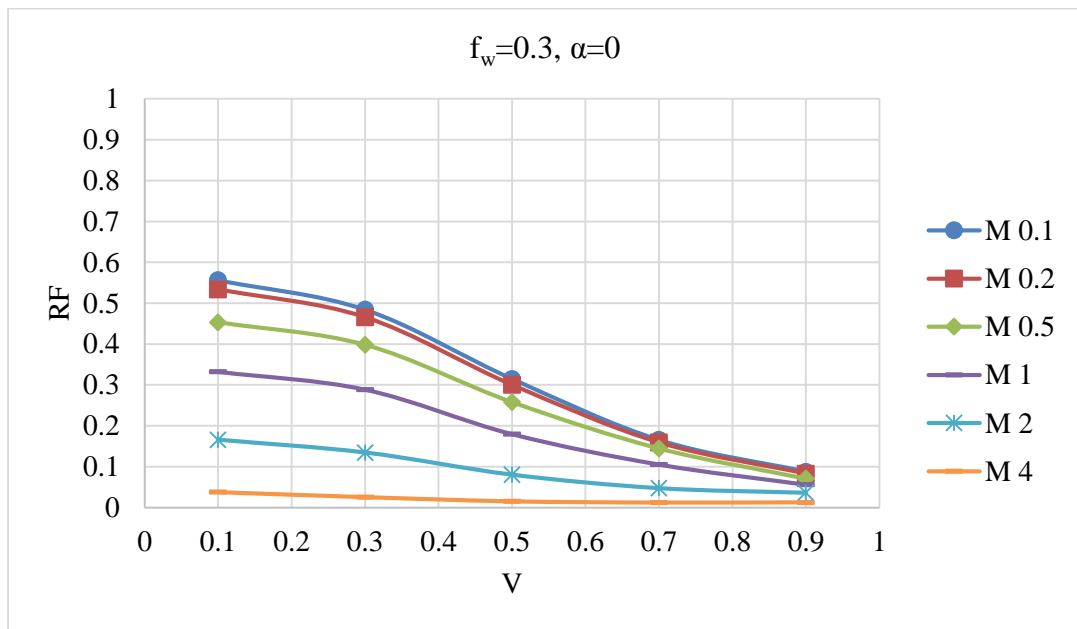


Figure A.56: Recovery factors after breakthrough ($f_w=0.3$) without crossflow ($\alpha=0$)
for system 3

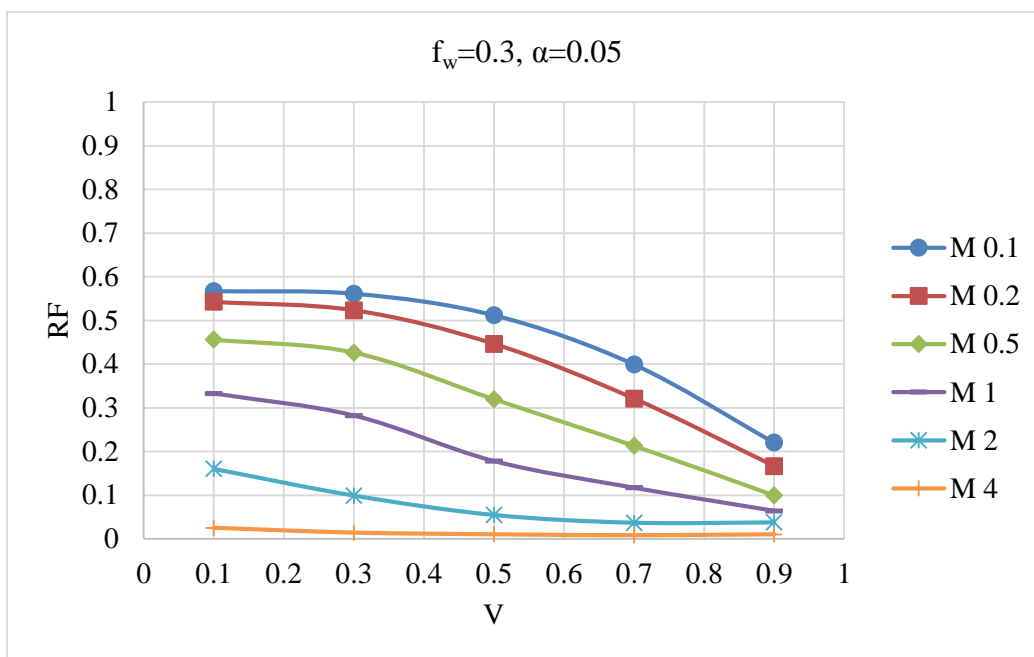


Figure A.57: Recovery factors after breakthrough ($f_w=0.3$) with crossflow ($\alpha=0.05$)
for system 3

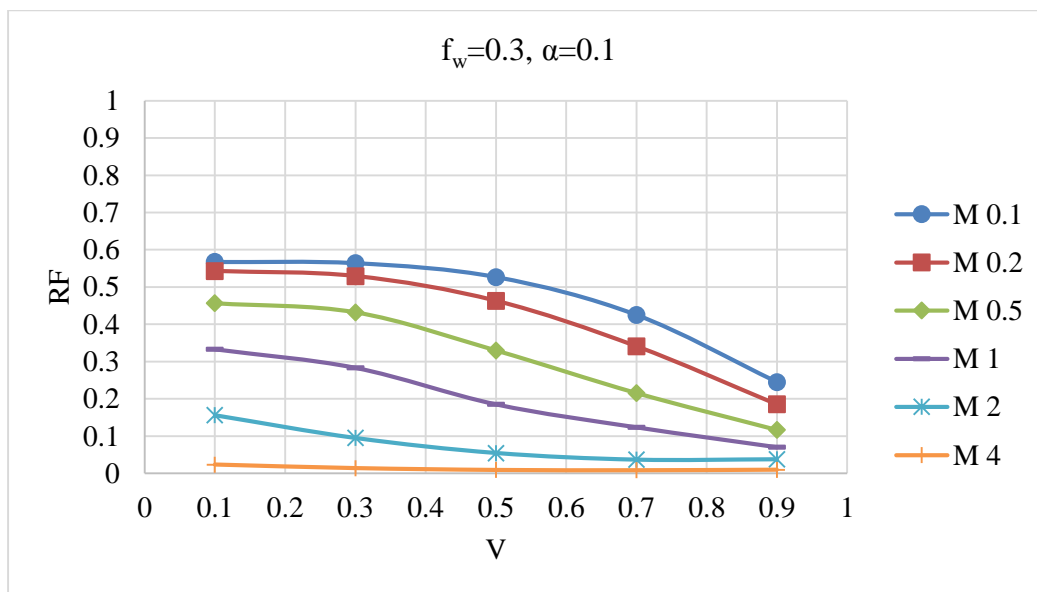


Figure A.58: Recovery factors after breakthrough ($f_w=0.3$) with crossflow ($\alpha=0.1$) for
system 3

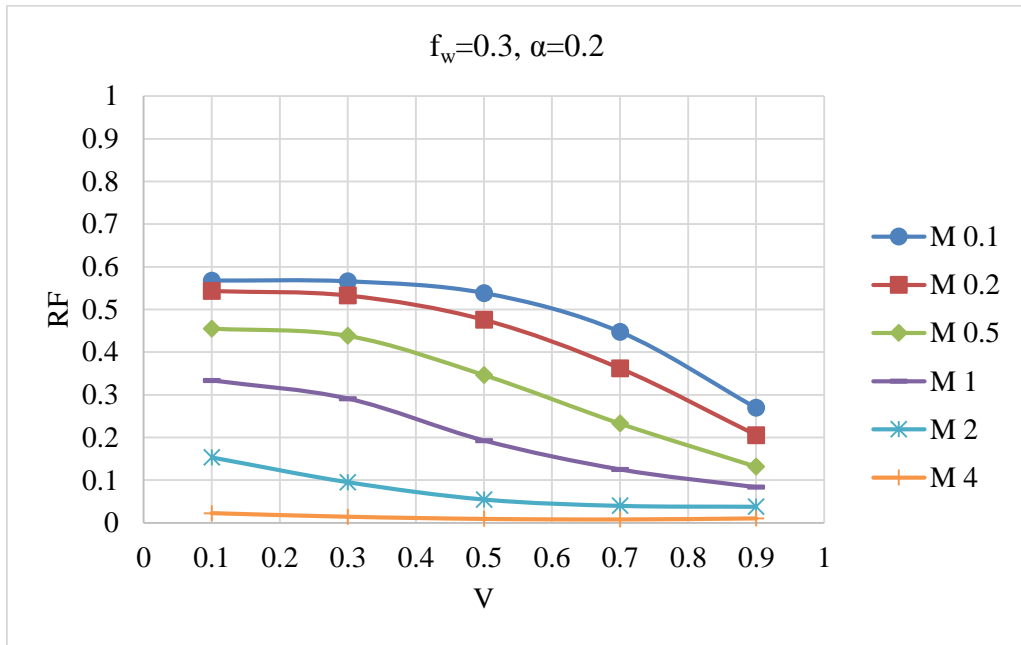


Figure A.59: Recovery factors after breakthrough ($f_w=0.3$) with crossflow ($\alpha=0.2$) for system 3

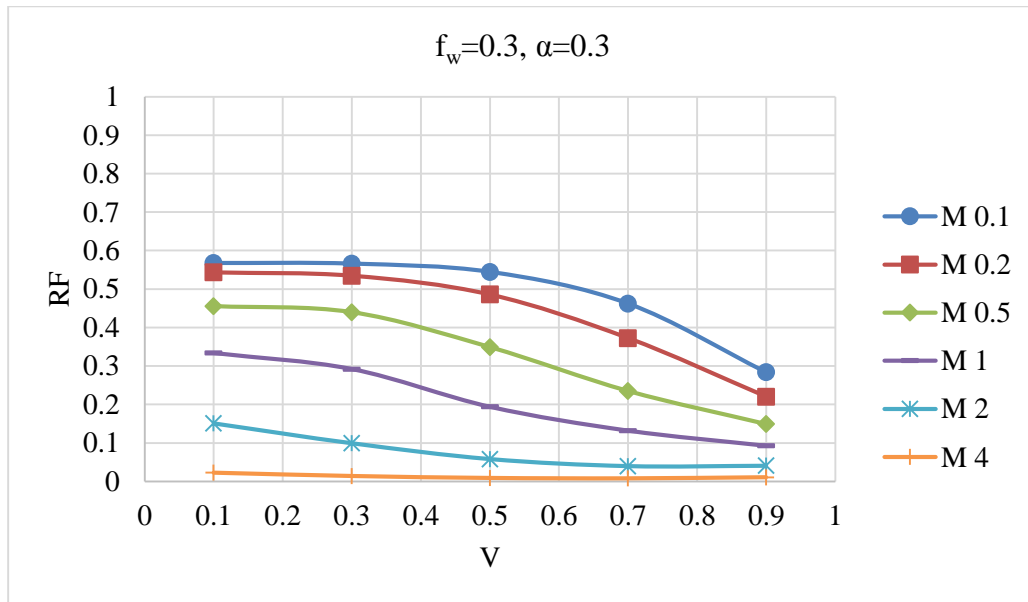


Figure A.60: Recovery factors after breakthrough ($f_w=0.3$) with crossflow ($\alpha=0.3$) for system 3

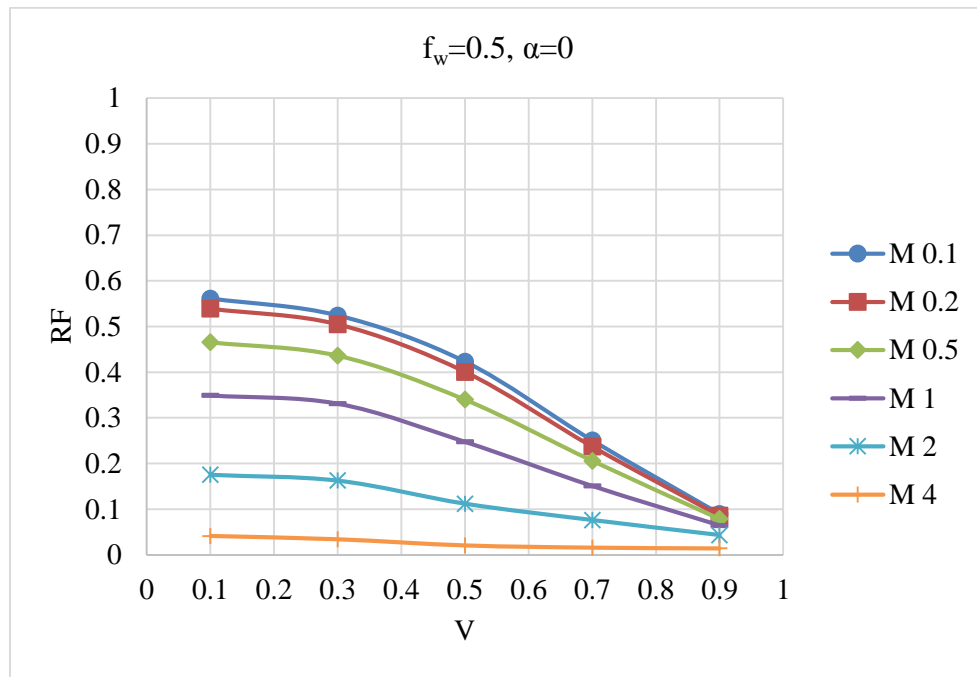


Figure A.61: Recovery factors after breakthrough ($f_w=0.5$) without crossflow ($\alpha=0$)

for system 3

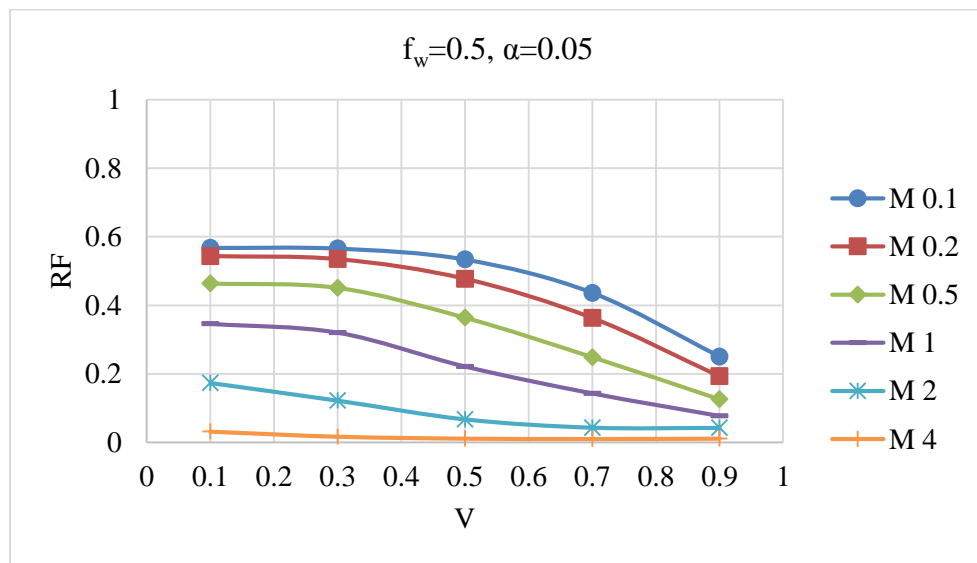


Figure A.62: Recovery factors after breakthrough ($f_w=0.5$) with crossflow ($\alpha=0.05$)

for system 3

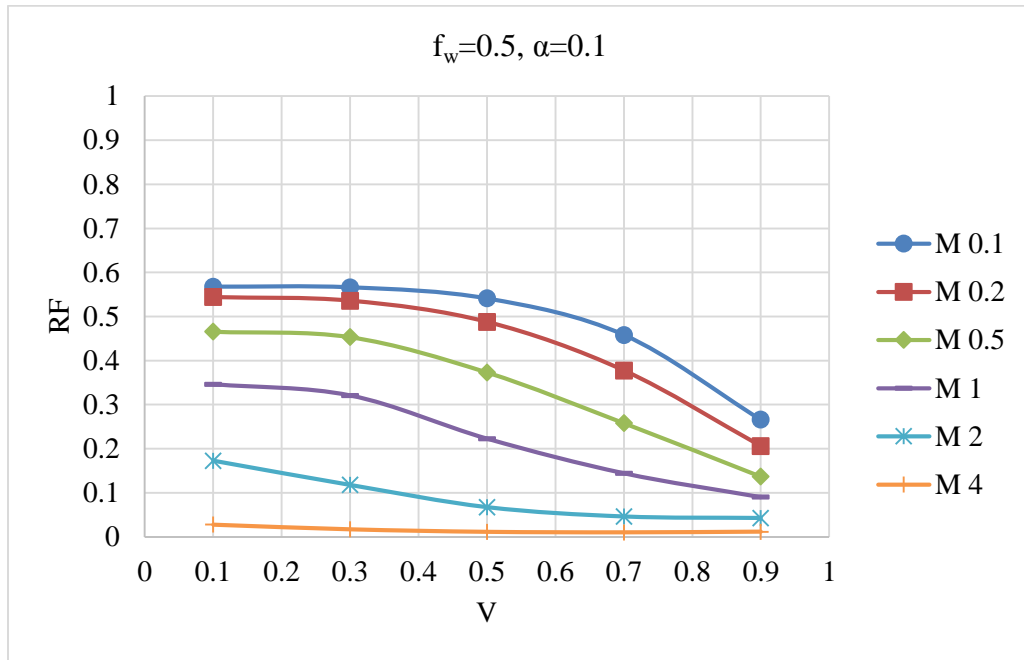


Figure A.63: Recovery factors after breakthrough ($f_w=0.5$) with crossflow ($\alpha=0.1$) for system 3

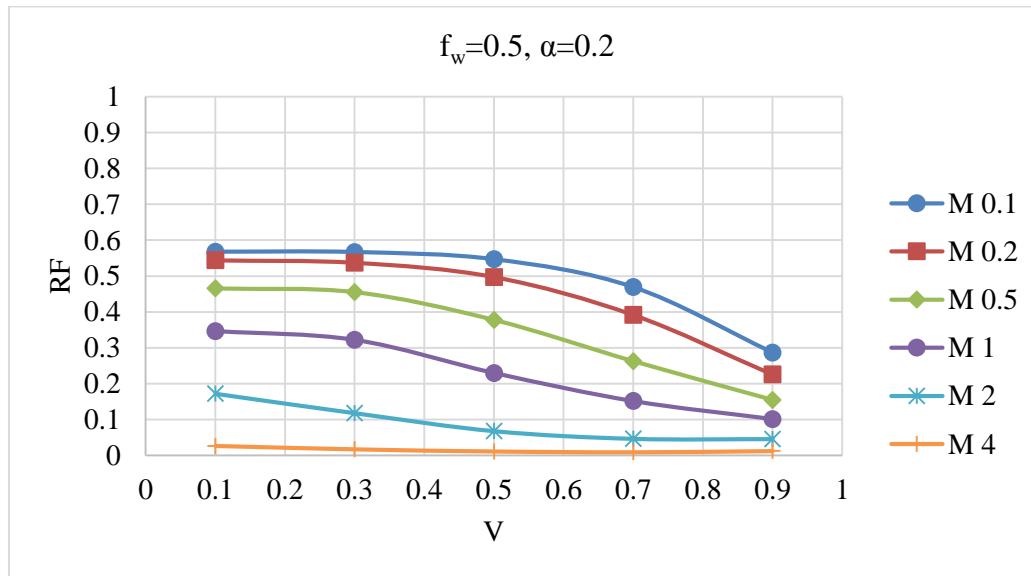


Figure A.64: Recovery factors after breakthrough ($f_w=0.5$) with crossflow ($\alpha=0.2$) for system 3

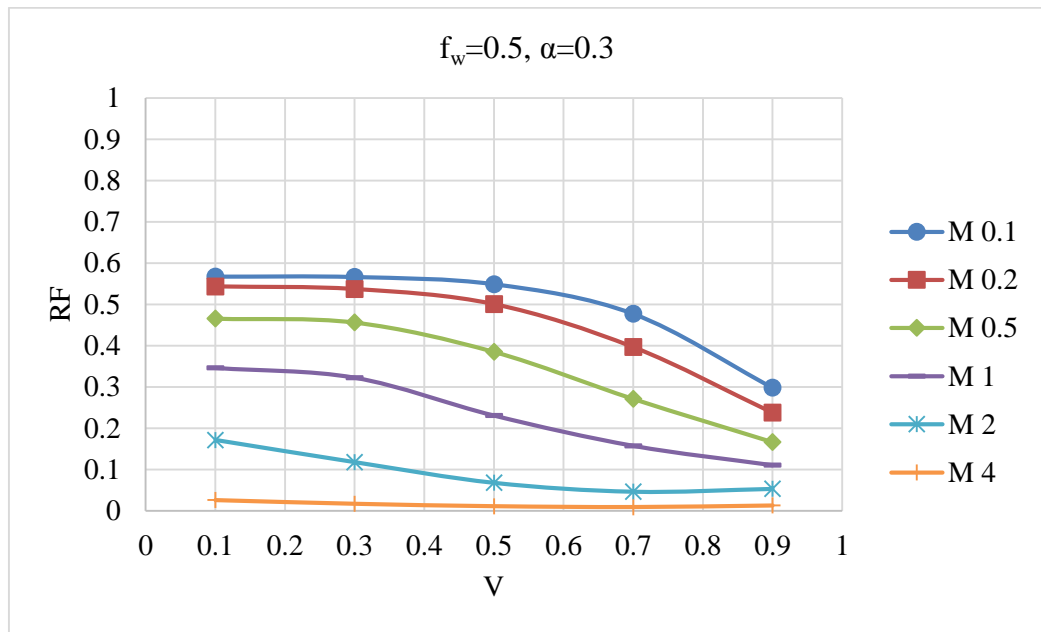


Figure A.65: Recovery factors after breakthrough ($f_w=0.5$) with crossflow ($\alpha=0.3$) for system 3

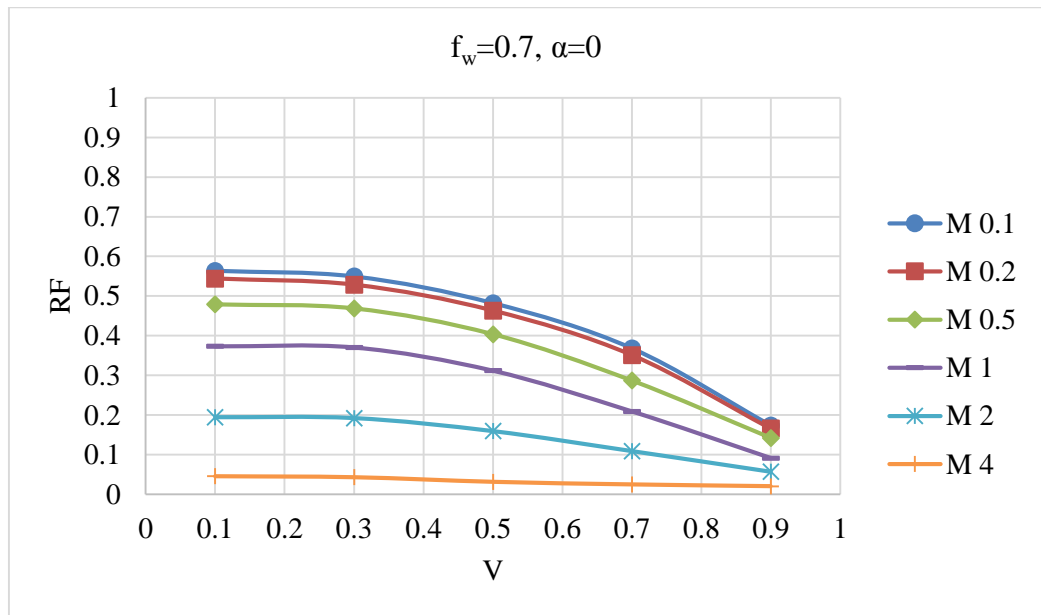


Figure A.66: Recovery factors after breakthrough ($f_w=0.7$) without crossflow ($\alpha=0$) for system 3

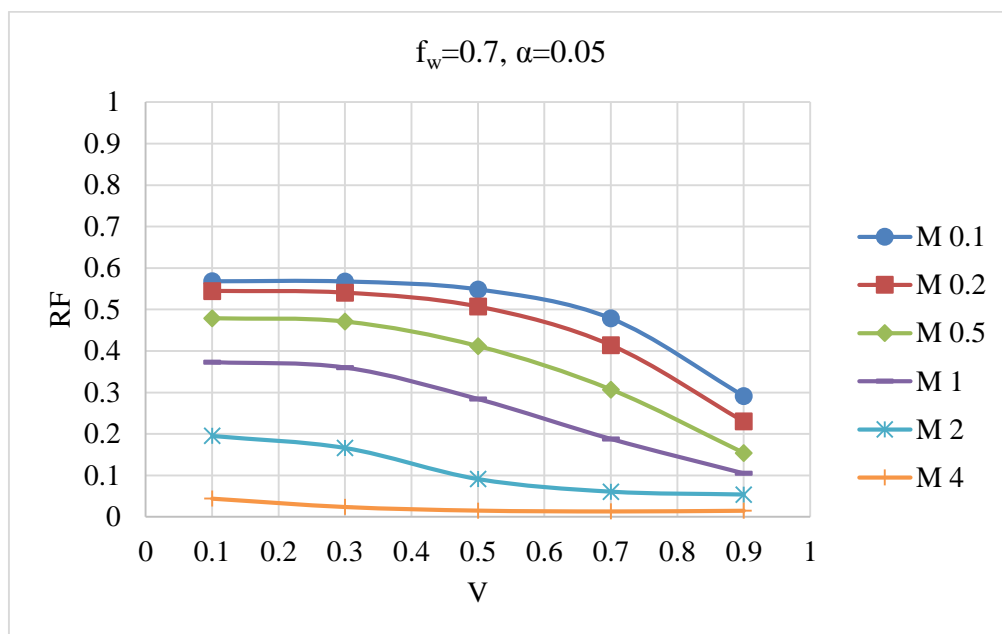


Figure A.67: Recovery factors after breakthrough ($f_w=0.7$) with crossflow ($\alpha=0.05$) for system 3

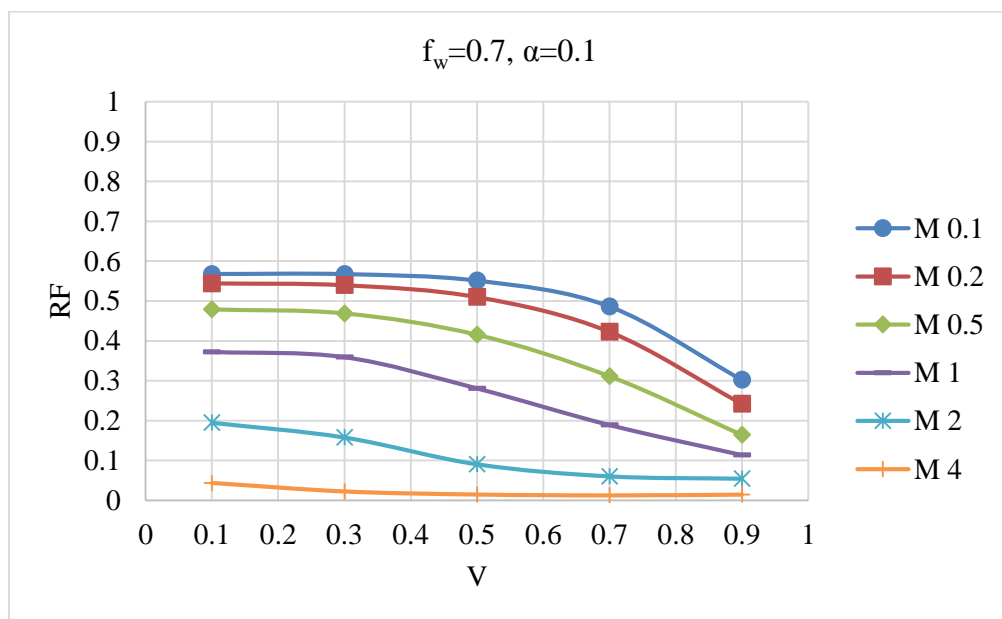


Figure A.68: Recovery factors after breakthrough ($f_w=0.7$) with crossflow ($\alpha=0.1$) for system 3

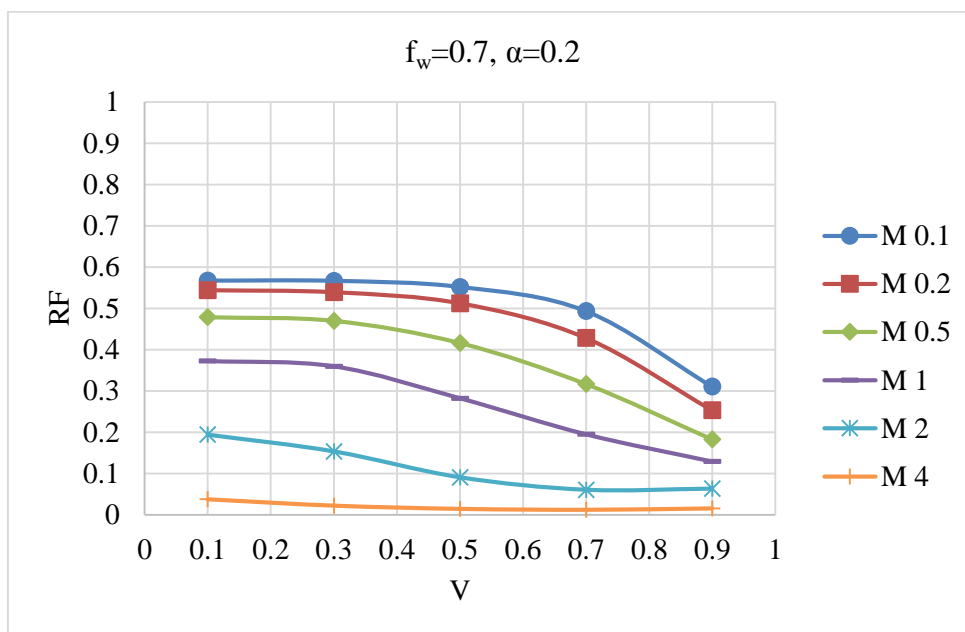


Figure A.69: Recovery factors after breakthrough ($f_w=0.7$) with crossflow ($\alpha=0.2$) for system 3

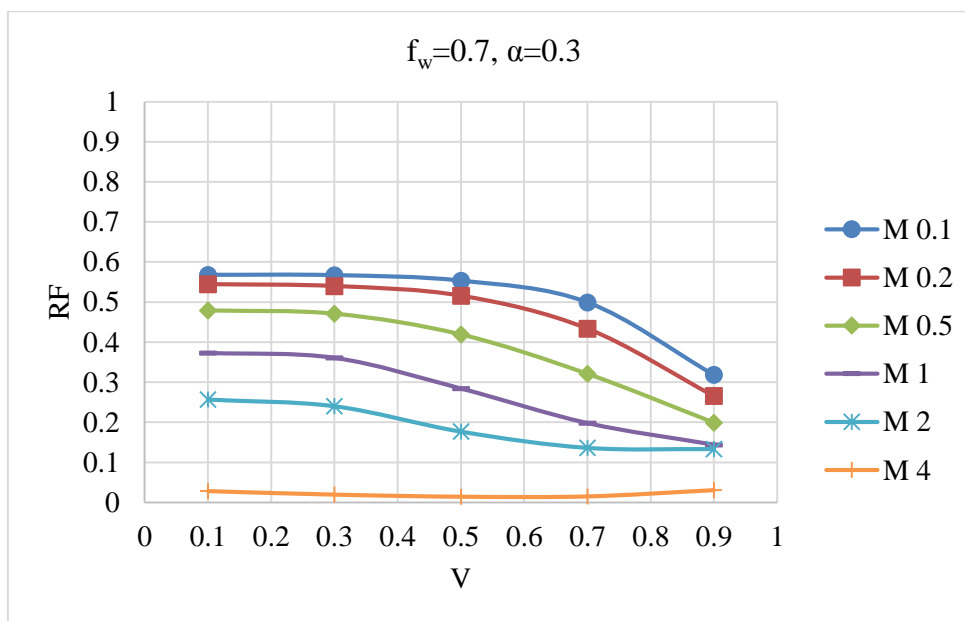


Figure A.70: Recovery factors after breakthrough ($f_w=0.7$) with crossflow ($\alpha=0.3$) for system 3

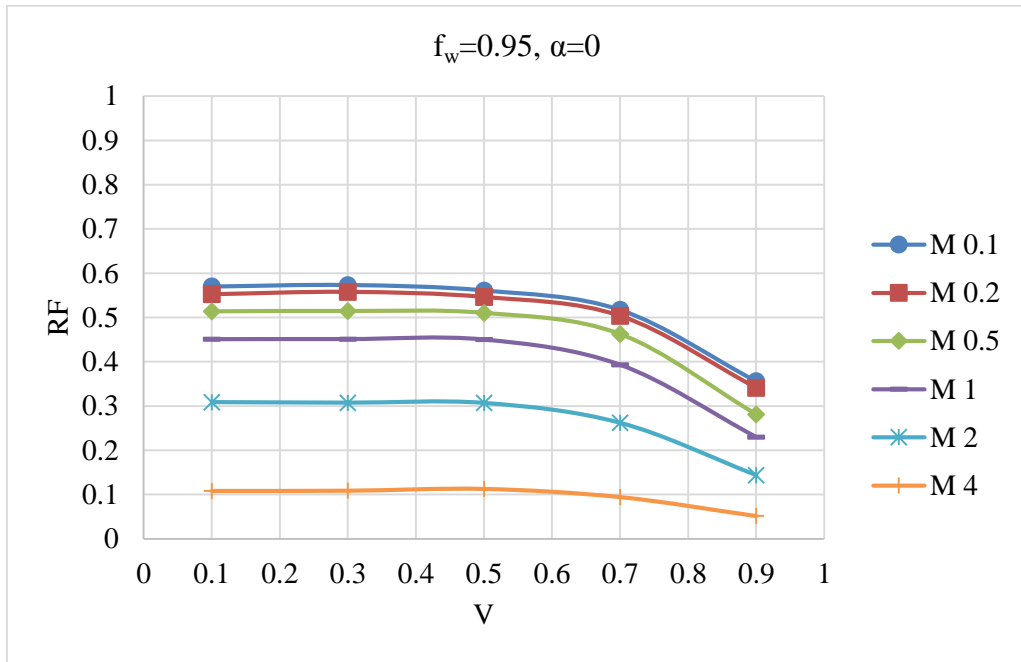


Figure A.71: Recovery factors after breakthrough ($f_w=0.95$) without crossflow ($\alpha=0$)
for system 3

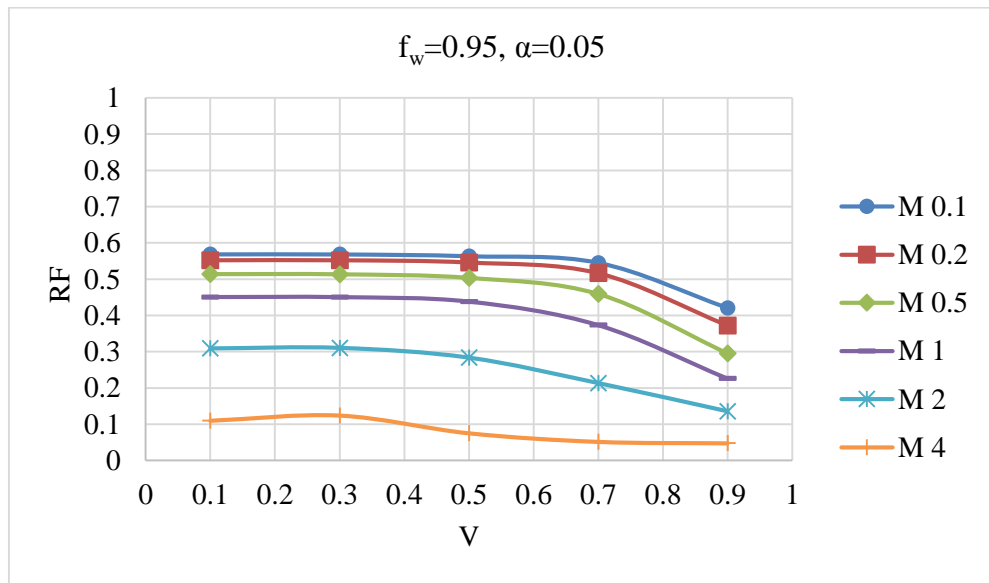


Figure A.72: Recovery factors after breakthrough ($f_w=0.95$) with crossflow ($\alpha=0.05$)
for system 3

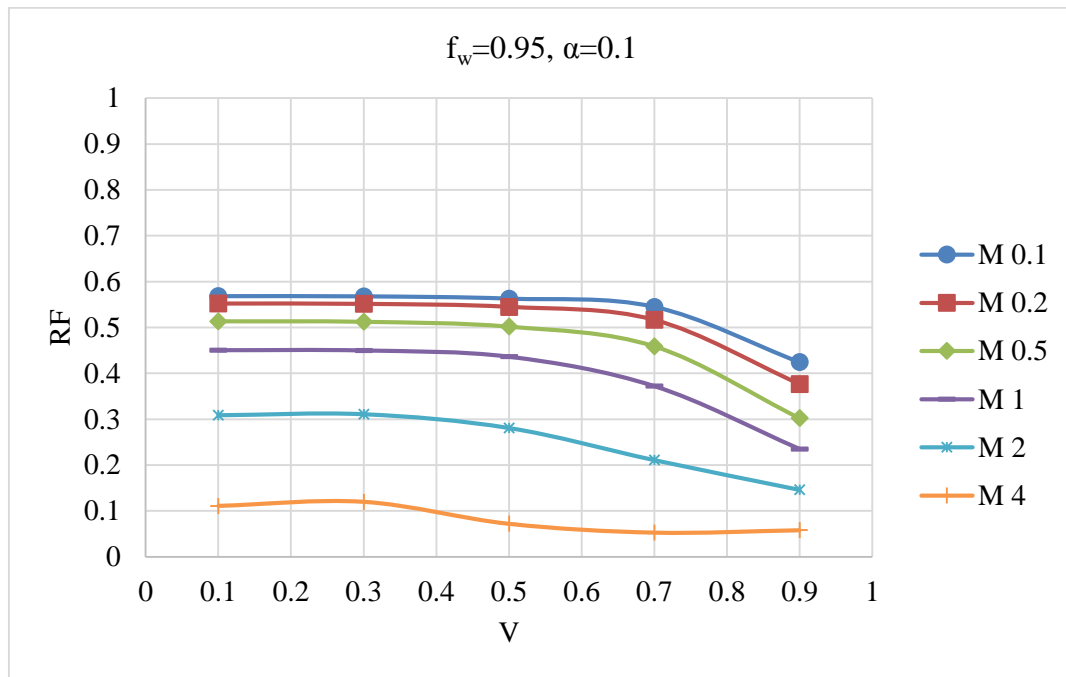


Figure A.73: Recovery factors after breakthrough ($f_w=0.95$) with crossflow ($\alpha=0.1$)

for system 3

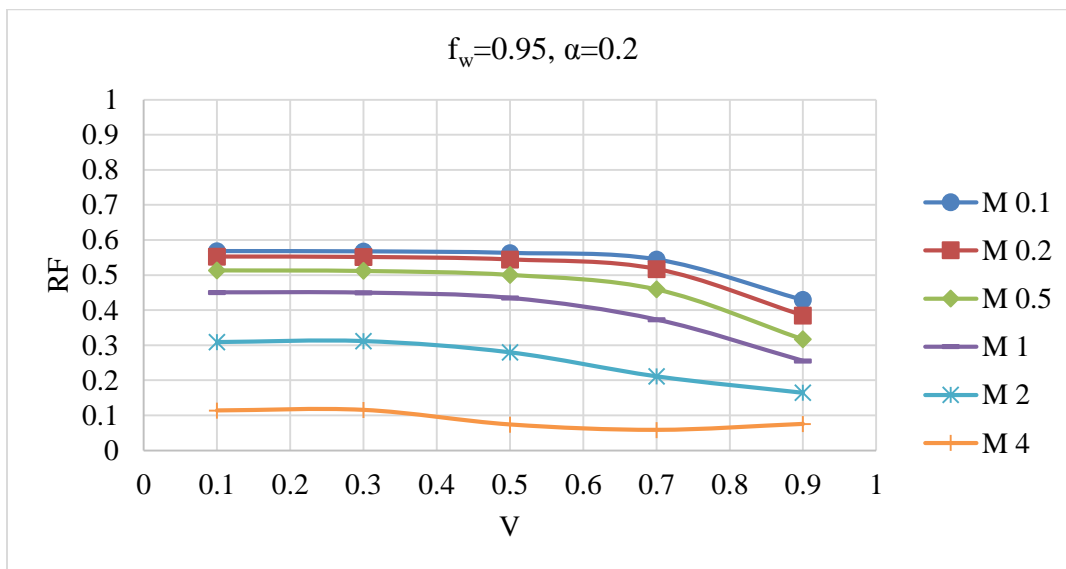


Figure A.74: Recovery factors after breakthrough ($f_w=0.95$) with crossflow ($\alpha=0.2$)

for system 3

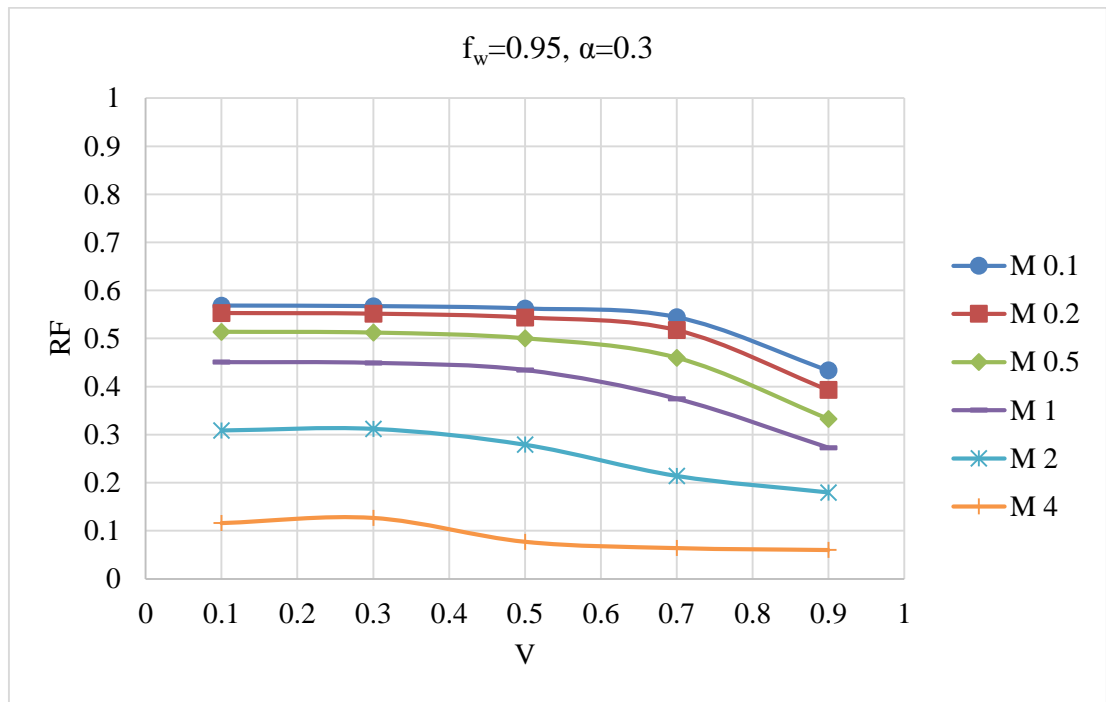


Figure A.75: Recovery factors after breakthrough ($f_w=0.95$) with crossflow ($\alpha=0.3$)
for system 3

Vitae

Name: Shams Kalam

Date of Birth: September 7, 1989

Permanent Address: B-59, Bilal Town, Malir Halt, Karachi, Pakistan.

Email Address: shamskalam@hotmail.com

Publications: A Review of Recent Developments and Challenges in IGIP Estimation of Coal Bed Methane Reservoirs. **SPE-178022-MS.**
A New Algorithm to Quantify Water Coning in Hydraulically Fractured Tight Oil Reservoirs. **IFEDC-2015482.**
Application of Artificial Intelligence for Water Coning Problem in Hydraulically Fractured Tight Oil Reservoirs. **OTC-26450-MS.**

Educational Qualification: **MS (Petroleum Engineering)** **March, 2016**
King Fahd University of Petroleum & Minerals,
Dhahran, Saudi Arabia.

Master in Energy and Environmental Economics and Management **June, 2013**
Eni Corporate University (Scoula Enrico Mattei)
San Donato Milanese, Italy.

B.E. (Petroleum Engineering) **December, 2011**
NED University of Engineering and Technology,
Karachi, Pakistan.